Title
Development of Dielectric Elastomer Nanocomposites as Stretchable and Flexible Actuating Materials

Author
Wang, Yu

Publication Date
2015

Peer reviewed|Thesis/dissertation

UNIVERSITY OF CALIFORNIA,

IRVINE

Development of Dielectric Elastomer Nanocomposites as Stretchable and Flexible Actuating Materials

DISSERTATION

submitted in partial satisfaction of the requirements

for the degree of

DOCTOR OF PHILOSOPHY

in Materials Science and Engineering

by

Yu Wang

Dissertation Committee:

Professor Lizhi Sun, Chair

Professor Lorenzo Valdevit

Professor James Earthman

2015

DEDICATION

To

my parents,

Limin Zhang and Jian Wang

and my wife,

Miho Wang

TABLE OF CONTENTS

LISTS OF FIGURES

Page

Chapter 1

Chapter 2

Chapter 3

Chapter 4

Chapter 5

Chapter 6

LIST OF TABLES

Page

Chapter 5

Chapter 6

ACKNOWLEDGEMENTS

I would like to express my sincere gratitude to my advisor, Professor Lizhi Sun, for his continuous guidance and support during my graduate studies. His great integrity, graciousness will always be my pursuit. Without his encouragement and patience, this work would not have been possible.

I am also grateful to my dissertation committee members, Professor Lorenzo Valdevit from Department of Mechanical and Aerospace Engineering, and Professor James Earthman from Department of Chemical Engineering and Materials Science for their insightful advises and valuable discussion in completing this dissertation.

I would like to thank Dr. Jian-Guo Zheng at UC Irvine for guiding me and helping me with the facilities including scanning electron microscopy, transmission electron microscopy, atomic force microscopy and laser Doppler vibrometry. SEM work was performed at the Laboratory for Electron and X-ray Instrumentation (LEXI) at UC Irvine, using instrumentation funded in part by the National Science Foundation Center for Chemistry at the Space-Time Limit (CHE-082913).

I also would like to thank my friend, Dr. Ken Nagata, for his help in developing batch scripts to run finite element models on high performance computing available at University of California, Irvine. I also enjoyed fruitful discussion with him on statistical approach to analyze the data.

I would like to thank Dr. Sungjun Kim and Professor G. P. Li in Electrical Engineering and Computer Science at University of California, Irvine for their help and insightful discussion on the dielectric properties measurement.

I would like to thank Mr. Dongxu Liu for his insightful advices for solid mechanics. Thanks also go to professor Sun's group members, Mr. Yongxue Li, Mr. Ping Zhang and Mr. Robbie Damiani for their encouragement during my study. Special thanks go to Dr. Rui Li for his kind help and care from my first day in Professor Sun's group, as well as the insightful advice for my career.

Lastly, I would like to thank my wife, Miho Wang, for her love, encouragement and support during my work towards Ph.D. degree. Without her love, this work would not have been possible. Special thanks also go to my dear parents, Limin Zhang and Jian Wang for their endless love and support throughout my life. I owe to them every success I have in my life.

This work is sponsored by the National Science Foundation (NSF) under Grants CMMI-0800417 and CMMI-1229405. The supports are gratefully acknowledged.

CURRICULUM VITAE

Yu Wang

2009	B.S., Materials Engineering University of Tokyo, Tokyo, Japan
2010	M.S., Materials Science and Engineering University of California, Irvine, CA
2015	Ph.D., Materials Science and Engineering University of California, Irvine, CA
2015-	Engineer Ford Motor Company, Dearborn, MI

ABSTRACT OF THE DISSERTATION

Development of dielectric elastomer nanocomposites as stretchable and flexible actuating materials

By

Yu Wang

Doctor of Philosophy in Materials Science and Engineering

University of California, Irvine, 2015

Professor Lizhi Sun, Chair

Dielectric elastomers (DEs) are a new type of smart materials showing promising functionalities as energy harvesting materials as well as actuating materials for potential applications such as artificial muscles, implanted medical devices, robotics, loud speakers, micro-electro-mechanical systems (MEMS), tunable optics, transducers, sensors, and even generators due to their high electromechanical efficiency, stability, lightweight, low cost, and easy processing. Despite the advantages of DEs, technical challenges must be resolved for wider applications. A high electric field of at least 10-30 $V/\mu m$ is required for the actuation of DEs, which limits the practical applications especially in biomedical fields. We tackle this problem by introducing the multiwalled carbon nanotubes (MWNTs) in DEs to enhance their relative permittivity and to generate their high electromechanical responses with lower applied field level. This work presents the dielectric, mechanical and electromechanical properties of DEs filled with MWNTs.

The micromechanics-based finite element models are employed to describe the dielectric, and mechanical behavior of the MWNT-filled DE nanocomposites. A sufficient number of models are computed to reach the acceptable prediction of the dielectric and mechanical responses. In addition, experimental results are analyzed along with simulation results. Finally, laser Doppler vibrometer is utilized to directly detect the enhancement of the actuation strains of DE nanocomposites filled with MWNTs. All the results demonstrate the effective improvement in the electromechanical properties of DE nanocomposites filled with MWNTs under the applied electric fields.

Chapter 1 Introduction

1.1 Applications and Challenges of Dielectric Elastomers

An actuator is a mechanical device which controls the system. Conventional actuators include electronic actuators, motors, hydraulic cylinders and piezoelectric actuators [1]. Those actuators are complex to transmit energy with poor efficiency at small scales. In addition, there are limitations with respect to the size, shape, response speed, which motivate researchers to work on alternative materials for actuators. New high-performance actuator materials are demanded for the applications of micro robots [2], portable micro devices, stretchable electronics [3, 4] and medical purposes.

Electro active polymers (EAPs) have been attracting attention in the field of electromechanical actuation and sensing. Dielectric elastomers (DEs), an emerging area of EAPs, have been showing promising functionalities as energy harvesting materials [5-8] as well as actuating materials for potential applications such as artificial muscles [6, 9-12], implanted medical devices, robotics [2, 13], loud speakers [14, 15], automotive control, micro-electro-mechanical systems (MEMS), tunable optics [16], responsive prosthetics[17], transducers[18], sensors, and even generators[19-21] due to their high electromechanical efficiency, durability, stability, lightweight, low cost, and easy processing[1, 6, 9, 19, 22-26].

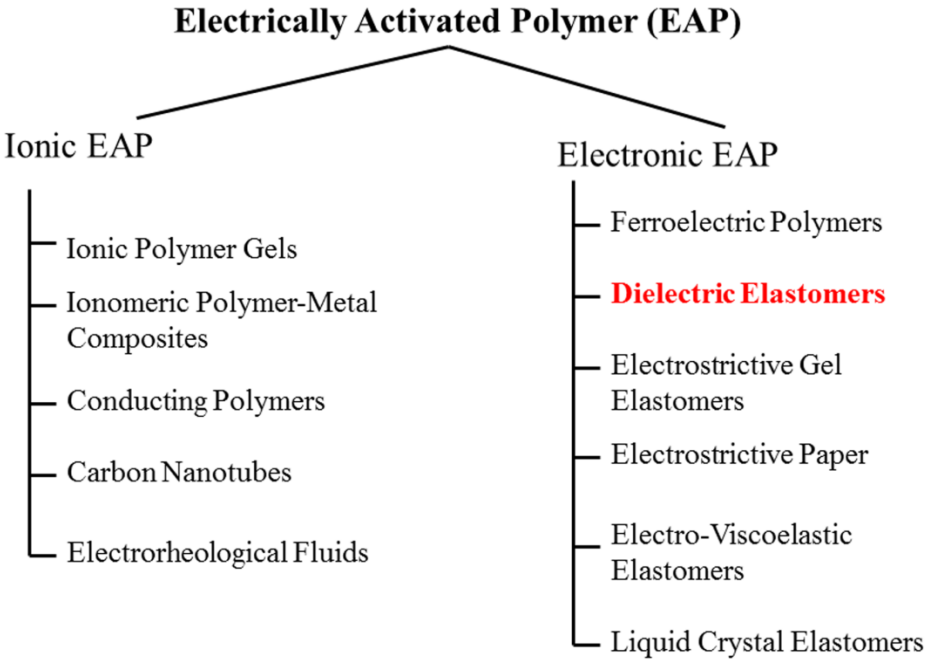

Fig. 1. 1. Classifications of actively deformable polymers (Figure modified from [27]).

DE material is an elastic polymer with dielectric properties. As DE materials are insulators, the material can be used as a medium in structures such as capacitors. In another word, DE actuators can be described as compliant capacitors [28] with the incompressible and yet highly deformable elastomer material sandwiched by two compliant electrodes [29] as shown in Fig. 1.1. When potential difference is applied to the compliant electrodes on both surfaces of the DEs, positive charges accumulate on one electrode, and negative charges on the other. As a result, Coulomb force arises due to the attraction force by the opposite charges on the different electrodes, and repelling force by like charges on each electrode, resulting in a pressure referred to as Maxwell Stress [22]. The area covered by compliant conductive electrodes deforms and expands its area

under applied electric field. For example, acrylic-based DEs are reported to have up to 380 % in-plane strain [25, 30].

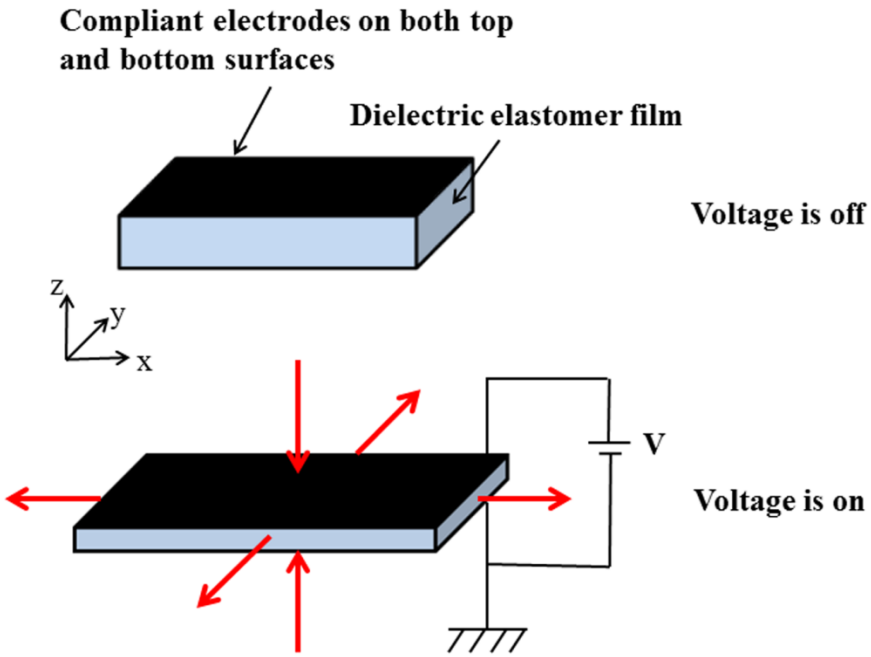

Fig. 1. 2. Principle of operation of dielectric elastomers (DEs).

There are two potential elastomers for DEs, one is acrylic-based elastomers [31-34], and the other is silicone-based elastomers [35, 36]. Michel, S., *et al.* summarizes that acrylic-based elastomers provide higher strain response while silicone-based elastomers enables faster response, at least 50-67 times faster due to the higher viscoelastic losses in acrylic-based elastomers [1, 37]. Another significant fact which needs to be remarked here is that

electromechanical response of silicone-based elastomers is time-independent while that of acrylic-based elastomers is strongly dependent on time and history. It is assumed that the creep processes are not completed within an activation cycle. As a result, the acrylic-based elastomers possess risks of damages and unstable actuations which require additional control system. Some approaches have been proposed to minimize the viscosity in acrylic-based elastomers such as pre-strain [38-41], however, pre-strain causes increased materials stiffness and slightly reduced dielectric constant [28]. Therefore, for fast response actuation purposes, silicone-based elastomers are favored.

Despite the advantages of DEs, technical challenges must be resolved for wider applications. A high electric field of at least 10-30 $V/\mu m$ is required for the actuation of DEs, which limits the practical applications especially in biomedical fields [6, 11]. A common solution to the disadvantages of DEs is to enhance their relative permittivity by implementing ceramic powders with high dielectric constant such as TiO_2 particles[42, 43], $BaTiO_3$ nanoparticles [43-46] and $PbTiO_3$[47, 48] to generate high electromechanical responses with lower applied field level. However, high loading, up to 20-30 vol. % of these particles are required for meaningful increase, at which the ceramic powders filled composite materials could lose its flexibility, leading to limited improvement of the electromechanical response. Recently, carbon nanotubes have been reported to efficiently enhance the relative permittivity with a small loading fraction up to 2 weight % (wt. %) due to its high aspect ratio and conductivity while avoiding the unwanted increase of the materials rigidity [49-53].

1.2 Historical Overview

Electromechanical responses of DEs are of interest in various fields as mentioned earlier. Pelrine first demonstrated a silicone-based dielectric elastomer actuation [22], and also developed a simple model for pure DEs to correlate the thickness strain as

$$s_z = -\frac{\varepsilon_0 \varepsilon}{Y}\left(\frac{V}{d}\right)^2$$

where, s_z is the thickness strain of the film, ε_0 permittivity of vacuum (8.85×10^{-12} F/m), ε dielectric constant of the material, Y the modulus of elasticity, V the applied voltage, d the thickness of the film. Pelrine has also pointed out that the breakdown and pull-in instabilities of the DEs could occur under certain thickness strain.

Since the pioneering work done by Pelrine, much effort has been made by many researchers to explore the applications of DEs [25, 54]. Extensive research has been done on the selection of elastomers and the selection of the curing agent in the 2000s [27, 32]. Some of the efforts have been done to improve the electromechanical response of DEs by pre-stretch [6, 32, 41, 55]. Li reported that pre-stretch can even stabilize the actuation of DEs as well as improve the breakdown strength of DEs [40]. Suo *et al* also developed the theory of DE actuating principles, and extensively investigated the DE breakdown and pull-in instability mechanism in a numerical approach [7, 29, 33, 56-63]. In addition, they investigated the theoretical maximum extractable energy that could be obtained from DE generators [5]. The selection of electrode materials is also an active research field as the electrodes cover the entire active region of DEs without restricting

the deformation [1]. So far, carbon grease [22], carbon black, and carbon nanotubes [64] are proposed to meet the requirements.

Much investigation has also been carried out to enhance the electromechanical properties of DEs through improving the effective dielectric constant of DEs by adding ceramic fillers such as TiO_2 particles [42, 43], $BaTiO_3$ nanoparticles[43-46] and $PbTiO_3$ [47, 48] as mentioned earlier. However, it is reported that the dielectric breakdown occurs, especially under high concentration of the fillers [45]. Consequently, it is desired to add a type of filler with small concentration which can still significantly improve the electromechanical response of DEs.

Some of the ideas have been proposed to utilize carbon nanotubes as fillers to DEs [52, 65]. The idea comes from that only a small amount of CNTs can drastically increase the dielectric constant [53, 66-68] without changing the elastic modulus much [68], resulting in higher electromechanical response. Carbon nanotubes (CNTs) are allotropes of carbon with a cylindrical nanostructure discovered by Iijima [69] back in early 1990s. CNTs can be classified into 2 categories, single-walled carbon nanotubes (SWNTs) and multi-walled carbon nanotubes (MWNTs). A SWNT is composed of a single graphene in a cylindrical nanostructure while a MWNT is made up of multi-layer of graphene sheets. Both types of CNTs possess remarkable characteristics such as high thermal conductivity, high electrical conductivity, and high mechanical strength. Extensive research has been done to implement CNTs in polymer matrix in order to obtain composite materials with improved mechanical properties or high electrical conductivity. One of the challenges in using CNTs as fillers to polymer matrix is the dispersion of CNTs. CNTs naturally hold themselves together due to Van der Waals forces. Many research efforts have been made to improve the dispersion of CNTs applying multiple approaches such as ultra-sonication and functionalization of the CNTs. Moreover, the introduction of well-dispersed

MWNTs can potentially enhance the scratch resistance for wider applications. Some researchers have demonstrated that blending rigid and tough polymer particles like PMMA can enhance the scratch resistance of the relatively soft polymers [70].

We aim to develop a new generation of DEs by incorporating MWNTs to the DEs as fillers. We experimentally and numerically investigate the dielectric or mechanical property modification with the addition of MWNTs to DEs. Finally, we experimentally demonstrate that, with addition of MWNTs, the DE nanocomposites show improved electromechanical properties. An integrated research is summarized on the synthesis, characterization, modeling and simulation of DEs and DE nanocomposites.

1.3 Scope

This research is to investigate the electromechanical response enhancement by adding CNTs in DEs. Here, the first goal is to successfully develop a set of methods to fabricate the novel DE nanocomposites. In the next step, Laser Doppler Vibrometer is utilized to characterize the electromechanical response of the DE nanocomposites. This is among the few efforts to precisely investigate the electromechanical properties of DEs and DE nanocomposites. Last but not least, representative unit-cell models with multiple CNTs are developed for the first time to investigate how the microstructure of the DE nanocomposites affects the dielectric and mechanical properties by applying finite element analysis, and also compared with the experimental results.

This dissertation is organized as follows:

Chapter 2 presents the fabrication process of DEs and DE nanocomposites. The dispersion process of CNTs is also discussed. First, literature review is conducted and the current research status on the fabrication of DEs and DE nanocomposites, and CNT dispersion issues are summarized. Next, the fabrication procedures and materials characterization of the fabricated specimens are presented. Lastly, fabrication process and CNTs dispersion are summarized.

Chapter 3 presents the measurement of the electromechanical properties of DEs and DE nanocomposites by Laser Doppler Vibrometer. First, literature review on the electromechanical measurement of DEs is summarized. Next, the electromechanical measurement system is described and the technical issues are addressed. Finally, the obtained electromechanical response of DEs and DE nanocomposites are evaluated and analyzed to demonstrate the electromechanical response enhancement of DE nanocomposites filled with CNTs.

Chapter 4 covers the experimental study of dielectric and mechanical properties of dielectric elastomer nanocomposites filled with CNTs. First, literature review on the dielectric and mechanical measurement is summarized. Next, the measurement procedures are described. Finally, the measurement results are discussed, and the major findings are summarized.

Chapter 5 covers the filler orientation effects on dielectric properties of DEs and DE nanocomposites. First, literature review on the efforts to enhance the dielectric properties of elastomer nanocomposites is summarized. Next, representative unit-cell models are proposed and the correlation between the microstructure and the effective dielectric properties of DE nanocomposites is investigated. Finally, proposed random orientation models are evaluated by comparing the simulation results with the experimental data.

Chapter 6 presents mechanical properties of DEs and DE nanocomposites. First, literature review on the mechanical properties of CNTs filled elastomers. Next, representative unit-cells are used to analyze the mechanical properties of the nanocomposites. Finally, proposed random orientation models are evaluated by comparing the simulation results with the experimental data.

Chapter 7 concludes the dissertation by summarizing the major contributions. In addition, some suggestions for the future work are also discussed.

Finally, an appendix is included. It gives the batch commands to run COMSOL Multiphysics on High Performance Computing (HPC) facilities available at University of California, Irvine.

Over 170 references are cited.

Chapter 2 Materials Processing Techniques for Fabrication of DE Nanocomposites Filled with MWNTs

2.1 Introduction

Polymer/CNTs composites are promising new materials with excellent mechanical, thermal and electrical functionalities due to the unique properties such as high aspect ratio and high conductivity of CNTs. The addition of CNTs to polymer matrix enables the conductive elastic polymers (elastomers) to be utilized in stretchable electronics [71], MEMS [72], actuators and sensors [72, 73].

Polymers can be reinforced in strength and stiffness by adding particulate fillers in them. To obtain materials with great mechanical properties, various kinds of nanoparticles have been used such as silica, titanium [74] and polymethyl methacrylate (PMMA) [70]. Especially carbon nanotubes (CNTs) [69] have been considered to be the potential filler which can reinforce the mechanical properties of polymers in the last 20 years [74]. With the great progress achieved on CNTs, CNTs have been used to synthesize not only various polymer/CNTs composites [75] but also various CNTs/metal oxide hybrids [76], where CNTs can serve as high-performance supporting materials. CNTs can also be applied in nano-electronic devices [77], or in the automobiles and aerospace industries due to the dissipation of electrostatic charges [78]. The critical challenge, however, is the dispersion control of CNTs inside polymer matrix.

CNTs can easily form aggregates and bundles due to van der Waals force. Aggregation of CNT could limit the advantage of the CNT aspect ratios. As a result, the aggregated CNTs could have

poor interfacial bonding with the surrounding elastomer matrix. This weak interfacial bonding between the matrix and CNTs can result in the poor load transfer within the polymer nanocomposites.

For the past 15 years, the dispersion of CNTs has been under extensive investigations. The well dispersed CNTs have been demonstrated to enhance the mechanical, thermal and electrical properties of polymer/CNTs composites. CNTs surface functionalization [79-85] and the utilization of solvent [86-93] such as acetone and ketone have been attempted to improve the dispersion in polymer matrix as well. Poor dispersion and poor interfacial bonding are the limiting factors of the full utilization of the carbon nanotube as a reinforcing filler in elastomer matrices [74].

The selection of solvent has a significant influence of the dispersion of carbon nanotubes in elastomer matrix [92]. Acetone is a simple polar organic solvent and a common chemical commodity. Acetone is utilized as a solvent to dilute the pure elastomer and reduce the viscosity during the fabrication process [92].

In this chapter, the approaches to disperse MWNTs are to be briefly discussed. Utilization of acetone in MWNTs dispersion is to be discussed as well. Furthermore, the effect of acetone and ultra-sonication on MWNTs dispersion is to be discussed.

2.2 Materials, Fabrication, and Characterization

Alumilite HS III RTV high strength mold-making silicone rubber is chosen as elastomers. Acetone, from Fisher Scientific, is chosen as a solvent to help CNTs disperse in elastomers. MWNTs purchased from CheapTubes.com, are used as fillers in elastomers. MWNTs have outer diameter 20-30 nm, inside diameter 5-10 nm, length 10-30 μm and specific surface area $110 m^2/g$ according to CheapTubes.com.

Fig. 2.1 shows the flowchart of the DE nanocomposite processing steps. The fabrication process are consisted of five steps: (1) grinding the pristine MWNT aggregates with a mortar and pestle, (2) stirring and dispersing MWNTs in acetone solution by ultrasonic processor (Sonics & Materials, Inc., VCX 130 shown in Fig. 2.2) for hours, (3) pouring the elastomer matrix into the solution, (4) adding the curing agent once acetone evaporates and mixing the solution, and (5) vacuum degasing the mixture for minutes using MZ2C+2AK oil-free vacuum pump. Uniform dispersion of MWNTs in elastomer matrix can be a common challenge. Therefore, grinding and solution mixing with ultra-sonication are utilized to break the Van der Waals forces between MWNTs, and to minimize the formation of MWNT aggregates [94]. Vacuum degasing is utilized to eliminate air voids.

Next, spin coating technique is utilized to prepare nanocomposite films for electromechanical and dielectric property measurement. The thickness of the films for DEs and DE nanocomposites are controlled to be about 150 μm by controlling the revolution per minute (RPM) of the spin coater (Laurell Photoresist Spinner) as shown in Fig. 2.3. The spin coating time is 40 seconds.

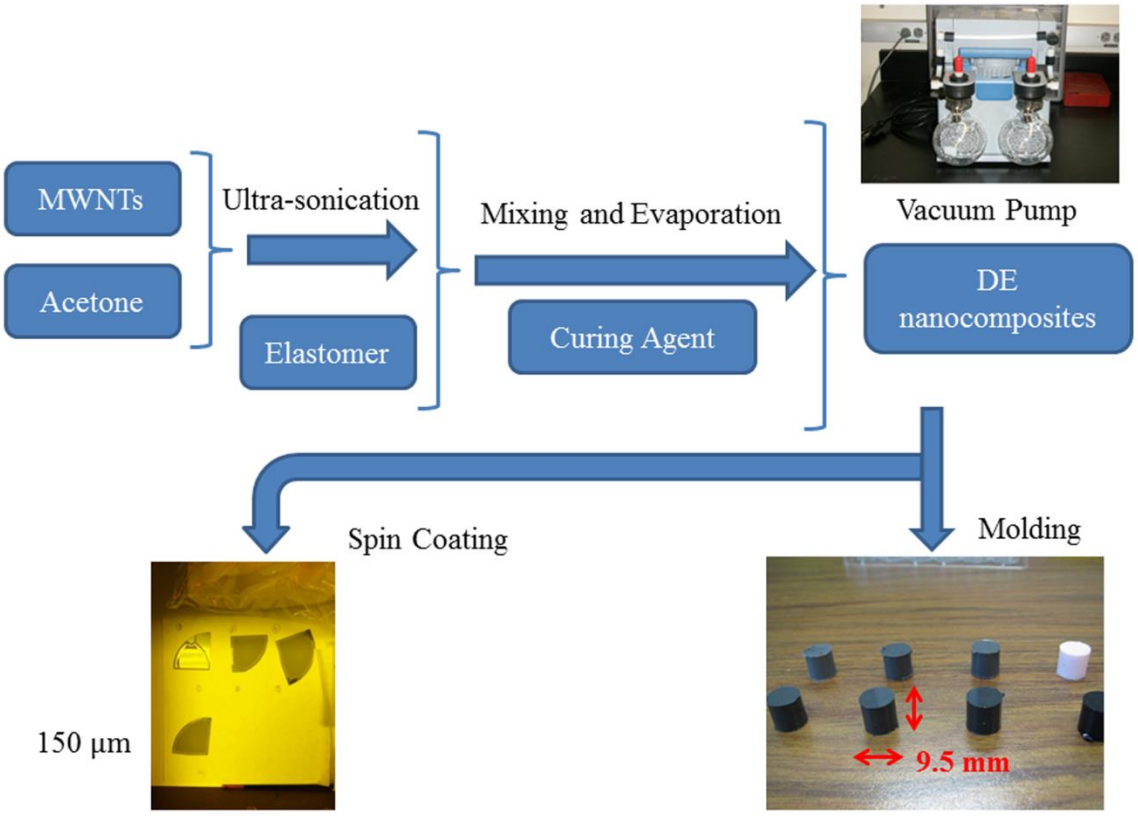

Fig. 2. 1. DE nanocomposite processing steps.

Fig. 2. 2. VCX 130 ultrasonic distributor for ultra-sonication processing.

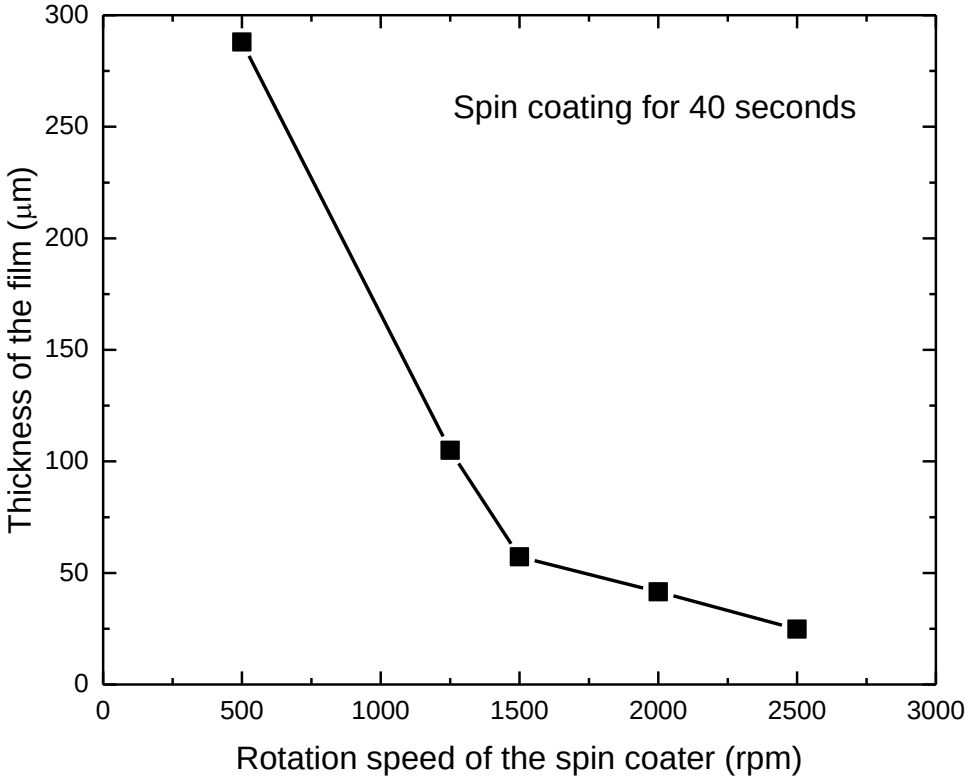

Fig. 2. 3. The relationship between the DE nanocomposite film thickness and the revolutions per minute (rpm) of the spin coater.

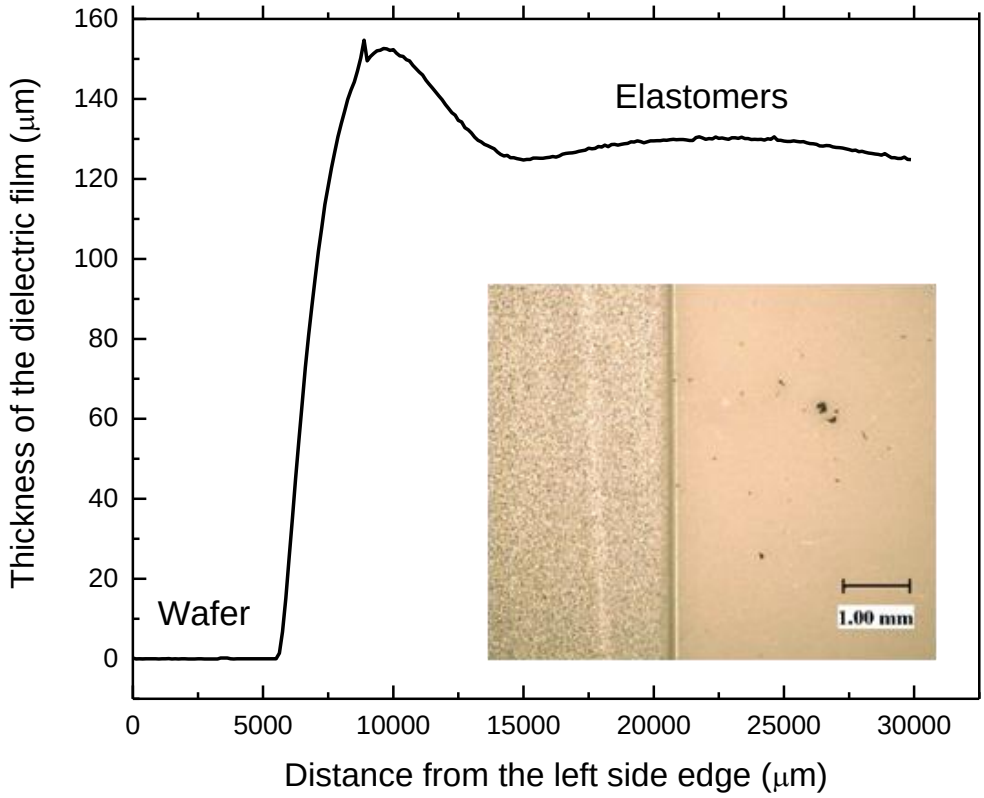

Fig. 2. 4. The thickness of the DE nanocomposite film measured by Digital Instruments Dektek 3 surface profiler.

DE Nanocomposite samples for mechanical testing are prepared by using the molding as shown in Fig. 2.1. The mold is in cylinder shape with diameter 9.5 mm and height 9.5 mm following ASTM Standard D 5992-96.

The elastomers completely cure after 72 hours. Then the thickness of the film is measured by Digital Instruments Dektek 3 surface profiler. Fig. 2.4 shows an example of the thickness measurement of a film fabricated by spin coating. The thickness at the edge is larger than other places because the uncured elastomers accumulate at the edge after the spin coating.

After fabrication, each sample is observed by FEI Quanta 3D FEG Scanning Electron Microscopy (SEM) and FEI/Philips CM-20 Transmission Electron Microscopy (TEM). Dielectric properties of nanocomposites are tested using HP 4280A 1MHz C Meter/C-V plotter at room temperature 24 ℃. Mechanical properties are tested by BOSE ElectroForce 3200 dynamic mechanical analysis (DMA) machine at 24 ℃. The details of the materials characterization are covered in the following chapters.

2.3 Results and Discussion

2.3.1 Acetone Effects in Dispersion of MWNTs in DE Matrix

Nanocomposites with 0.3 wt. % MWNTs are examined to investigate the acetone effect of acetone. Nanocomposites processed without and with acetones are compared. Fig. 2.5 shows SEM images of the clusters of MWNTs found in the nanocomposite materials processed without acetone. As seen in Fig. 2.5, various sizes of MWNT clusters are observed. The typical size of

the observed aggregates is in the range of 10-100 μm. In this study, the DE films are 100-200 μm in thickness. Thus, aggregates with 10-100 μm in size could easily be the sites of electrical conduction paths or a source of cracks [95] as can be seen in Fig. 2.5, causing the DEs to fail.

Fig. 2.6 shows SEM images of nanocomposites with acetone. The typical size of the clusters is found to be 5-20 μm, which is smaller than that of aggregates observed in the nanocomposites without acetone shown in Fig. 2.5. This shows that the acetone is playing a role in improving the dispersion of MWNTs. In addition, acetone dilutes the pure elastomer and reduces the viscosity during the fabrication process, which enables better mixing between the polymer matrix and each MWNT [92]. As a result, more interaction between DE matrix and MWNTs is enabled.

Although, acetone successfully reduces the aggregate size, the aggregates issues cannot still be fully solved using only acetone as can be seen in Fig. 2.6. Thus, other technique is also required for better dispersion of MWNTs in DE matrix.

In the next section, one of the powerful tool, ultra-sonication, is examined to investigate the effectiveness of the technique.

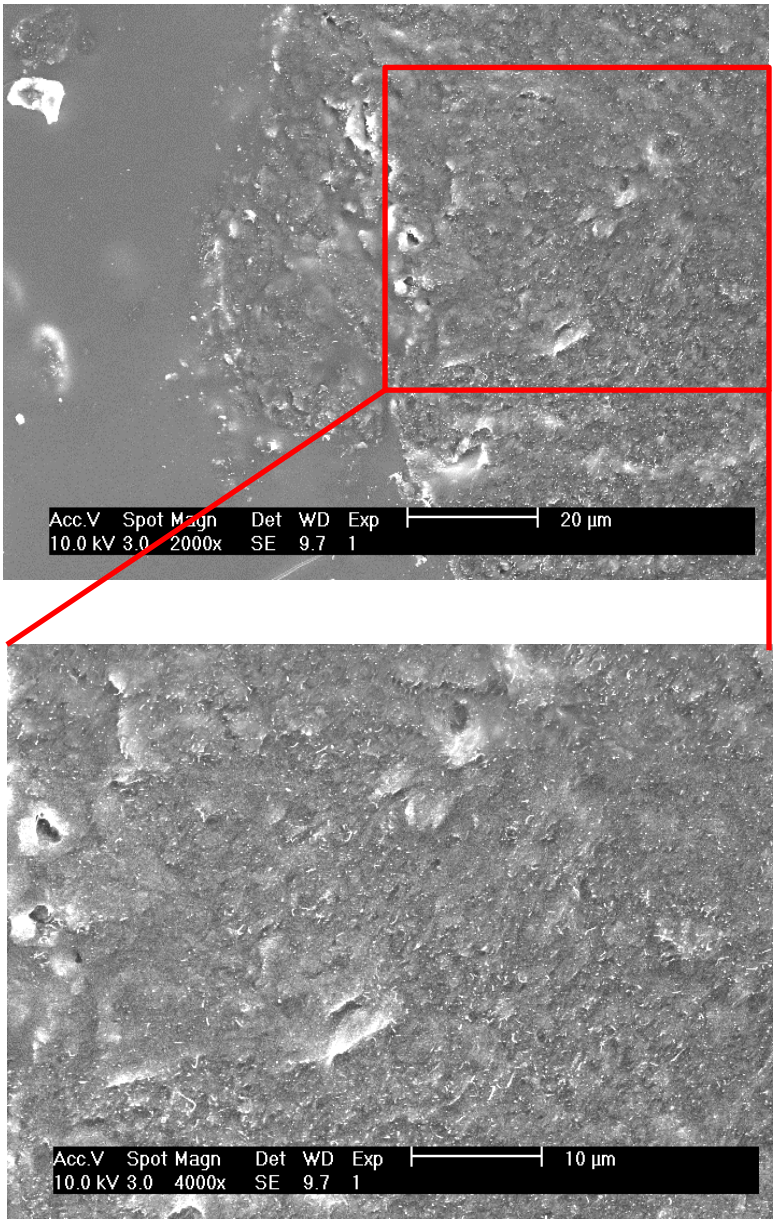

Fig. 2. 5. SEM images of nanocomposites with 0.3 wt. % MWNTs processed without acetone.

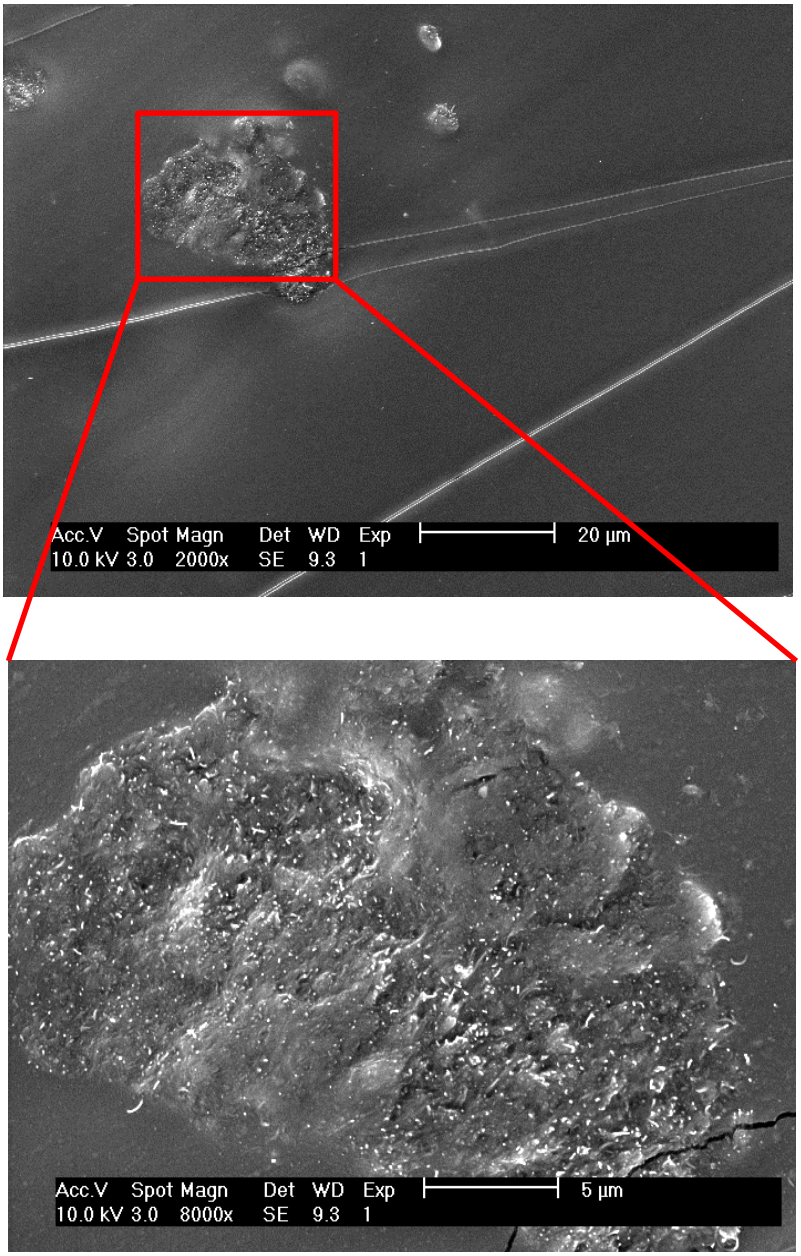

Fig. 2. 6. SEM images of nanocomposites with 0.3 wt. % MWNTs processed with acetone.

2.3.2 Ultra-sonication Effects

Poorly dispersed MWNTs usually form aggregates which work as stress concentration and initiator of cracks [95]. Ultra-sonication is a simple technique to utilize high-intensity acoustic energy to mix and disperse materials [95].

In this section, HS III dielectric elastomers with 0.3 wt % MWNTs processed with acetone are examined to investigate the dispersion of the MWNTs and material properties affected by the ultra-sonication.

Fig. 2.7, Fig. 2.8 and Fig. 2.9 show the dispersion of MWNTs before and after 0.5-hr or 4.0-hr ultra-sonication. Obviously, aggregates of MWNTs still exist even with 0.5-hr sonication. However, the typical size of the aggregates is 3-8μm, which is smaller than those observed in DEs with 0.3 wt. % MWNTs without ultra-sonication shown in Fig. 2.6 and Fig. 2.7. As shown in Fig. 2.9, the aggregates are not observed any more in the nanocomposite with 4.0-hr ultra-sonication process, and uniformly dispersed individual MWNTs are observed.

Fig. 2.10 shows the dynamic mechanical analysis results of nanocomposites with 0.3 wt. % MWNTs at 10 Hz. The introduction of 0.3 wt. % MWNTs in elastomer matrix indeed enhances the storage modulus of the nanocomposites. The specimen with 4.0-hr ultra-sonication improves the storage modulus by 25 % at all the dynamic strain amplitude range while the specimen with 0.5-hr ultra-sonication also improves the modulus by 11 % at all the dynamic strain amplitude. This demonstrates that the better dispersion of MWNTs is achieved, and larger interaction surface areas between the elastomer matrix and MWNTs enables larger load transfer under compression [95]. As a result, higher storage modulus is obtained.

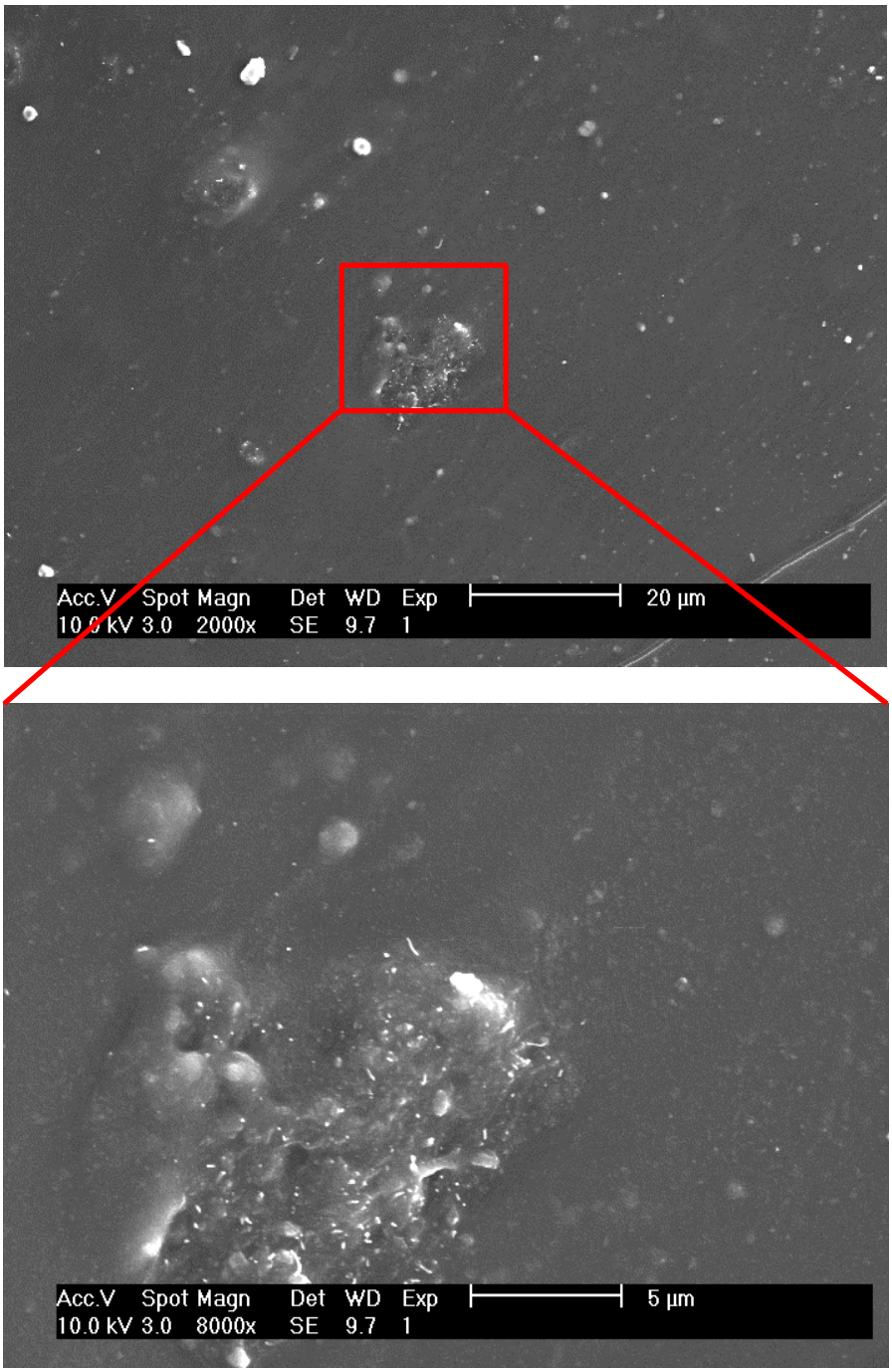

Fig. 2. 7. SEM images of nanocomposites with 0.3 wt. % MWNTs processed with acetone without ultra-sonication treatment.

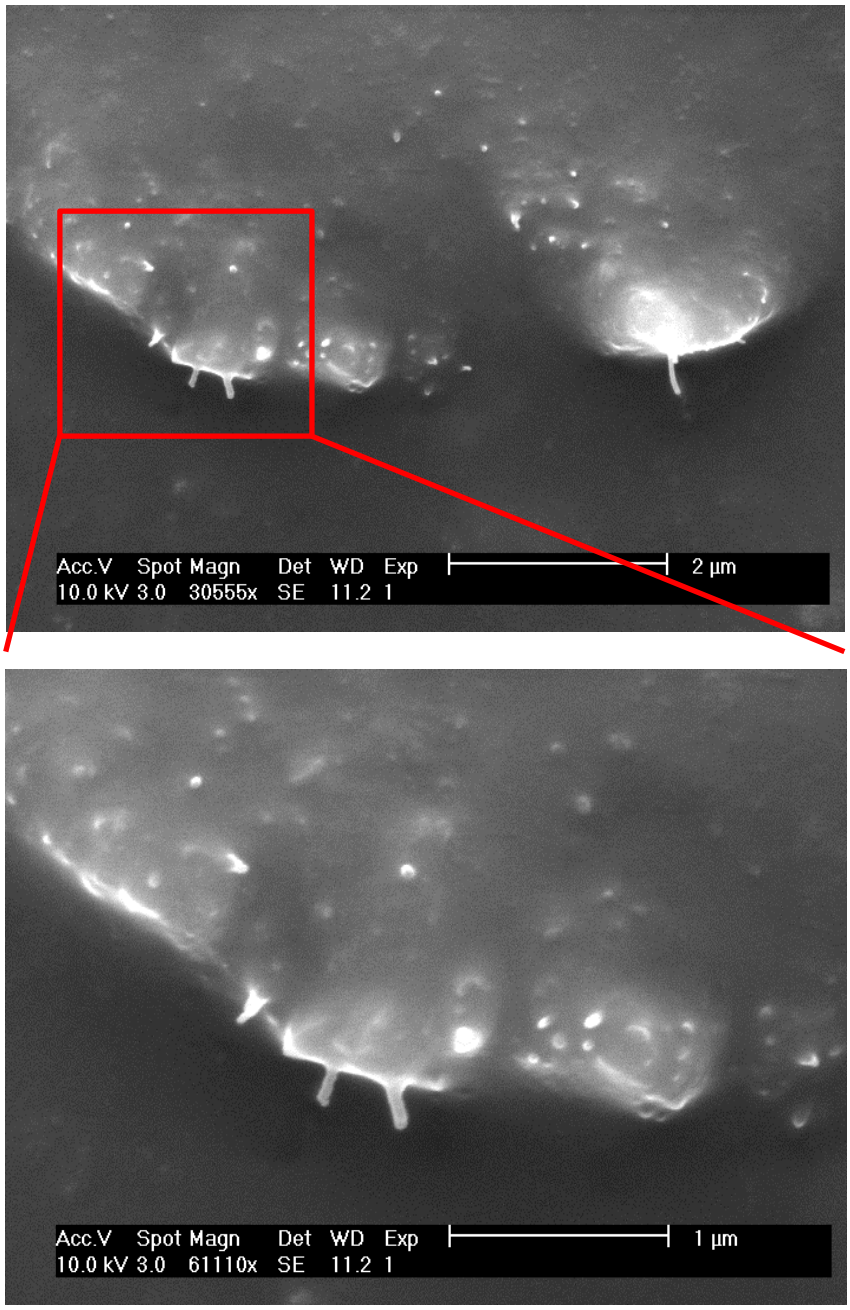

Fig. 2. 8. SEM images of nanocomposites with 0.3 wt. % MWNTs processed with acetone with 0.5-hr ultra-sonication treatment.

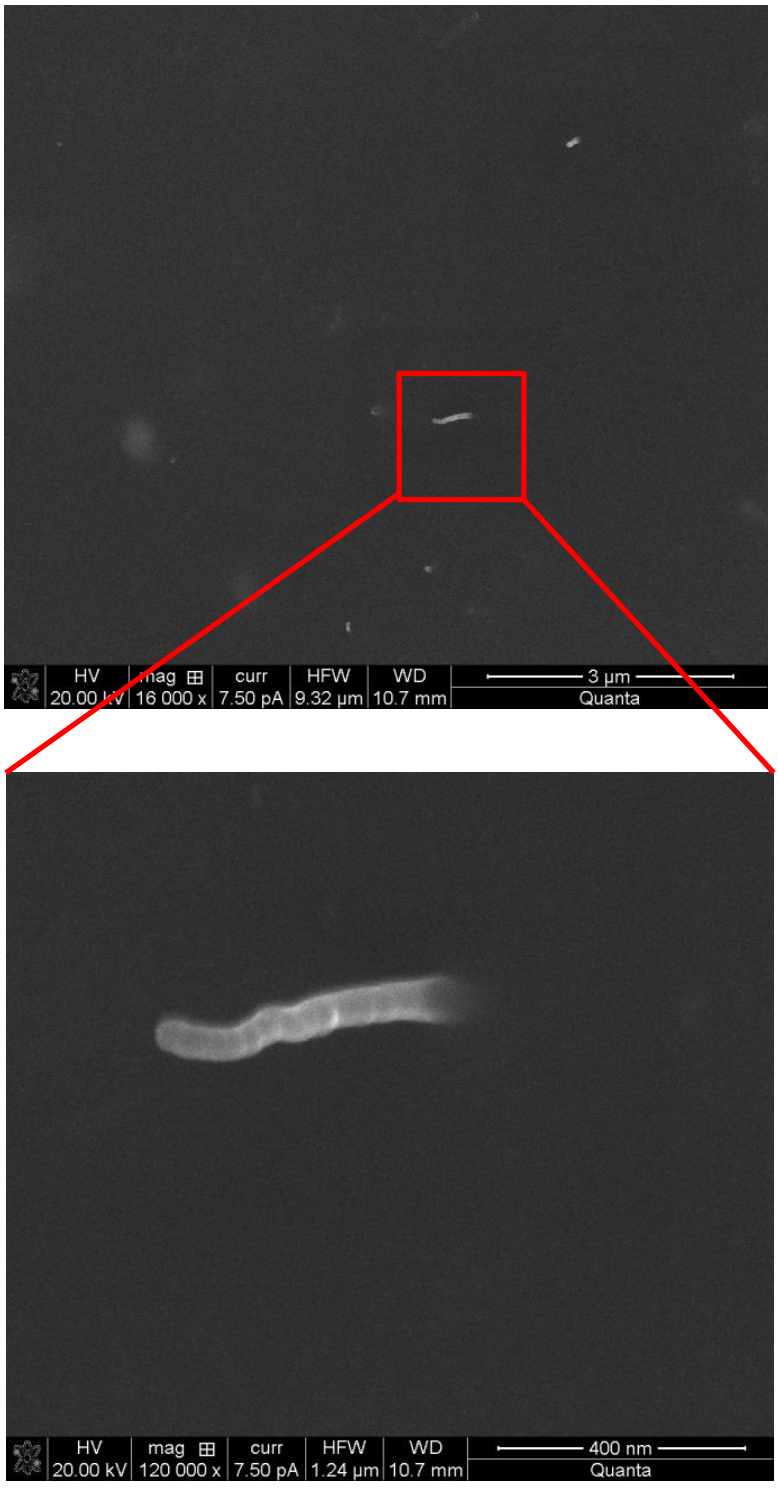

Fig. 2. 9. SEM images of nanocomposites with 0.3 wt. % MWNTs processed with acetone with 4.0-hr ultra-sonication treatment.

It is also shown that the loss modulus and loss factor are increased with the longer ultra-sonication. The 0.5-hr ultra-sonication increases the loss modulus up to 9 % while the 4.0-hr ultra-sonication increases the loss modulus by 40 %. Moreover, the 0.5-hr ultra-sonication increases the loss factor up to 15 % while the 4.0-hr ultra-sonication increases loss factor by 20-25 %. One possible reason behind this is related to the nature of bonding between DE matrix and MWNTs. Although improved dispersion enables the larger interaction area between DE matrix and MWNTs, the bonding between them is not strong enough. As a result, the energy due to the sliding and friction at the interfacial surface areas is dissipated under dynamic mechanical loadings. This phenomenon is not prominent for samples with 0.5-hr ultra-sonication as the existence of aggregates reduces the effective interaction surface areas between the elastomer matrix and MWNTs. However, the nanocomposites processed with 4.0-hr ultra-sonication show this trend as they have larger effective interaction surface areas enabled by improved MWNT dispersion. As a result, nanocomposites processed with 4.0-hr ultra-sonication shows larger loss modulus and loss factor.

In conclusion, ultra-sonication is proven to be an effective technique to help dispersion of MWNTs in elastomers as shown in SEM micrographs. Moreover, the introduction of ultra-sonication during the processing increases both storage, loss modulus and loss factor of nanocomposites under dynamic mechanical loadings, providing another clue for the improved dispersion of MWNTs in DE matrix.

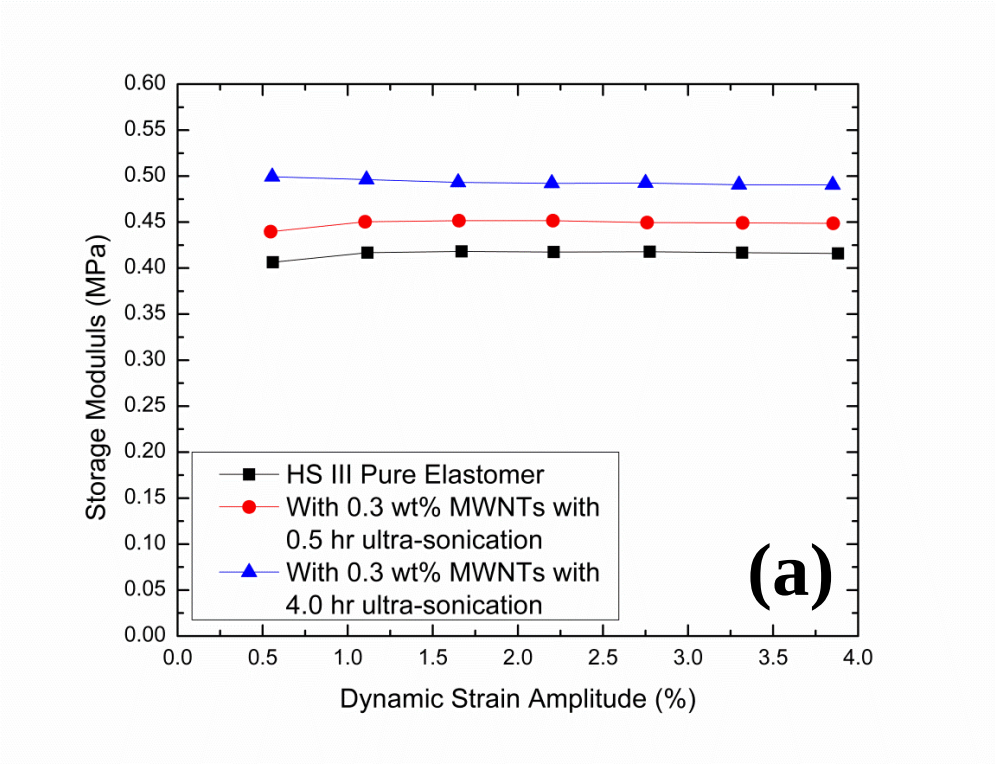
Storage Modululs (MPa)
Dynamic Strain Amplitude (%)
HS III Pure Elastomer
With 0.3 wt% MWNTs with 0.5 hr ultra-sonication
With 0.3 wt% MWNTs with 4.0 hr ultra-sonication
(a)

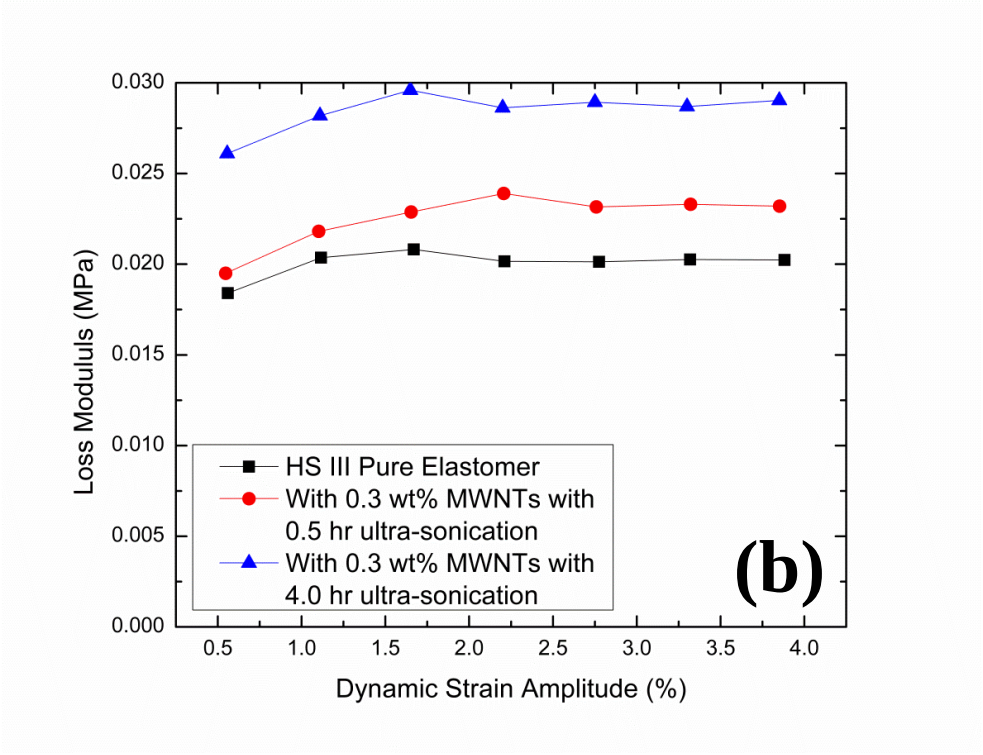
Loss Modululs (MPa)
Dynamic Strain Amplitude (%)
HS III Pure Elastomer
With 0.3 wt% MWNTs with 0.5 hr ultra-sonication
With 0.3 wt% MWNTs with 4.0 hr ultra-sonication
(b)

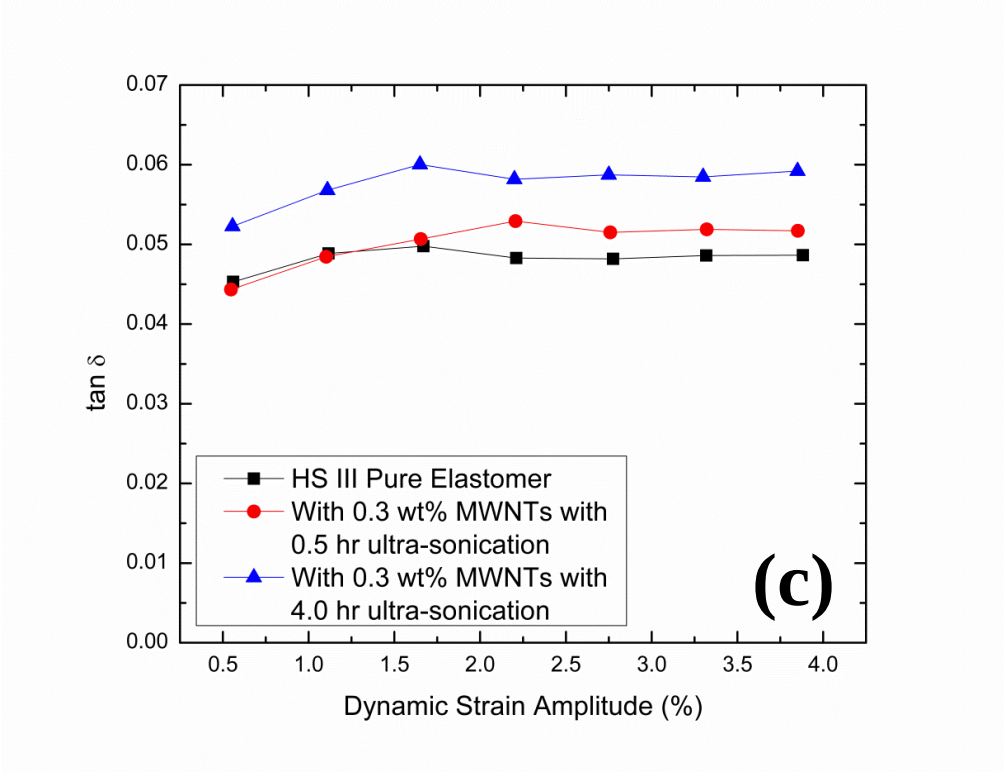

Fig. 2. 10. Dynamic strain sweeps of DE nanocomposites filled with 0.3 wt. % MWNTs processed with acetone and ultra-sonication (a) Storage moduli and (b) loss moduli and (c) loss factors under compression loading. The test frequency is 10 Hz.

2.3.3 Damages to MWNTs Caused by Ultra-sonication

Although Fig. 2.9 demonstrates that the acetone and 4.0-hr ultra-sonication during the processing successfully minimizes the number and size of MWNT aggregates, it does not mean longer ultra-sonication can further improve the dispersion of MWNTs. The next section discusses the damages to MWNTs by ultra-sonication during the material processing.

Although ultra-sonication significantly improves the dispersion of MWNTs in matrix, the damages are caused to MWNTs [95-99] because of the energy introduced by ultra-sonication. It is reported that the aspect ratio strongly depends on the material processing, and 420, 80 and 8 are reported as MWNT average aspect ratio under different treatments even for the same type of MWNTs [98].

In this study, SEM and TEM are utilized to investigate the aspect ratio of MWNTs after the processing. Fig. 2.11 shows the pristine MWNTs before the materials processing. According to specifications provided by CheapTubes.com, the diameter of MWNTs is 20-30 nm, and the length is 10-30 μm.

Fig. 2.12 shows 3 typical images obtained from TEM. Based on images obtained from TEM, the typical length of MWNTs ranges from 400 nm to 1 μm, which is shorter than the pristine MWNTs before the processing. The reasoning behind is associated with the lengthy time of ultra-sonication. The ultra-sonication is carried out at 130 Watts, 20 kHz. For nanocomposites with MWNTs, 4.0-hr ultra-sonication is applied in order to achieve the uniform distribution.

In conclusion, it is demonstrated the ultra-sonication technique successfully improves the dispersion of MWNTs in matrix. However, the aspect ratio (length/diameter) is shortened due to the energy introduced to MWNTs during the processing. The average aspect ratio of MWNTs after processing with acetone and 4.0-hr ultra-sonication is reduced to 20.

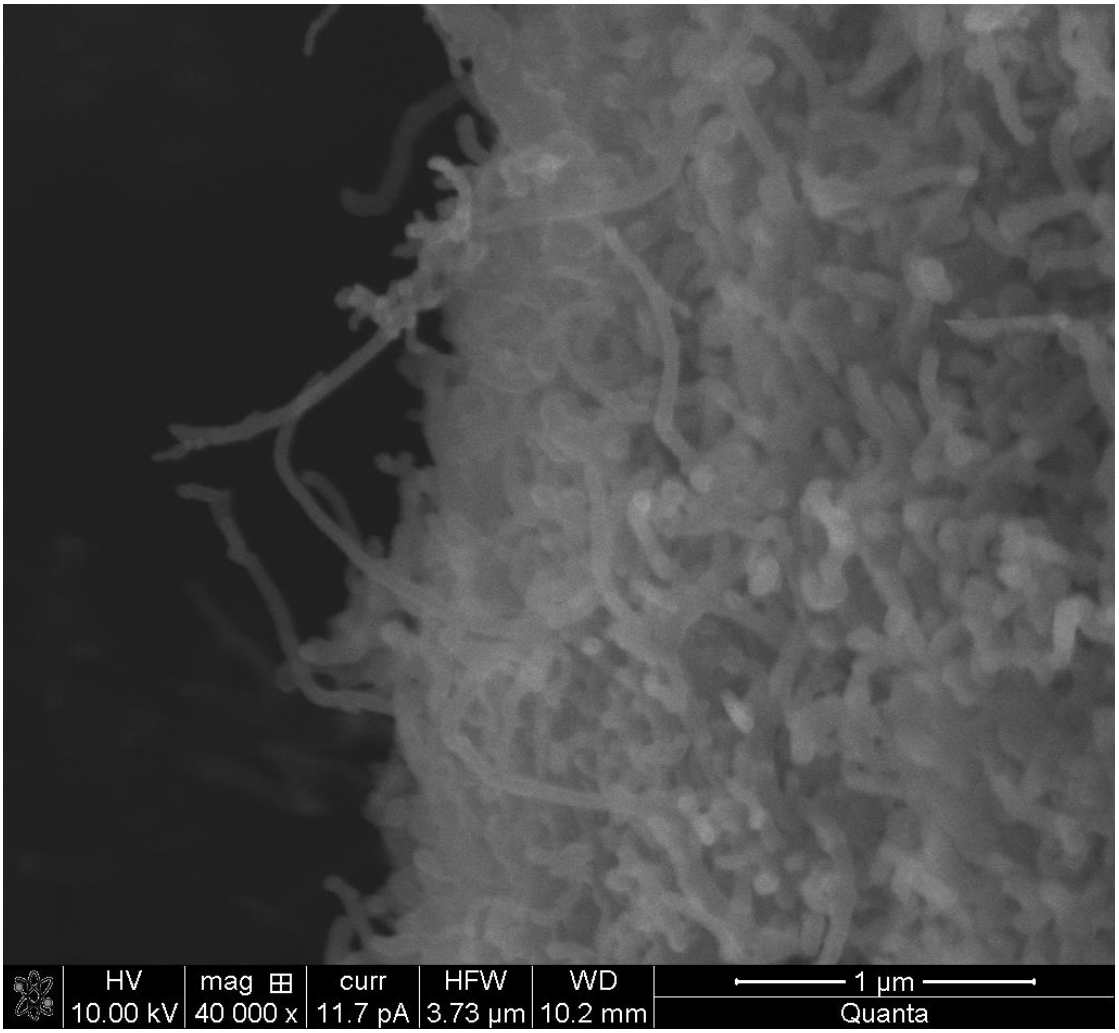

Fig. 2. 11. SEM micrograph of pristine MWNTs before the processing.

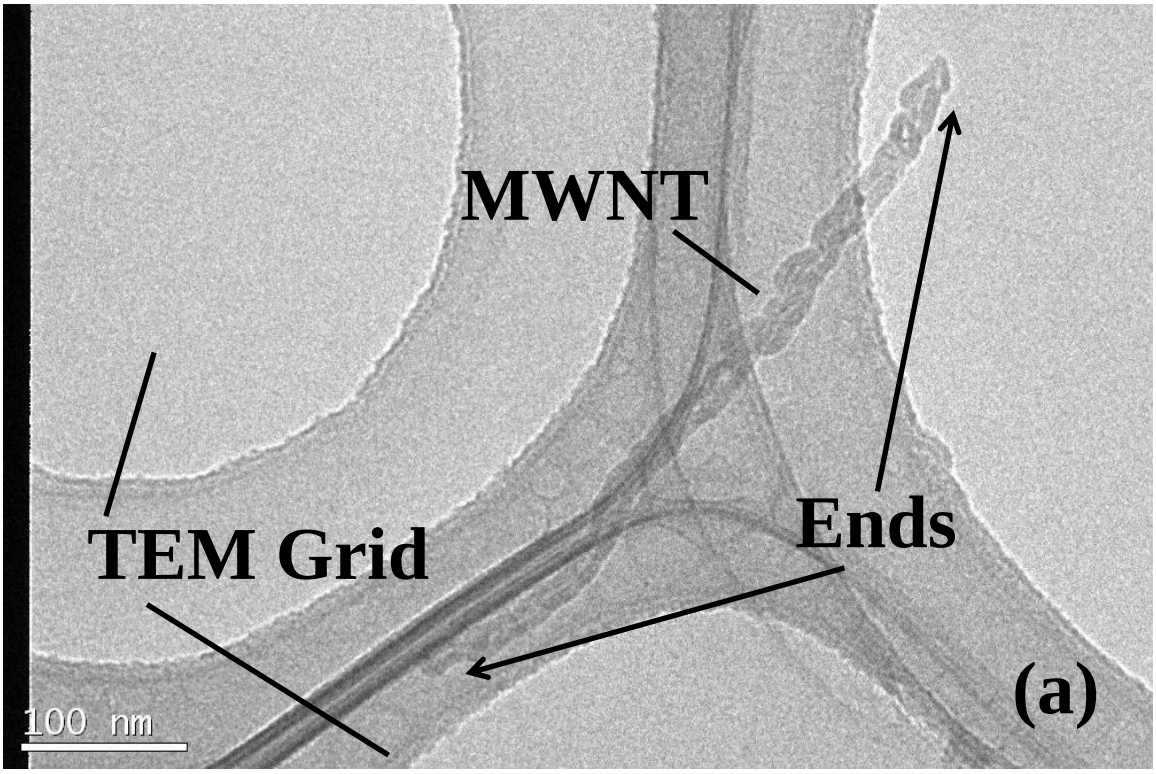
MWNT
TEM Grid
Ends
100 nm
(a)

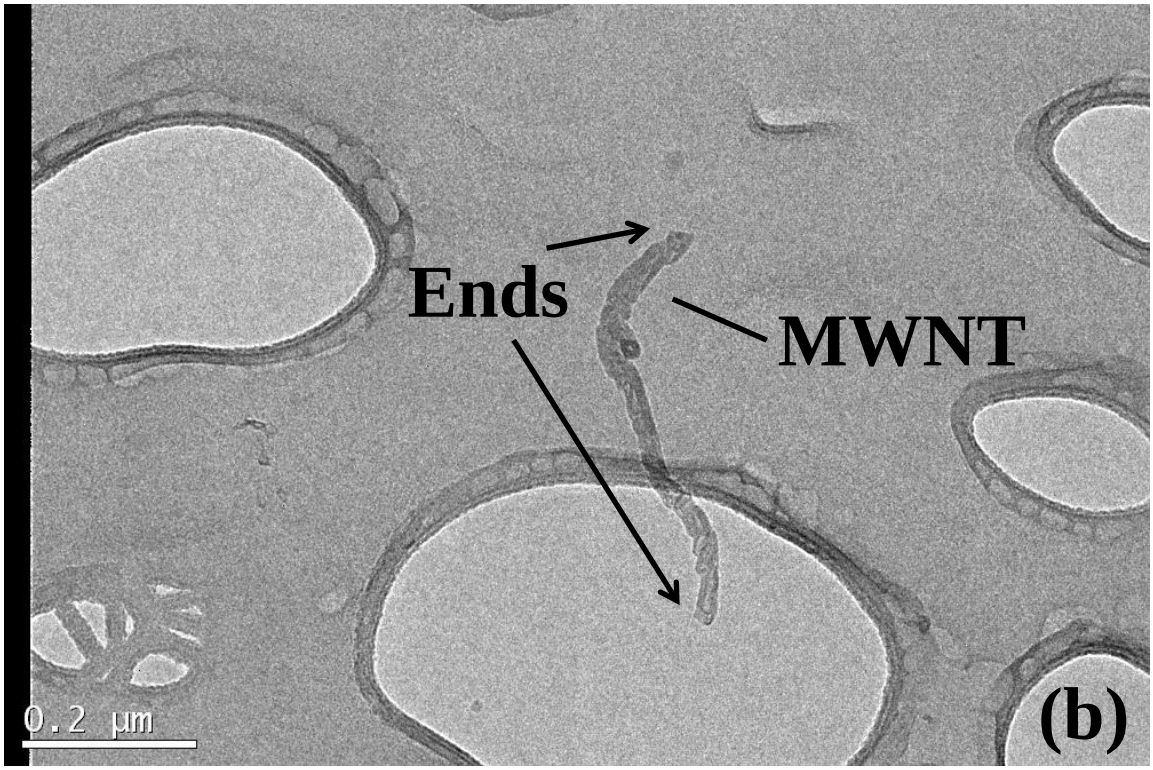
Ends
MWNT
0.2 µm
(b)

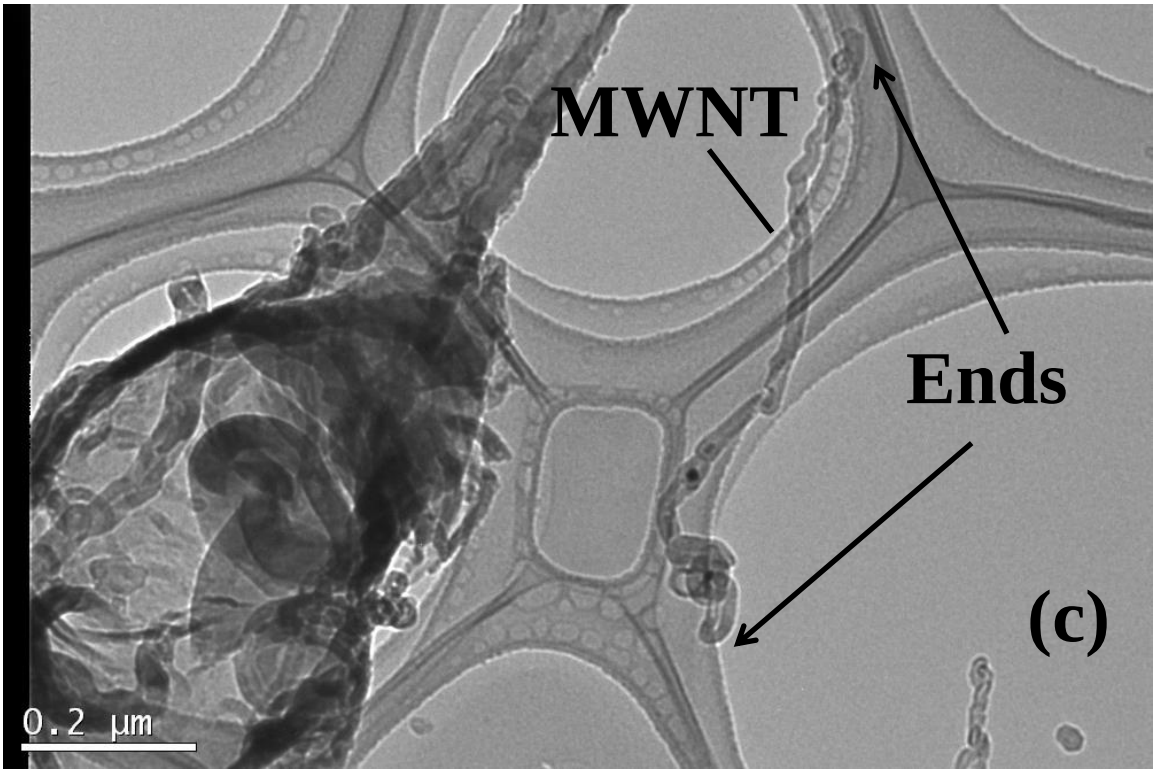

Fig. 2. 12. TEM images of MWNTs processed with acetone and 4.0-hr ultra-sonication treatment. (a), (b) and (c) show different MWNTs.

2.4Conclusions

Acetone and ultra-sonication are demonstrated to be an effective approach to disperse MWNTs in elastomer matrix. Acetone reduces the size of the aggregates, and also reduces the viscosity of elastomer, resulting in improved mixing of elastomer and MWNTs. Ultra-sonication further improves the dispersion of MWNTs by adding energy to break the van der Waals force between each MWNT. The shortcoming of ultra-sonication is the damages to MWNTs as mentioned earlier, resulting in shortened aspect ratio [96, 97].

Higher load transfer and larger energy dissipation are observed from the nanocomposites with MWNTs as a result of improved MWNTs in elastomers. Dynamic mechanical properties of polymer/CNTs composites have been proven to be closely correlated with the dispersion of CNTs. The increase of the storage modulus is associated with the MWNT dispersion improvement. As the dispersion improves, more elastomer-MWNT interaction is enabled. As a result, more dynamic loading can be carried due to the extended interfacial area between elastomer and MWNTs.

The loss modulus and loss factor are associated with the strength of the bonding between elastomer and MWNTs. As the dispersion improves, more elastomer-MWNT interaction is enabled. Although interfacial area between elastomer and pristine MWNTs increases, the bonding is unchanged by acetone or ultra-sonication after acetone evaporates. As a result, the friction is generated at the weak bonding sites when dynamic mechanical loading is applied.

In conclusion, ultra-sonication processing with acetone improves the dispersion of MWNTs in elastomers. All the nanocomposites filled with MWNTs tested in the later chapters are fabricated using the approach described in this chapter. Acetone along with 4.0-hr ultra-sonication is utilized for all DE nanocomposites filled with MWNTs.

Chapter 3 Experimental Study in Electromechanical Responses of Dielectric Elastomer Nanocomposite filled with Carbon Nanotubes.

3.1Introduction

An actuator is a mechanical device which controls the system or detects the system change. Dielectric elastomers (elastic+polymers) (DEs) are an emerging field of electro-active polymer (EAP) materials attracting attention in the field of actuators in the last 10 years [1, 22, 23] due to its softness, flexibility and the ability to convert electrical energy to mechanical energy and vice versa. Pelrine *et al*, first developed a model to describe the behavior of silicone based dielectric elastomers [22, 23, 25] and seek the possibility to use dielectric elastomers as actuators. They numerically showed "Maxwell stress", and correlated it to the electromechanical response of the dielectric elastomer materials. The detail is shown in literature [100]. An electromechanical response is the physical response of a mechanical system to electrical stimulation.

Soft elastomers, mostly silicone elastomers and acrylic elastomers are potential candidates as dielectric elastomers in electro-active polymer actuator technology. A comparison between these 2 types of elastomers were conducted by Michel [37], and it was revealed that the response time of silicone based elastomers are much faster than that of acrylic elastomers due to the viscosity of the materials. Moreover, the electromechanical response of silicone elastomers is time and history independent, while that of acrylic elastomers are strongly time and history dependent. In this study, silicone dielectric elastomers are to be used for analysis of electromechanical properties.

Fillers are extensively utilized to enhance the specific polymer materials properties [44]. We aim to develop a new generation of DEs by incorporating MWNTs to the DEs as fillers. In order to enhance the electromechanical response of DE nanocomposites, MWNTs are introduced as fillers to DEs. The idea comes from that only a small amount of CNTs, conductive fillers, can drastically increase the dielectric constant [66-68] without changing the elastic modulus much [68]. Higher dielectric constant of nanocomposites brings more charges on the electrodes, resulting in larger deformation under the application of the electric fields.

There are candidate conductive fillers which can enhance the dielectric property of nanocomposite when the concentration is close to the electrical percolation threshold as shown in Fig. 3. 1. Lower percolation threshold means lower concentration is required to achieve the substantial dielectric property enhancement for the nanocomposites. Although, the elastic modulus varies from a material to another, concentration of the fillers is one of the primary factors deciding the stiffness of the nanocomposites.

It is known that MWNTs in a polymer matrix can increase the dielectric constant, especially, around the electrical percolation threshold [53, 66]. Charge accumulation occurs at the interface of two materials with different charge carrier relaxation time (Maxwell-Wagner effect) [101, 102]. In this study, there are two materials, DE matrix and MWNTs. Under applied electric fields, the charges in conducting fillers move inside the fillers, imparting to them a dipole moment; hence the aspect ratio of fillers is closely related to the dielectric constant of nanocomposites as a dipole moment depends on the distance between the unlike charges. Furthermore, when the concentration of conductive fillers is smaller than the percolation threshold, more “micro capacitors” are formed with the increase of the concentration, leading to enhanced dielectric constant of nanocomposites [66, 103, 104]. The “micro capacitors” are assumed to be formed by

MWNTs separated by DE matrix as the insulating medium, thus the number of capacitors is closely related to the dispersion of MWNTs inside DE matrix. The similar dielectric constant enhancement was also observed for epoxy resin or polydimethylsiloxane filled with conductive fillers/carbon black [102, 105], graphite powders [106], onion-like carbon [107] and metals [108]. However, the high aspect ratio of MWNTs leads to lower percolation threshold, resulting in the more efficient dielectric property enhancement.

We demonstrate that, with addition of MWNTs, the nanocomposites show improved deforming properties. An integrated research plan is proposed to study the synthesis, characterization, modeling and simulation in order to understand the deforming mechanisms of DE nanocomposites.

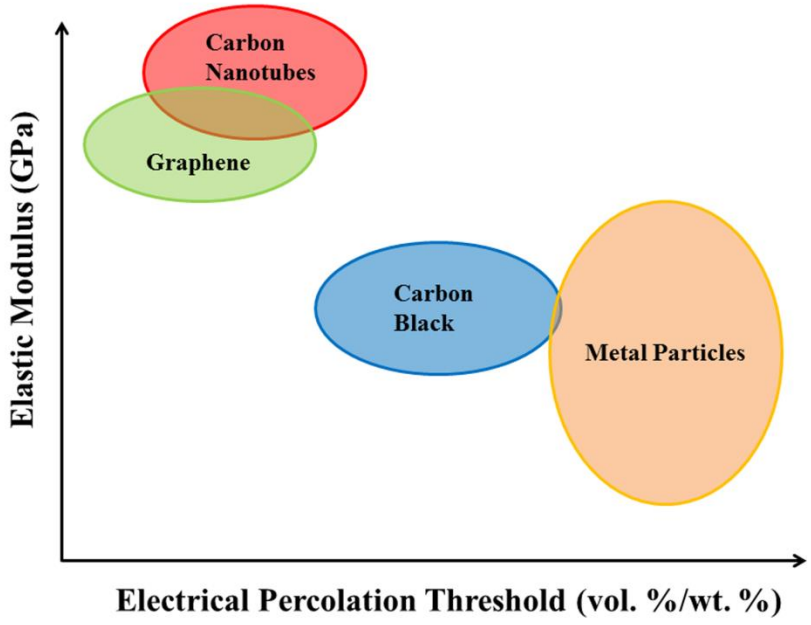

Fig. 3. 1. Potential fillers which can enhance the electromechanical response of DEs.

In most of the previous studies, DE actuation is characterized by the area changes using digital cameras or CCD (charge-coupled device) cameras [17, 22, 38, 43, 55, 59, 64, 109-117]. Based on the area change, the strain in the thickness direction is calculated. Although the area measurement by cameras is a simple and easy approach to indirectly detect the electromechanical response of materials, it could lose its accuracy especially when the material deformation becomes larger due to the limited depth of field of the camera. In addition, the electromechanical detection by cameras is based on the incompressibility assumption, thus it is not a direct approach to measure the electromechanical response.

Very little attention has been paid so far to direct measurement of the electromechanical response of the nanocomposite materials based on the thickness strain measurement [118]. However, laser Doppler vibrometry system turns out to be a very accurate way to measure the surface displacement, and even hundreds of nanometer displacement can be detected.

In this study, laser Doppler vibrometry technique is employed to directly characterize the electromechanical properties of the DEs and DE nanocomposites filled with MWNTs.

3.2 Materials, Fabrication, Characterization and Electromechanical Measurement

Dielectric elastomer nanocomposites filled with MWNTs are fabricated using the steps described in the previous chapter. The thickness of the films is controlled to be about $150\,\mu m$ by adjusting the rotation speed of the spin coater.

Micro System Analyzer (Polytech MSA 500) is used to obtain the surface displacement of top and bottom surfaces with compliant electrodes in addition to optical images of the surface area change when subjected to applied electric field. Although Micro System Analyzer can provide the optical images, it is not accurate to measure the area change under materials deformation due to the depth of field of the lens. Depth of field is defined as the vertical distance in the specimen, measured from above and the below the exact plane of focus, which still yields an acceptable image [119]. The depth of field for optical lens 2X, 10X, and 20X by Mitutoyo are $\pm 91\,\mu m$, ± 3.5 and $\pm 1.6\,\mu m$ [119]. 10X and 20X optical lenses can easily lose the focus when larger deformation is introduced. Thus, measurement by optical lens could mislead the displacement results. As a result, measurement without the depth of field issue needs to be addressed. Laser Doppler vibrometry function of Micro System Analyzer is one of the best options to accurately capture the electromechanical response of the materials even under large deformation as the system is using the laser to detect the frequency change due to the samples surface motion (Doppler Effect). Doppler Effect refers to a change in frequency of a propagating wave caused by a relative movement between the source and the receiver. This principle could be applied to the frequency change of the laser. The displacement/velocity decoders detect the frequency change between the frequency of the incoming laser wave and the reflected laser wave. Then vibrometer calculates the displacement based on the detected surface motion velocity.

The laser Doppler vibrometer setup is described in Fig. 3.2. DE and DE nanocomposite specimens are connected to Matsusada AU-10P30-LC power supplier. Electric fields are applied in 4 cases shown in Fig. 3.3 to investigate how each case affects the displacement.

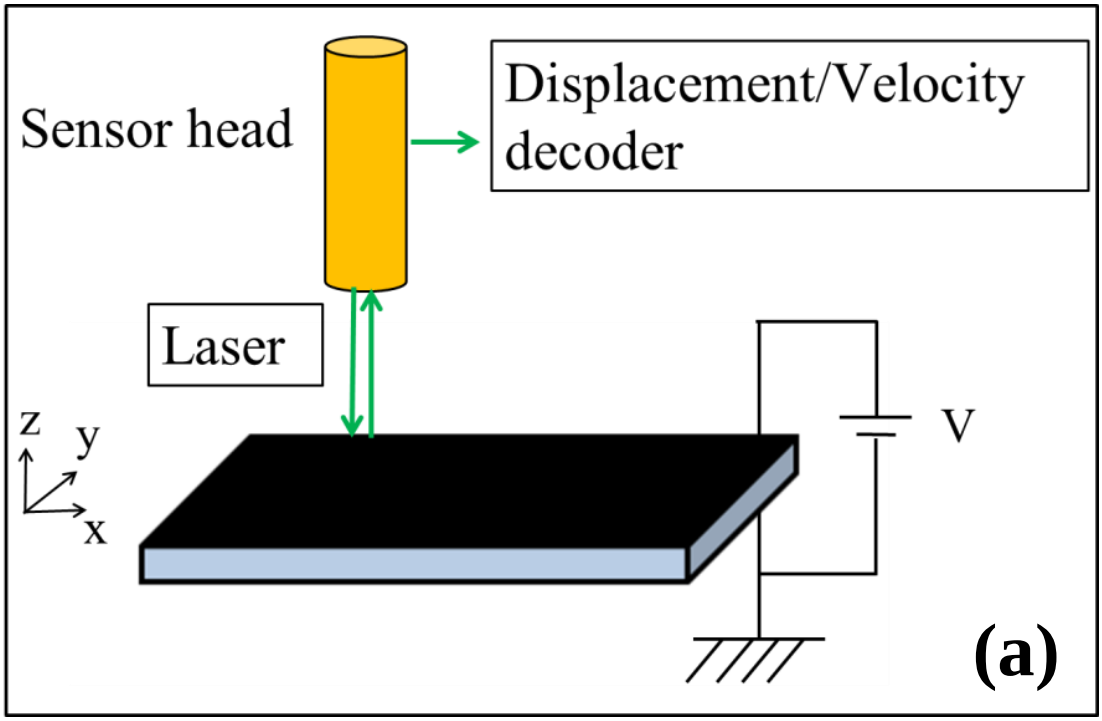

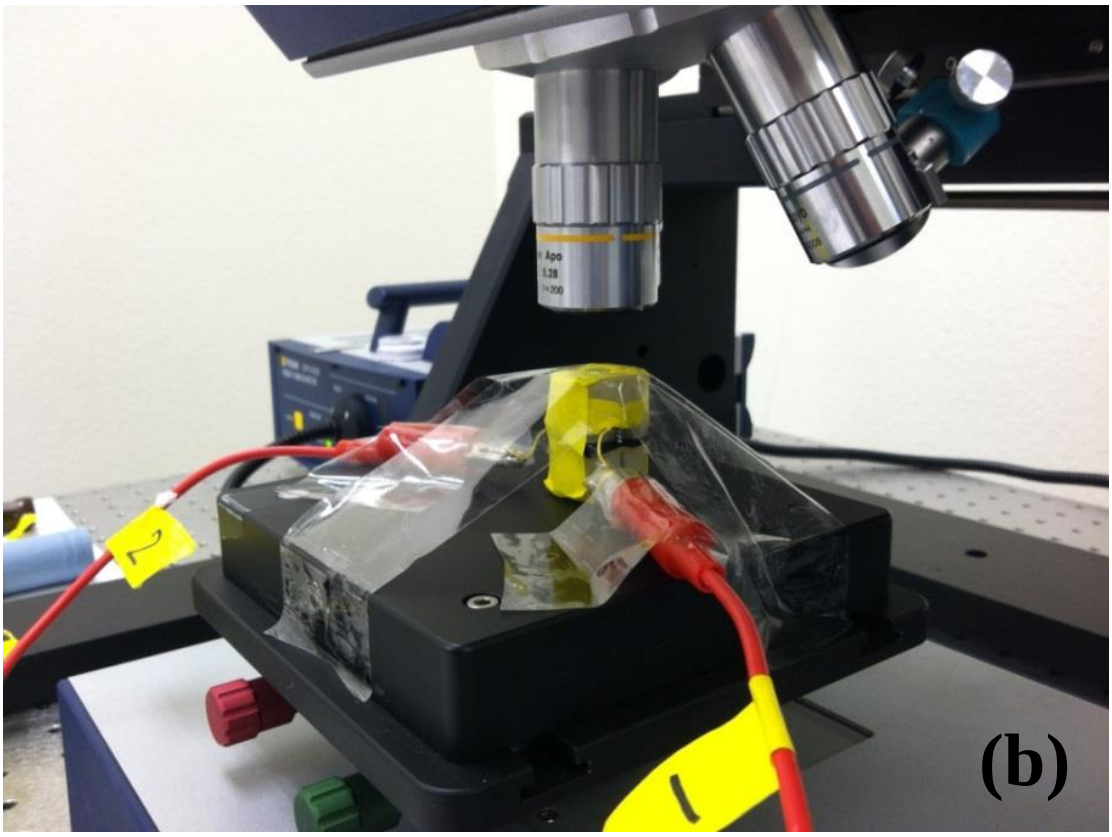

Fig. 3. 2. (a) The principle of and (b) set up of laser Doppler vibrometer.

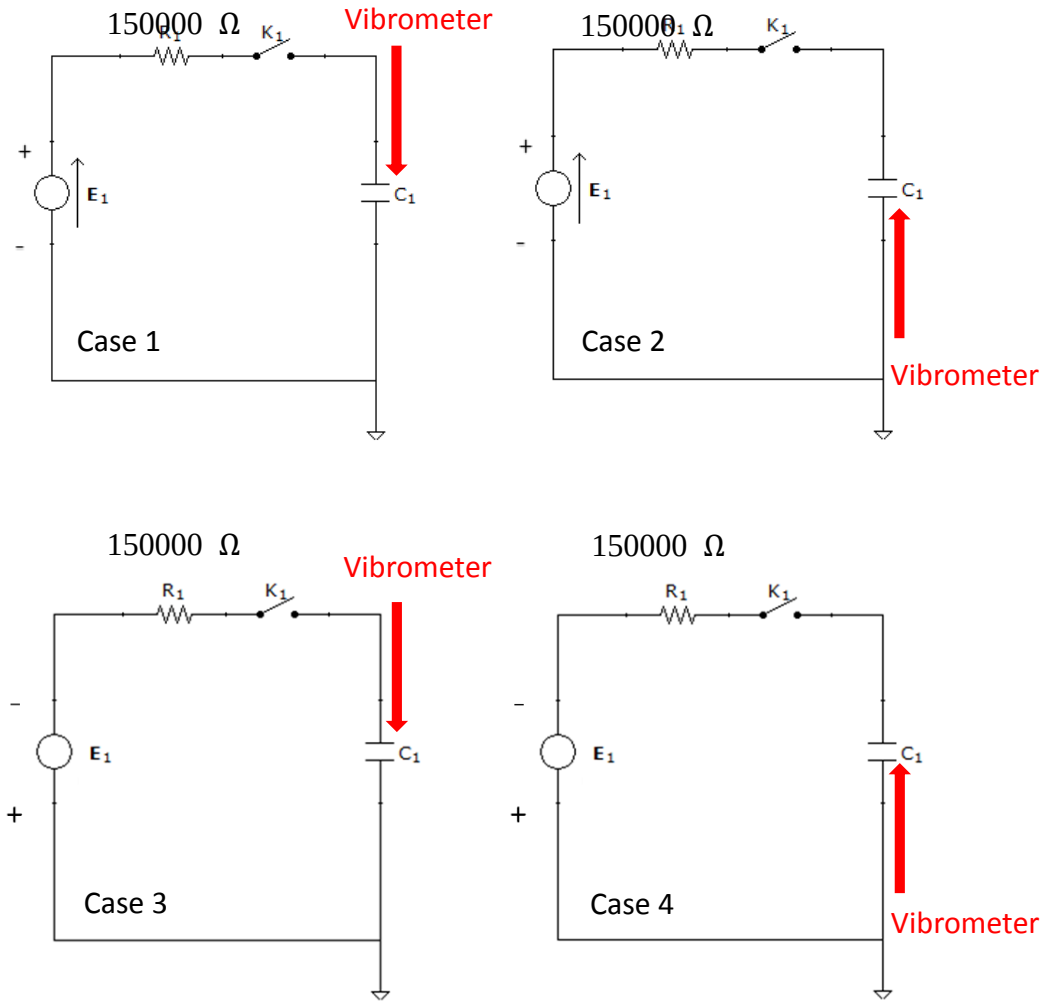

Fig. 3. 3. Loading cases of applied electric fields and laser Doppler vibrometer setup.

3.3 Results and Discussion

3.3.1 Selection of Electrodes

The selection of the electrode materials is an area of ongoing research. Compliant electrodes are key factor to the development of EAP technology as they maintain the uniform contact over the entire active region of the elastomer [1]. The requirements for the compliant electrodes are: (1) capable of large deformation without restricting dielectric elastomer performance, and (2) not losing the conductivity and contact with elastomers even under mechanical loading. A number of potential materials are proposed for compliant electrodes including carbon black, carbon nanotubes [64, 120], grease electrodes [22], rubber electrodes, dust electrodes, and glue electrodes [1].

Elastomer electrodes with MWNTs are tested in this study. In order to ensure the conductivity, 2 wt. % MWNTs are introduced. However, the primary drawbacks are that thickness cannot be controlled well, and uniform coverage is a challenging issue. As seen in Fig. 3.4, the cured elastomer electrodes are uneven compared to the dielectric elastomer film. This is because the higher viscosity of elastomer with more than 2 wt. % MWNT prevents the uniform spreading on spin coater even before curing. The network formed by MWNTs prevents the flow of the elastomers even during the spin coating process. Thus, the random thickness can be easily observed from Fig. 3.5. In addition, conductive elastomer with MWNTs have MWNT concentration more than 2 wt. % at which the electrodes are not as compliant as the dielectric elastomer any more, resulting in the restriction of DE deformation.

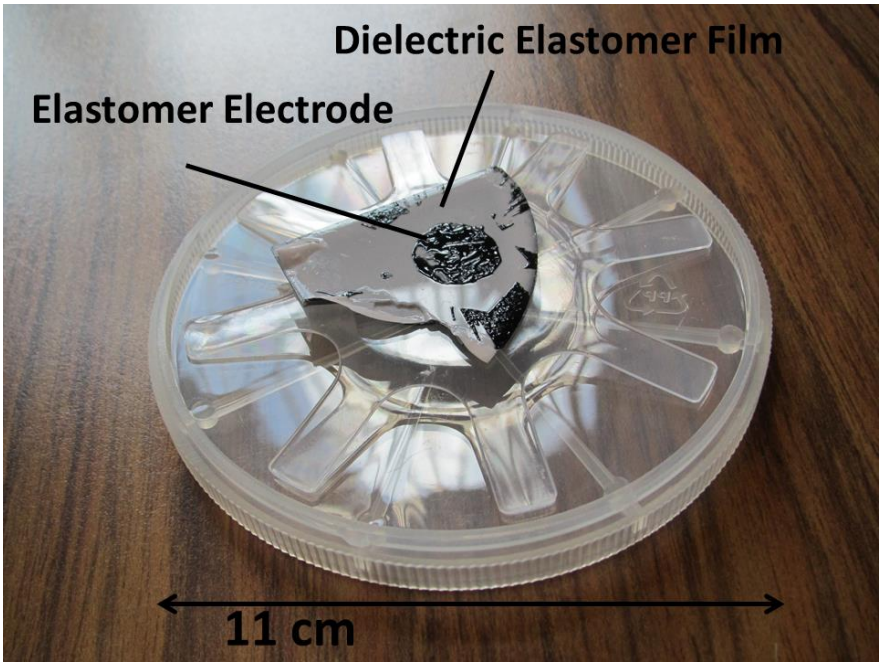

Fig. 3. 4. Elastomer electrodes coated on dielectric elastomer after spin coating.

In this study, a mixture of silicone-polymer-based graphite grease and carbon-filled silicone is used as proposed by Pelrine [22].

Carbon conductive grease from MG Chemicals, and RTV 60-CON adhesive sealant from Stockwell are utilized as compliant electrode materials. These two raw materials are mixed 1:1 by weight, and then mixed with acetone followed by ultra-sonication for 1 minute. Then, the mixture is air-brushed on the surface of the DEs using MASTER airbrush S68 with TC-828 twin tank compressor at 400 kPa. Once acetone evaporates, the electrodes are well attached to the DE surfaces.

Both sides of the film are coated with the compliant electrodes as shown in Fig. 3.5. The center of the dielectric elastomer film is sandwiched by electrodes on both surfaces. The diameter of the compliant electrodes is 2.38 mm. Fig. 3.6 shows the thickness measurement of the compliant

electrodes by HS200 Confocal Microscope/Profiler. The typical thickness of the complaint electrodes is about $20\,\mu\text{m}$, and the thickness is consistent at locations far away from the edges. Fig. 3.6 (b) shows the center of the electrode. From Fig. 3.6 (b), some locally uneven locations are found. However, the maximum surface height change is about 4.0 μm within $174\mu\text{m}\times139\mu\text{m}$ area as shown in Fig. 3.6 (b), which is within the thickness fluctuation observed in Fig. 3.6 (a) left side of the white line. In addition, the diameter of laser spot used in the measurement is $3\text{-}10\,\mu\text{m}$. As a result, the surface roughness within the laser spot is negligible. Thus, it is concluded that the carbon conductive grease from MG Chemicals, and RTV 60-CON adhesive sealant from Stockwell provides more uniform electrodes than the elastomer electrodes whose rough surface is visible.

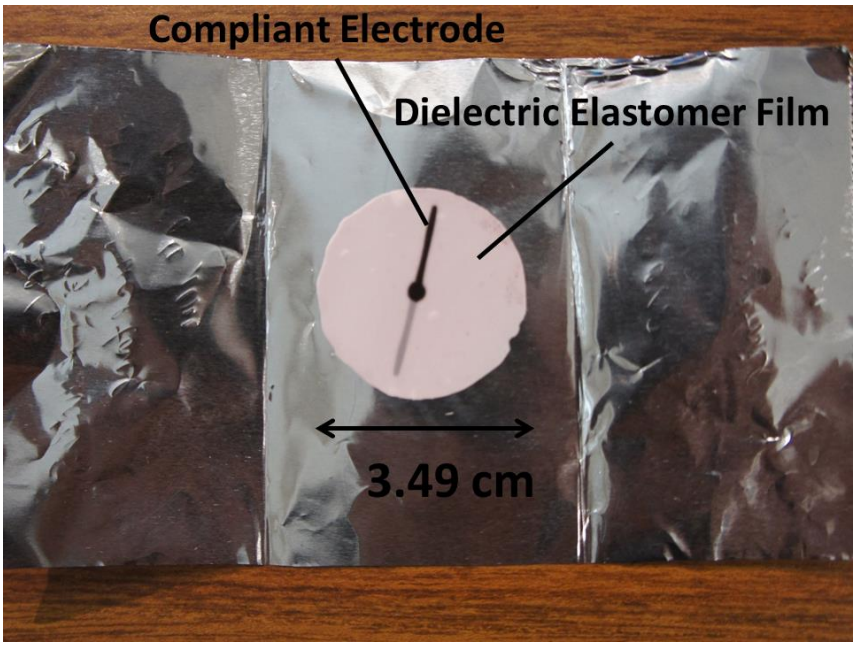

Fig. 3. 5. Fabricated DE film specimen coated with compliant electrodes.

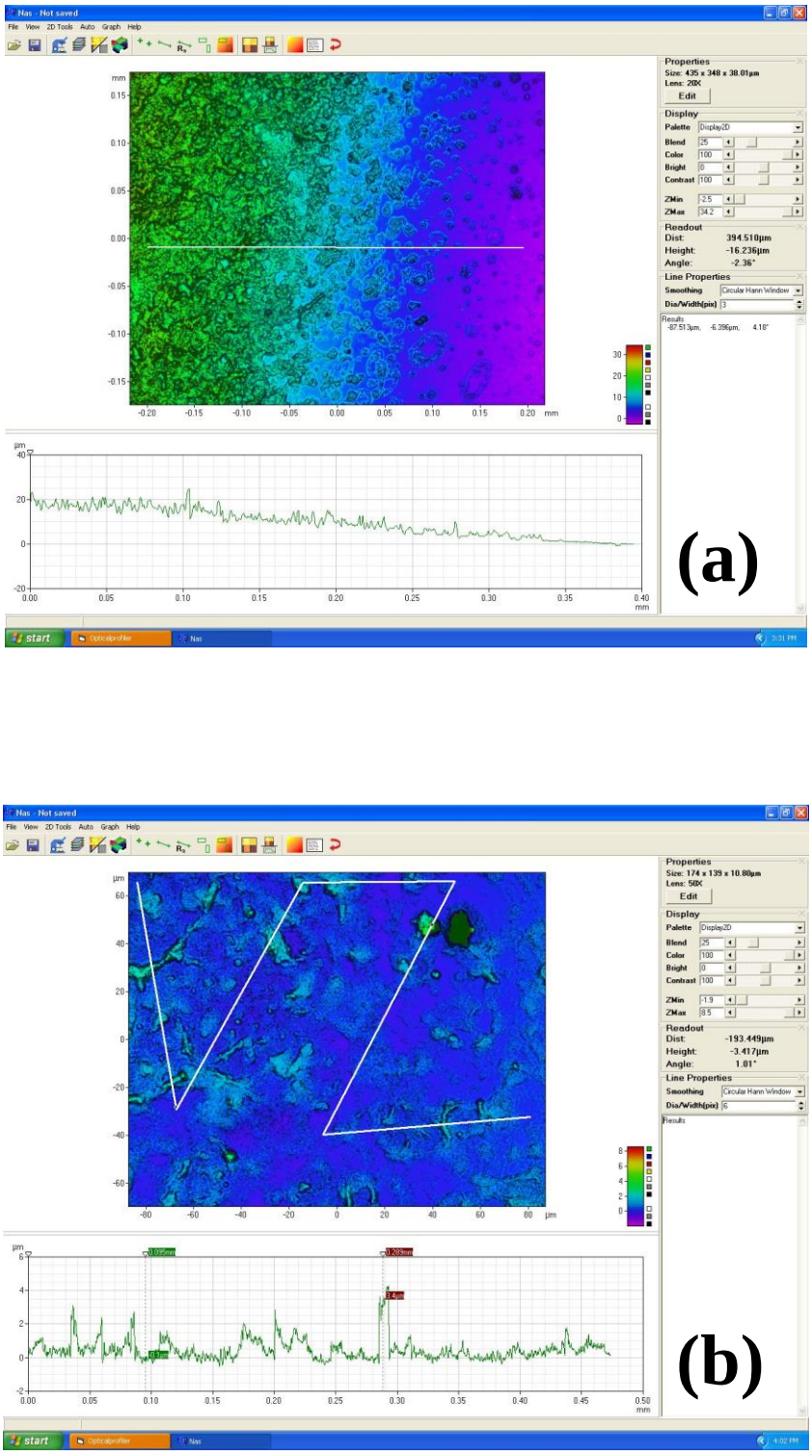

Fig. 3. 6. Thickness measurement of compliant electrodes air brushed on the dielectric elastomers by HS200 Confocal Microscope/Profiler.

Atomic Force Microscopy technique is also used to characterize the top surface of nanocomposites and electrode surfaces. It is utilized to make sure that the displacement results obtained by vibrometer are not affected by the roughness of the surfaces.

Within $75\mu m \times 75\mu m$ area of the electrode surface in Fig. 3.7 (a), the maximum height difference is $1.195\mu m$ with the average roughness is $117.3\ nm$. For pure elastomers, the surface roughness is very similar. This indicates the spin coating technique could fabricate the thin films of elastomer materials without creating the large variation in thickness enough to affect the displacement measurement. In addition, the surface of the electrodes is also examined. Within $115\mu m \times 115\mu m$ area of the nanocomposite surface in Fig. 3.7 (b), the maximum height difference is $2.62\mu m$ with the average roughness is $176.7\ nm$. This indicates that the displacement measurement could potentially affect the measured displacement, but the effect is very limited especially the displacement measurement is carried out at high electric field. In order to minimize the roughness effects, at least 5 random points are picked up for displacement measurement by laser Doppler vibrometer.

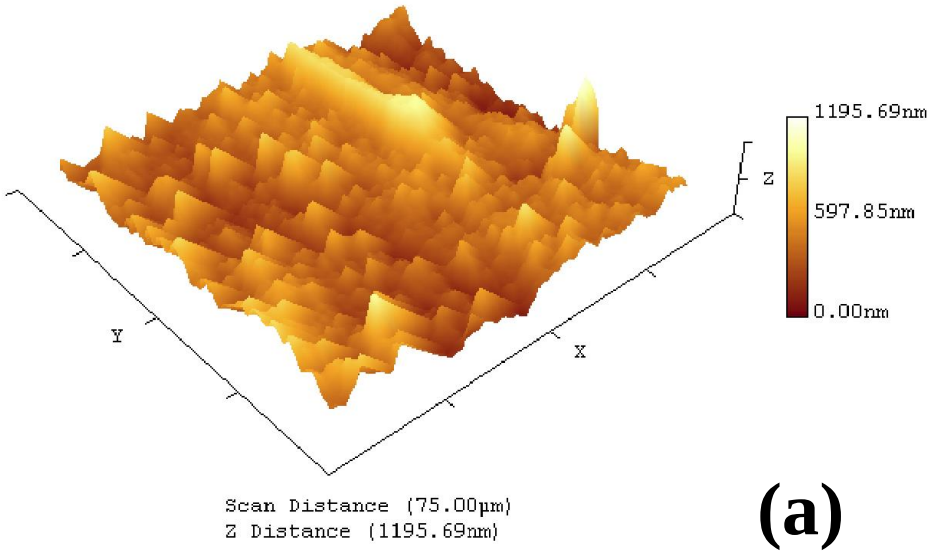

(a)

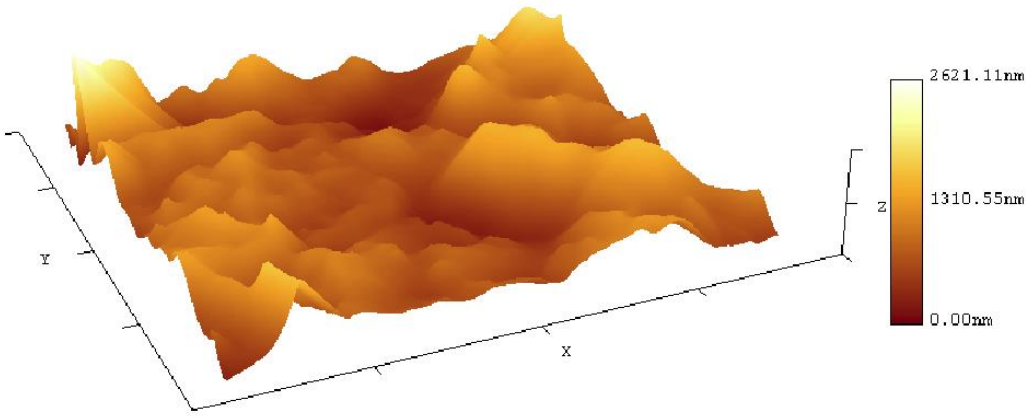

(b)

Fig. 3. 7. Surface roughness measurement of compliant electrodes by atomic force microscopy. (a) $75\mu m \times 75\mu m$ and (b) $115\mu m \times 115\mu m$ area.

3.3.2 Comparison Between the Ideal Maxwell Stress and Deformation by the Films

Ideal Maxwell stress proposed by Pelrine [22] is calculated to compare with the gravity effect on the deflection of the thin film [118]. The Maxwell stress is described as

$$p = \varepsilon\varepsilon_0 E^2 = 2.48\times10^{-11}\times E^2 (\text{Pa})$$

When $E = 10(\text{V/}\mu\text{m})$, then $p = \varepsilon\varepsilon_0 E^2 = 2.48\times10^{3}(\text{Pa})$. As a result, the force between the two electrodes can be calculated by multiplying the electrode area, and

$$2.48\times10^{3}\times\pi\times(2.38\times10^{-3}\div2)^2 = 110.4\times10^{-4}(\text{N})$$

On the other hand, the gravity applied to the DEs with compliant electrodes can be described as

$$1160\times\pi\times(2.38\times10^{-3}\div2)^2\times9.81 = 7.59\times10^{-6}(\text{N}) \ll 110.4\times10^{-4}(\text{N})$$

This simple calculation demonstrates the displacement measured by the vibrometer is mainly caused by the electromechanical stress instead of the gravity effect. For higher electrical field, the electromechanical stress is more dominant, thus, it can be concluded that the deflection due to the gravity has little effect on the measured electromechanical response. Thus, the addition of the measured displacement on both sides of the film can directly provide the strain in thickness direction.

3.3.3 The Displacement Measurement by Vibrometer

As mentioned in the previous chapter, the surface displacement of the DEs and DE nanocomposites is measured by vibrometer. The typical displacement measurement is shown in Fig. 3.8. It is shown that the HS III DEs immediately reach the relaxed state once the electric field is applied. As the relaxation process takes place momentarily under static case with constant applied voltage, viscoelasticity is not considered in this case. Thus the difference between the initial position and the final position of the surface is calculated and determined to be the surface displacement.

In addition, the surface returns back to the initial location once the applied electric field is removed. This demonstrates that the electromechanical response of HS III DEs induced by the applied electric field does not leave any residue strain, thus the each displacement measured is primarily due to the electromechanical response of DEs.

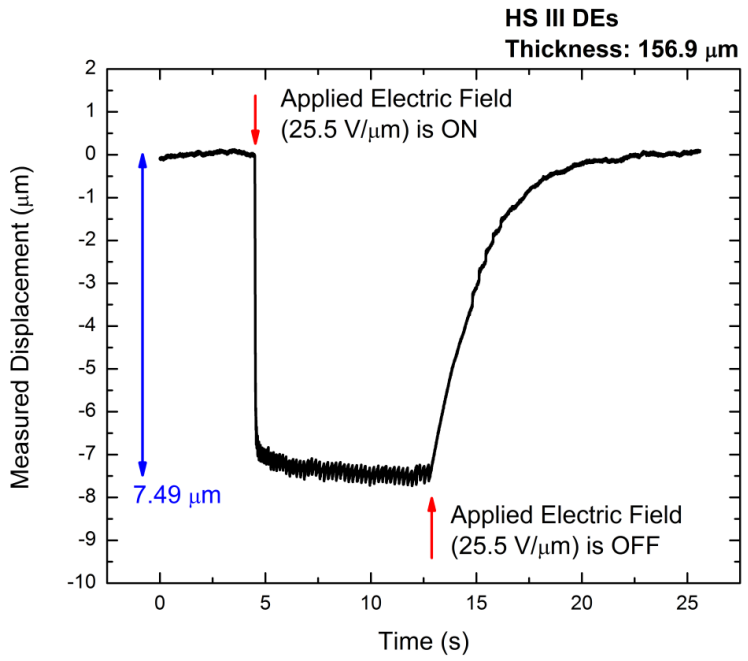

Fig. 3. 8. Displacement measurement of DE film specimen by laser Doppler vibrometer.

3.3.4 Boundary Conditions in Experiments and Thickness Strain

Boundary conditions are significant factors affecting the measured electromechanical response of the materials. In order to avoid the boundary condition effect, small tension is applied to place the DE thin films between 2 cylinder-shaped plastics as shown in Fig. 3.2 (b). In order to examine the validity of this method, a several measurements are performed.

Small tension is applied to the film specimens [118] to make the film flat enough to avoid the potential deflection due to the gravity or wrinkles, and then spread on the sample holder, then another half is used to fix the boundaries as shown in Fig. 3.2 (b).

Fig. 3.9 shows the optical image of DE before and after the application of electric fields at different boundary conditions. Fig. 3.10 shows the displacement for each case measured by vibrometer under different boundary conditions (boundary condition 1 & boundary condition 2). All the data points are average values from 5 measurement points at 5 random locations. It is reasonable to understand the displacement changes due to the different boundary condition. However, there are several things in common: (1) for case 1 and 3, boundary condition 2 provides larger displacement. (2) for case 2 and 4, boundary condition 1 provides larger displacement. The difference between case 1 and 3 is the applied voltage direction, and the displacement of same surface is detected by vibrometer. The same applies to case 2 and 4. The surface displacement of each case is turned out to have the order, which will be discussed in the next section.

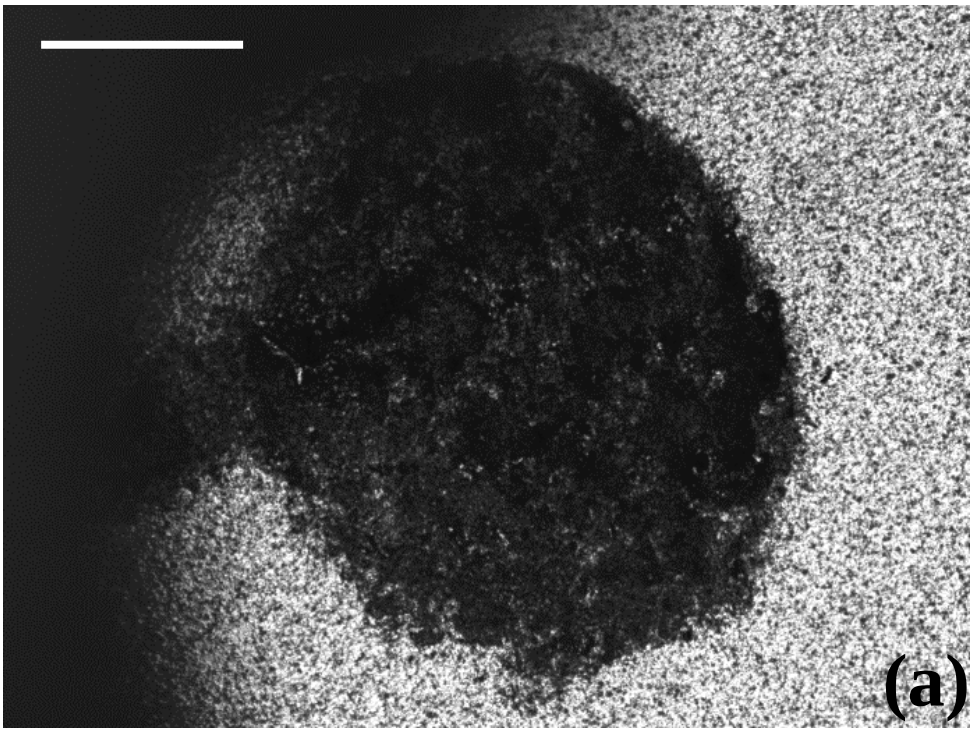
(a)

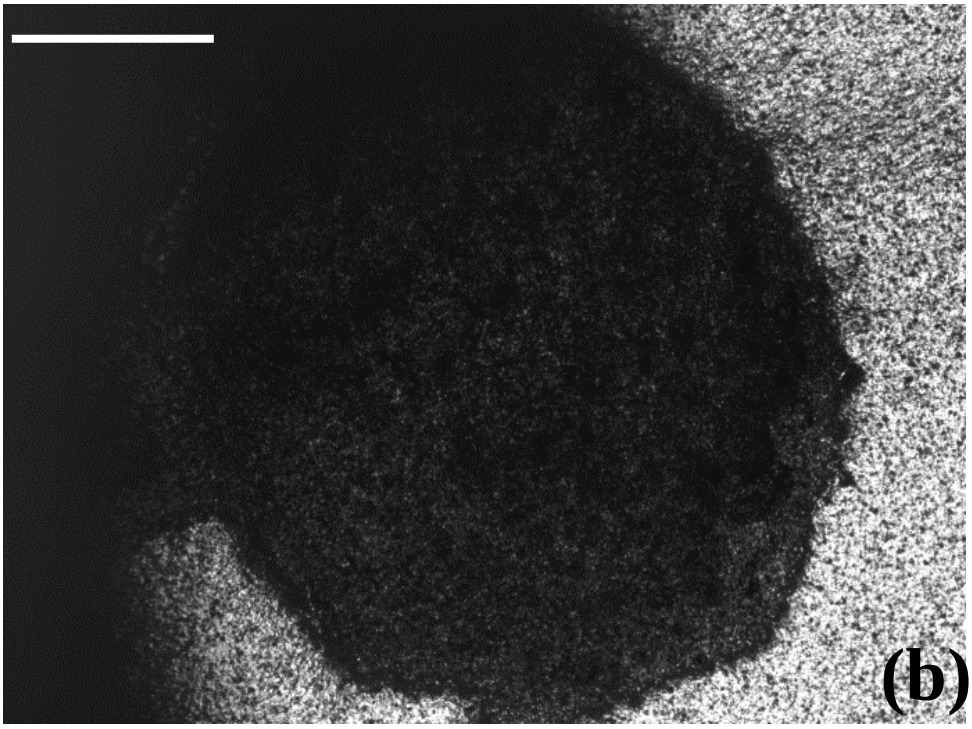
(b)

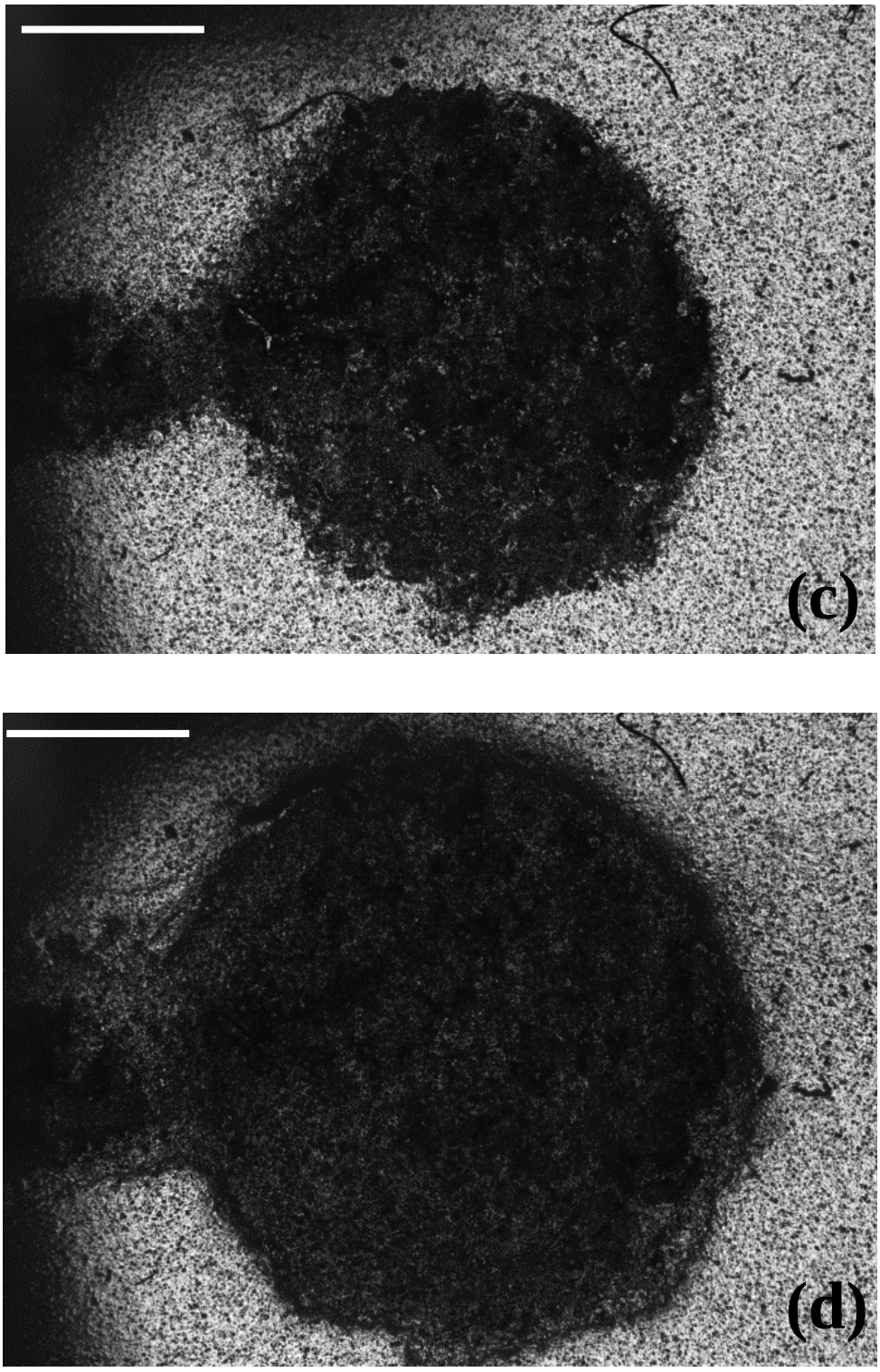

Fig. 3. 9. (a) Before and (b) after the application of 22.5 V/μm with boundary condition 1. (c) Before and (d) after the application of 22.5 V/μm with boundary condition 2. White scale bars are 1.5 mm.

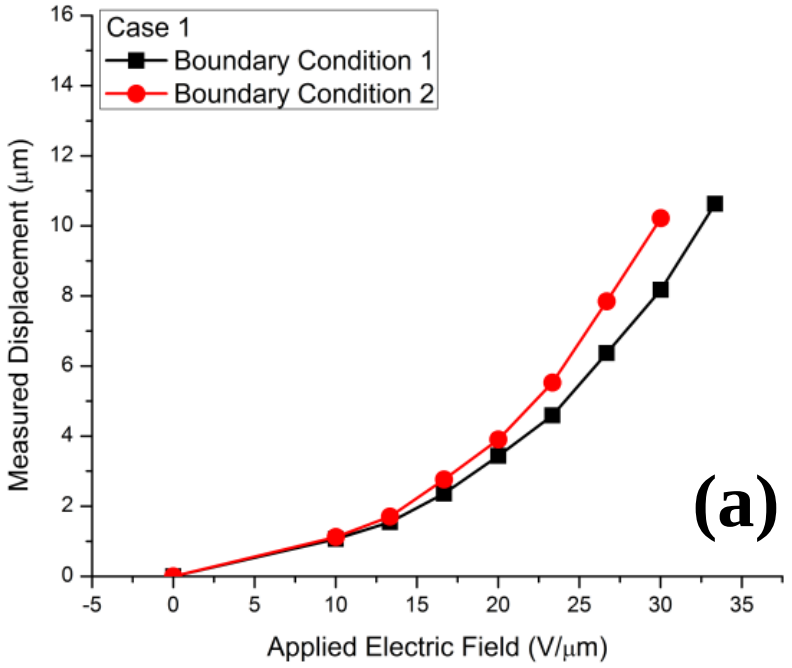
Case 1
Boundary Condition 1
Boundary Condition 2
Measured Displacement (μm)
Applied Electric Field (V/μm)
(a)

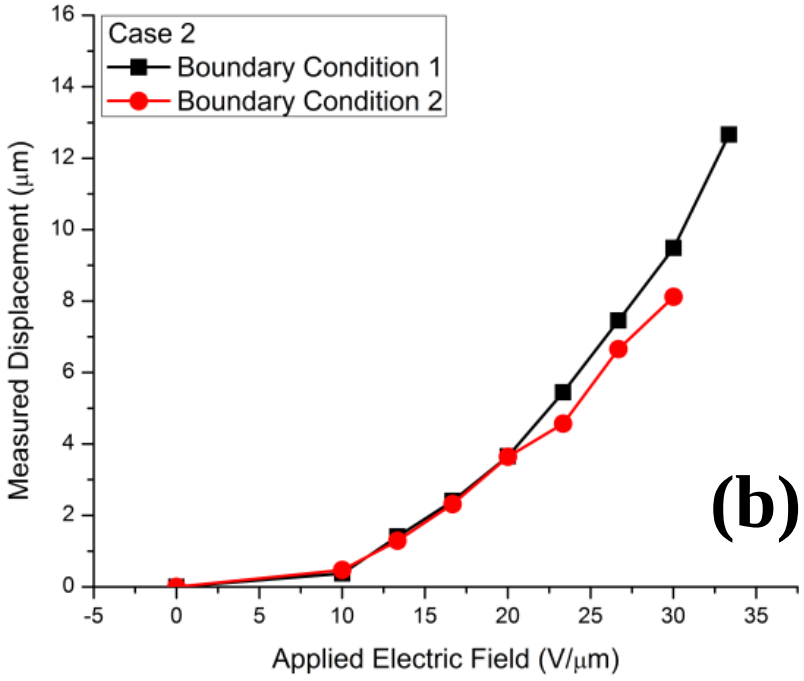
Case 2
Boundary Condition 1
Boundary Condition 2
Measured Displacement (μm)
Applied Electric Field (V/μm)
(b)

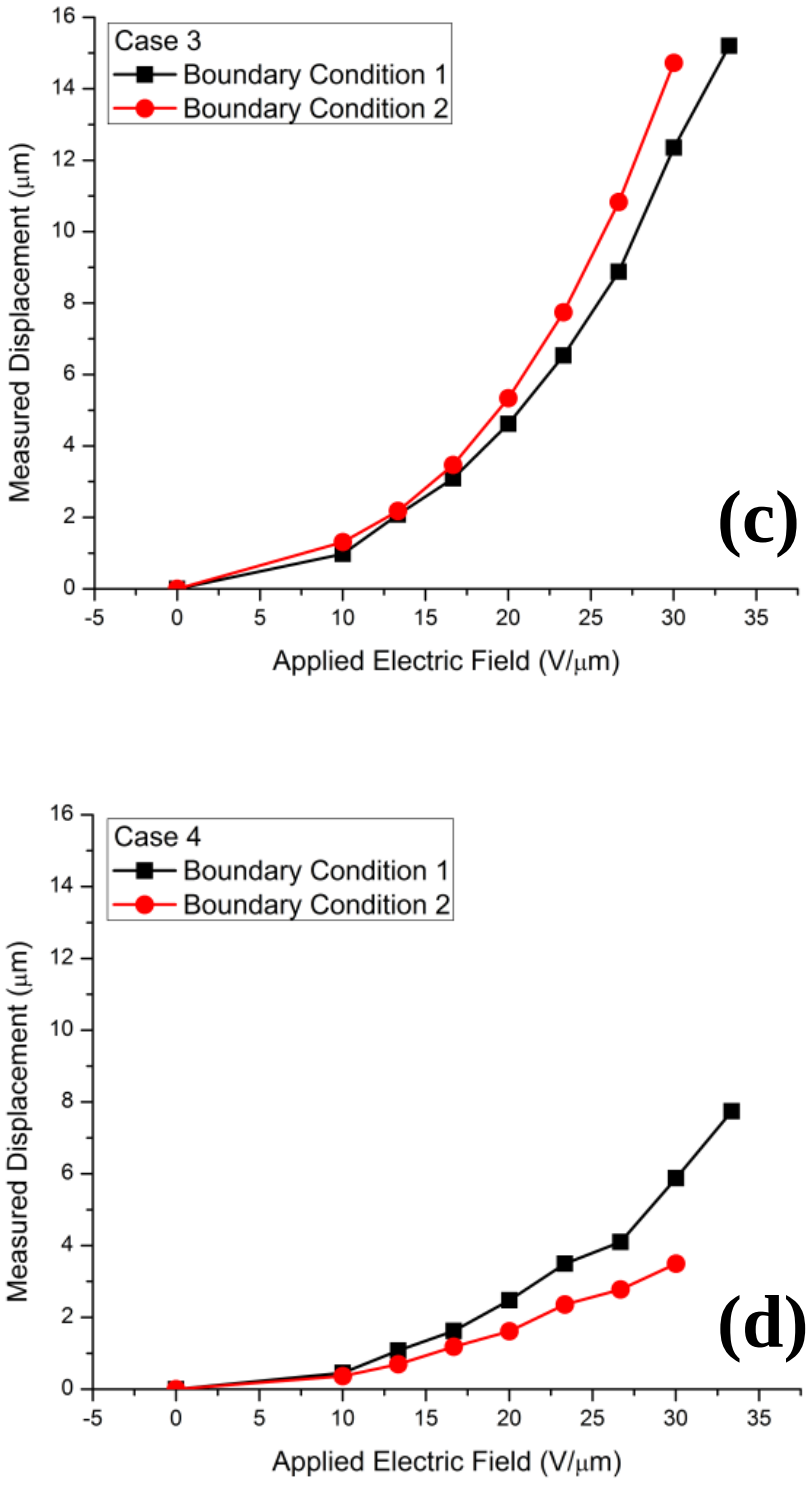

Fig. 3. 10. Measured displacement for (a) case 1, (b) case 2, (c) case 3, and (d) case 4.

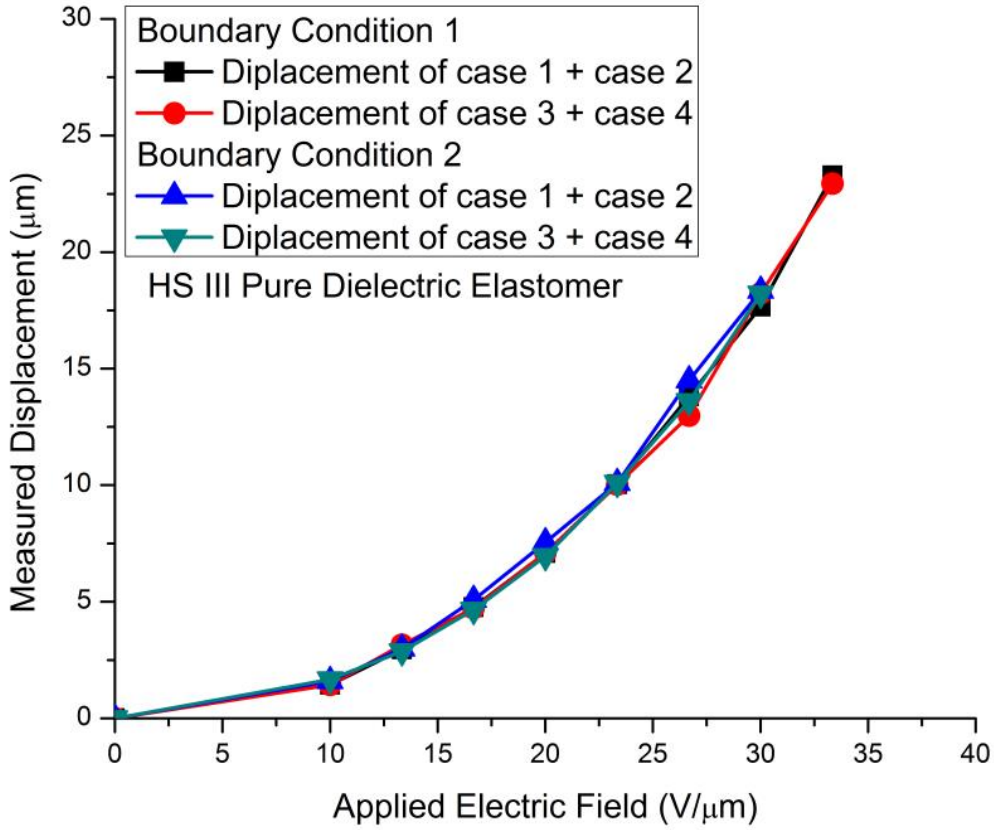

Fig. 3. 11. Measured displacement by laser Doppler Vibromter under different boundary conditions.

Vibrometer can only detect the displacement of the surface facing towards or outward the laser. However, by combining the displacement on both surfaces of DEs, thickness strain can be calculated. As mentioned earlier, the deflection by gravity is negligible compared to the displacement introduced by the electromechanical response of DEs.

Next, in order to determine the thickness strain of DEs under the applied electric fields, displacement of case 1 and 2 are added, and also displacement of case 3 and 4 are added to calculate the thickness strain. The added displacement is shown in Fig. 3.11. It is demonstrated

that 2 different boundary conditions provide consistent total displacement even under different boundary conditions, thus, it is validated that the total displacement or the thickness strain does not depend on the boundary conditions tested as long as small tension is applied and the DEs films are fully stretched in our sample holder described earlier. In addition, the measured thickness strain has a good agreement with that reported by Pelrine [22].

3.3.5 Acetone Effect on the Electromechanical Properties

Acetone is introduced during the fabrication process to improve the dispersion of MWNTs. Although acetone evaporation is accelerated by a hot plate during the processing, there could be residue acetone left in the processed materials. To examine the acetone effect on the electromechanical properties of the materials, pure DEs processed with or without acetone are compared shown in Fig. 3.12. Even though, DEs processed with acetone show slightly lower electromechanical response than DEs processed without acetone, the difference between two specimens is not pronounced. The largest difference observed at 26 V/μm is 12 %. Although the dielectric constant of acetone is 21.0 at 20 ℃ and the residue acetone is supposed to enhance the electromechanical response, the introduction of acetone actually lowers thickness strain under the same applied electric field according to Fig. 3.12. The potential causes of this difference could derive from the quality of the electrodes, specimen films, film thickness uniformity or measurement errors. More comparison needs to be carried out among DEs processed with or without acetone.

At this point, in order to have fair comparison with DE nanocomposites processed with acetone, DEs processed with acetone are chosen as a reference in this study.

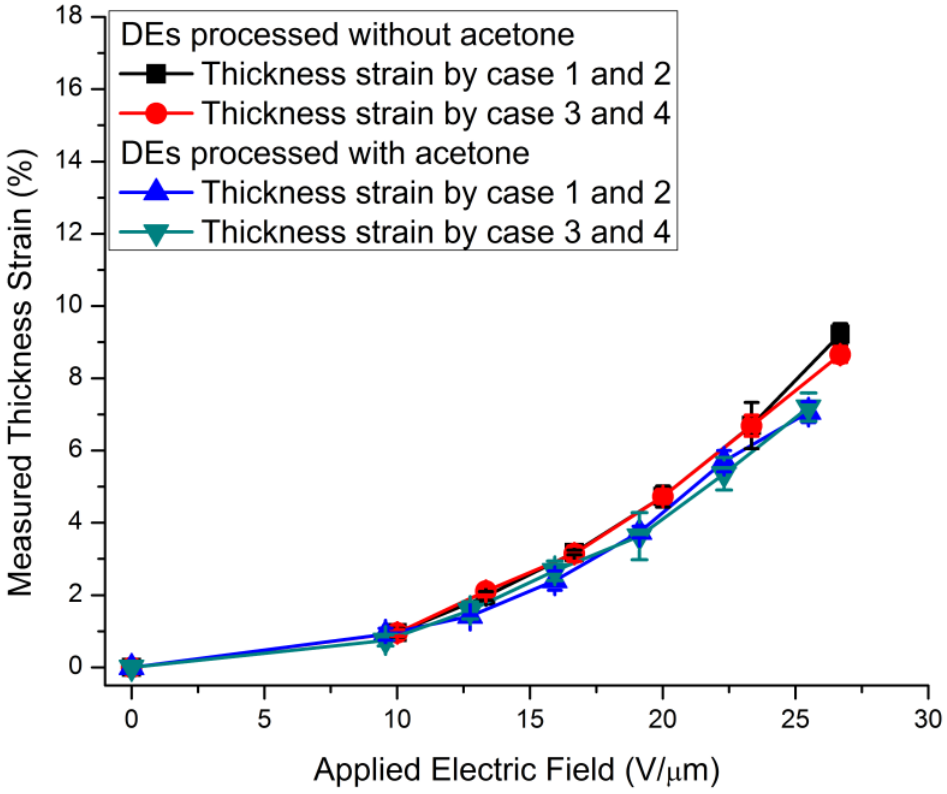

Fig. 3. 12. Measured displacement by laser Doppler vibrometer of specimens processed with or without acetone.

3.3.6 Surface Displacement Order

Surface displacement on the DEs is captured by laser Doppler vibrometer. The displacement for each case is detected and compared. It is found that the magnitude of the displacement for each

case has the order depending on the materials. For instance, regardless of the boundary conditions, the magnitude of the displacement of pure DEs is found to be

$$|d_3| \geq |d_2| \geq |d_1| \geq |d_4|$$

where d_i is the measured displacement in case i (i=1, 2, 3, 4). Although the identical surface is measured for case 1 and 3, the displacement in case 3 is always larger than that of case 1. This is true for displacement in case 2 and 4: displacement of case 2 is larger than that of case 4 although the identical surface is measured.

For all the nanocomposites filled with MWNTs, the magnitude of the displacement gives $|d_2| \geq |d_3| \geq |d_4| \geq |d_1|$ as shown in Fig. 3.13 and Fig. 3.14. The measured displacement order is correlated with the materials. The introduction of MWNTs in DEs has enhanced the displacement measured from case 2 and 4 compared to case 1 and 3.

Although the reasons for these orders are not revealed yet, some of the potential causes involve the material characteristics, fabrication processing, or the uniformity of the film specimens or electrodes. More investigation is required to find out the causes of the displacement orders.

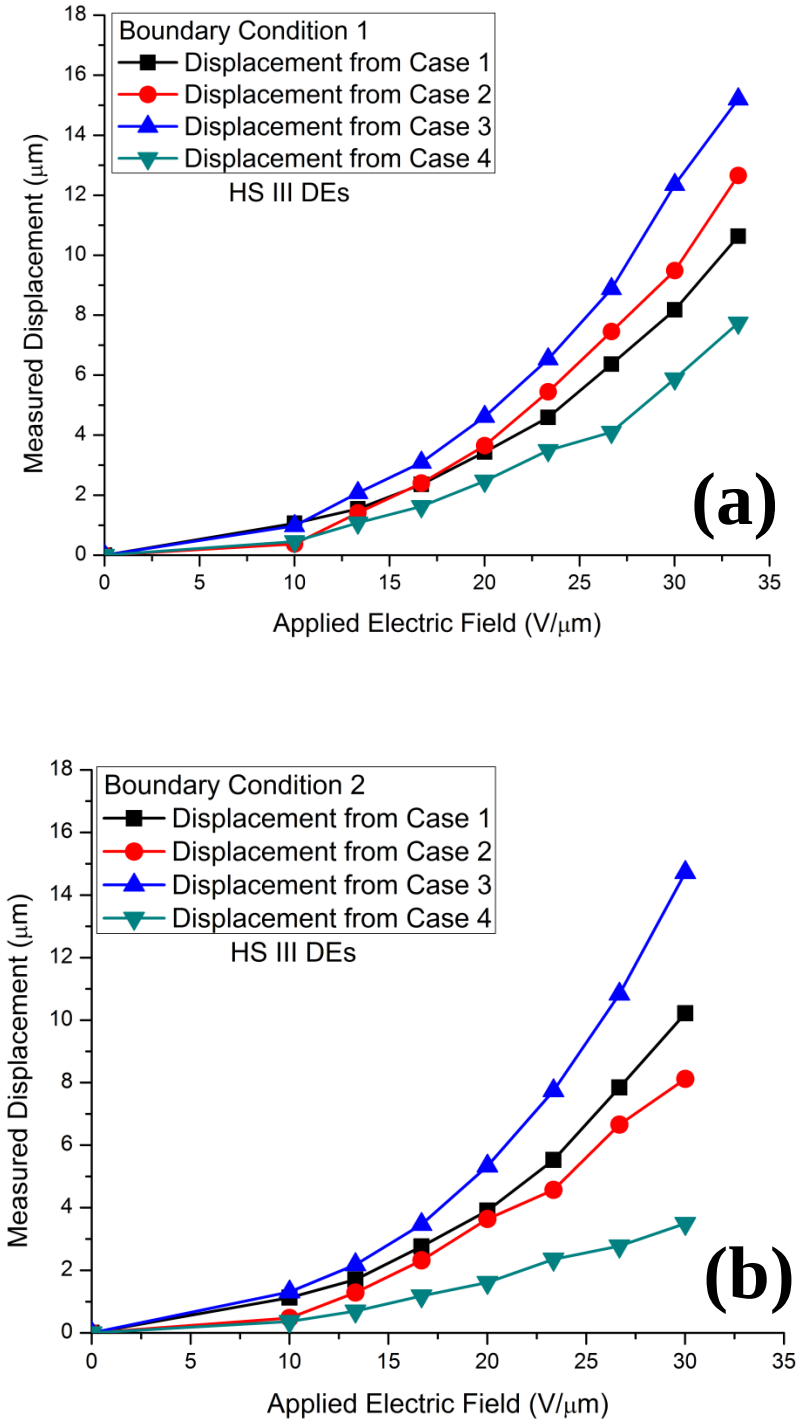

Fig. 3. 13. Measured displacement by laser Doppler Vibrometer under different boundary conditions.

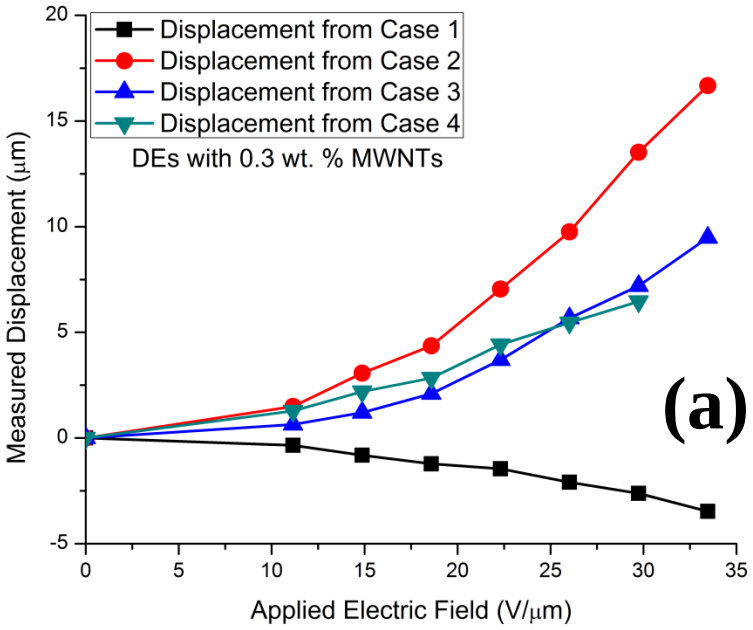
Displacement from Case 1
Displacement from Case 2
Displacement from Case 3
Displacement from Case 4
DEs with 0.3 wt. % MWNTs
Measured Displacement (μm)
Applied Electric Field (V/μm)
(a)

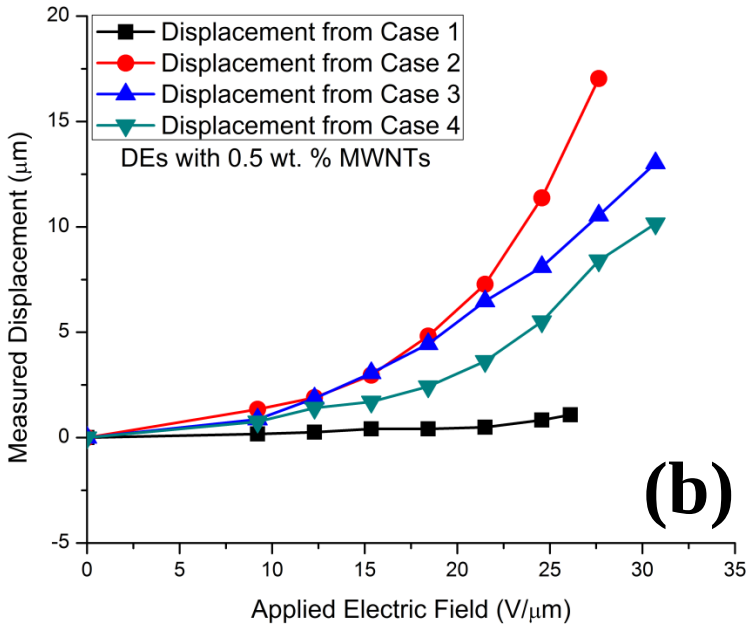
Displacement from Case 1
Displacement from Case 2
Displacement from Case 3
Displacement from Case 4
DEs with 0.5 wt. % MWNTs
Measured Displacement (μm)
Applied Electric Field (V/μm)
(b)

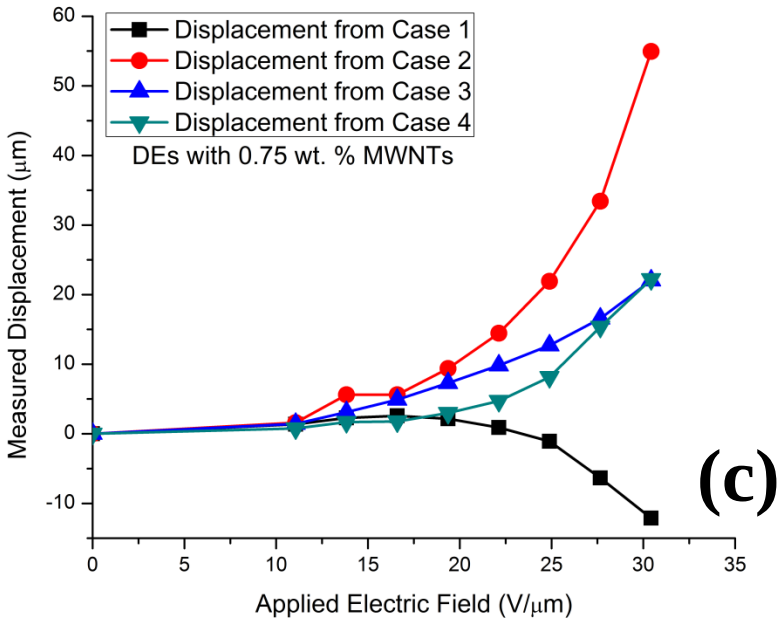

Fig. 3. 14. Measured displacement by laser Doppler vibrometer of dielectric elastomer nanocomposite specimens with (a) 0.3 wt. %, (b) 0.5wt. % and (c) 0.75 wt. % MWNTs. Positive displacement here is defined as the displacement in compression direction while negative displacement is defined as the displacement in tension direction.

3.3.7 Loading Cases Order

The electromechanical measurement is carried out in the order of case 1-case 3-case 4-case 2 for easiness. To examine the order effect on the material electromechanical response, the measurement order is reversed. Fig. 3.15 shows that the measurement order does not significantly affect the measured electromechanical response of the materials. This result also has a significant implication because the displacement order discussed earlier is not caused by the order of the applied electric fields or the residue charges on the compliant electrodes. Thus,

for electromechanical measurement for other nanocomposites, the measurement order is fixed to case 1-case 3-case 4-case 2.

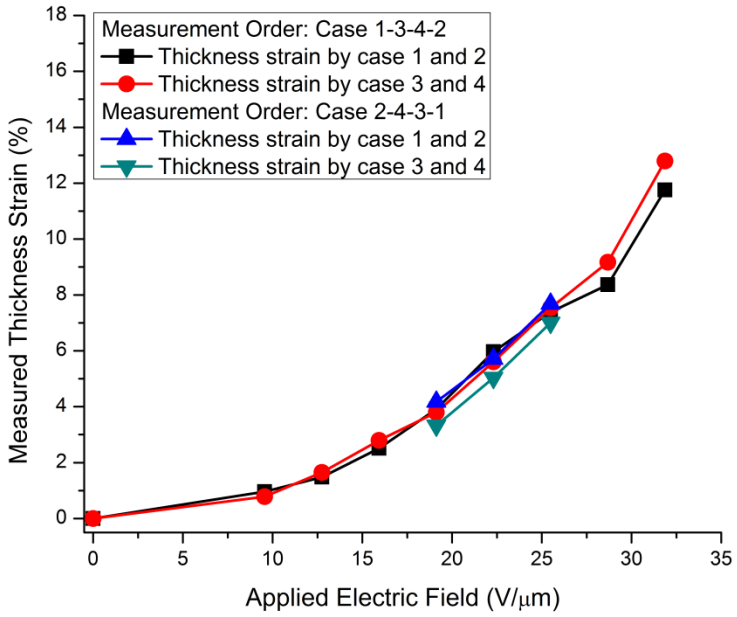

Fig. 3. 15. Measured displacement by laser Doppler of pristine DE under the different order of the applied electric fields.

3.3.8 Thin Alloy Coating on the Electrodes

Micro System Analyzer uses the Doppler Effect by the laser. In order to get the accurate measurements, reflected laser from the specimen surface is a key player. The compliant electrodes used in this study are black-colored, thus, detecting enough intensity of the reflected laser is a common challenge. In order to solve this problem, Au-Pd thin layer (1-2 nm) is deposited on the surface of the electrodes to improve the intensity of the reflected signal. Fig. 3.16 shows the optical microscope images of the compliant electrodes without or with the Au-Pd

thin layers. From Fig. 3.16 (e-h), it is obvious that the compliant electrodes with Au-Pd layer have better light reflection, making the measurement easier. However, from Fig. 3.16 (e-f), the electrode surface looks uneven. Fig. 3.16 (g-h) shows the zoomed-in images from (e-f). From Fig. 3.16 (e-f), Au-Pd thin layer and gaps between the layers are observed. The gaps are produced right after the electromechanical deformation is introduced for the first time. Gaps have already been created before Fig. 3.16 (g) and (h) are captured. It should be noted that the discontinuous displacement is observed by vibrometer for specimens with coated electrodes. Under applied electric field, some locations show little displacement while the others (gaps) show large displacement. This can be explained by the poor adhesion between the Au-Pd thin layer and the electrodes. The Au-Pd layer attached to the electrode deforms with electrodes although Au-Pd layer poorly attached to the electrode does not deform along with the electrodes. As a result, the non-uniform displacement measurement results as well as light reflection is observed from the Au-Pd layer on the electrodes shown in Fig. 3.16 (e-f).

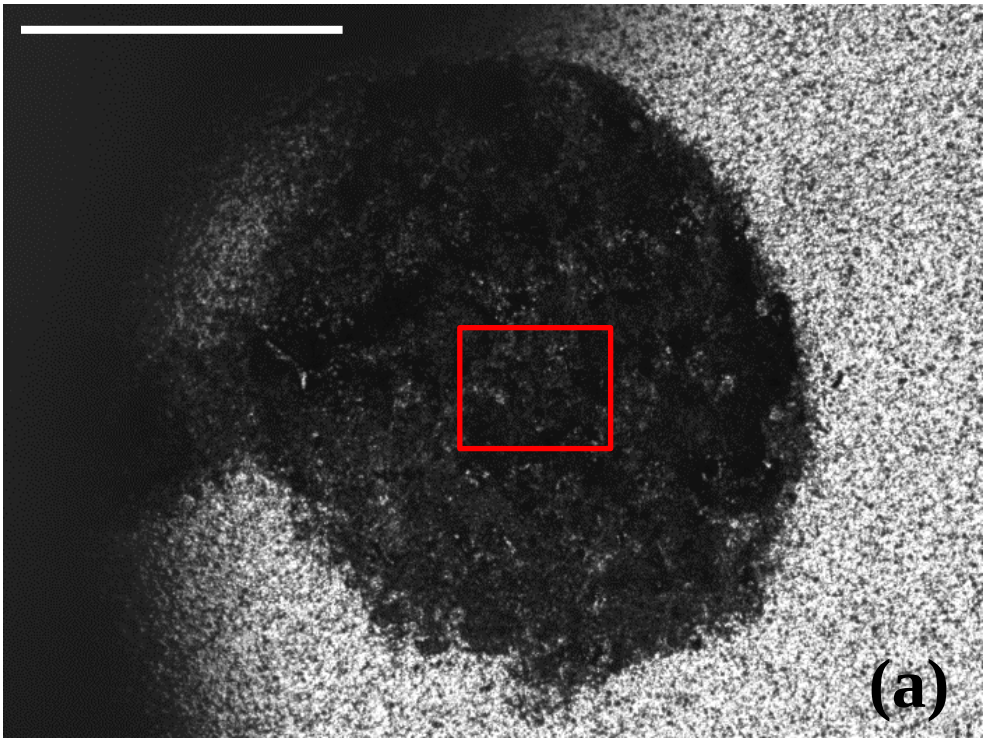
(a)

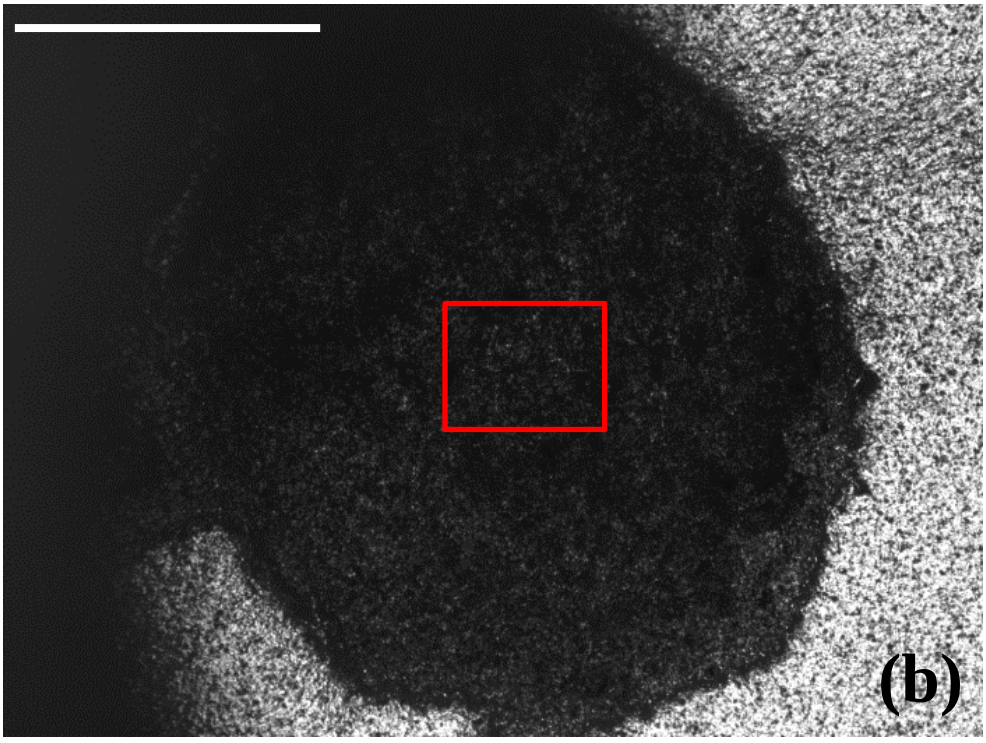
(b)

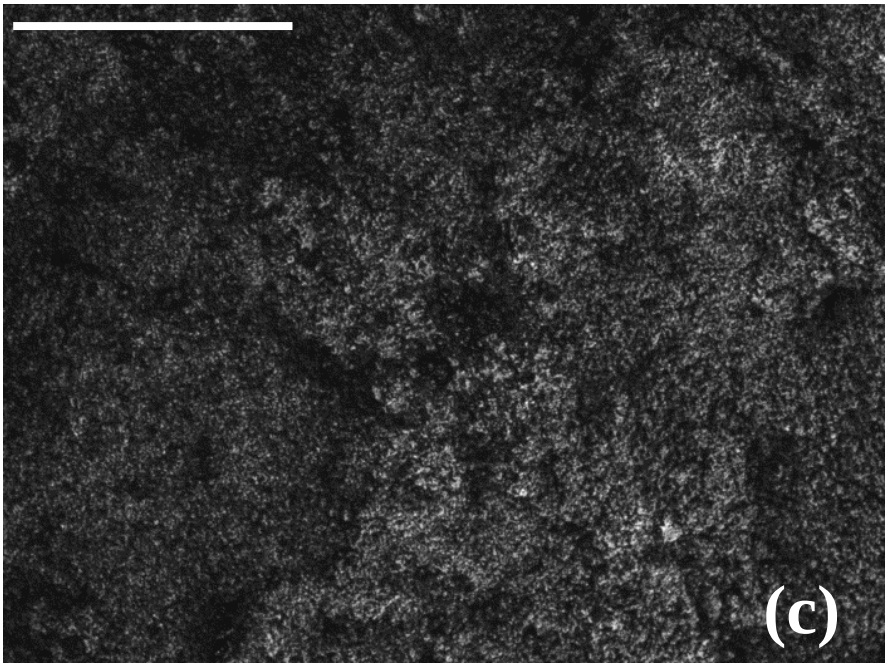
(c)

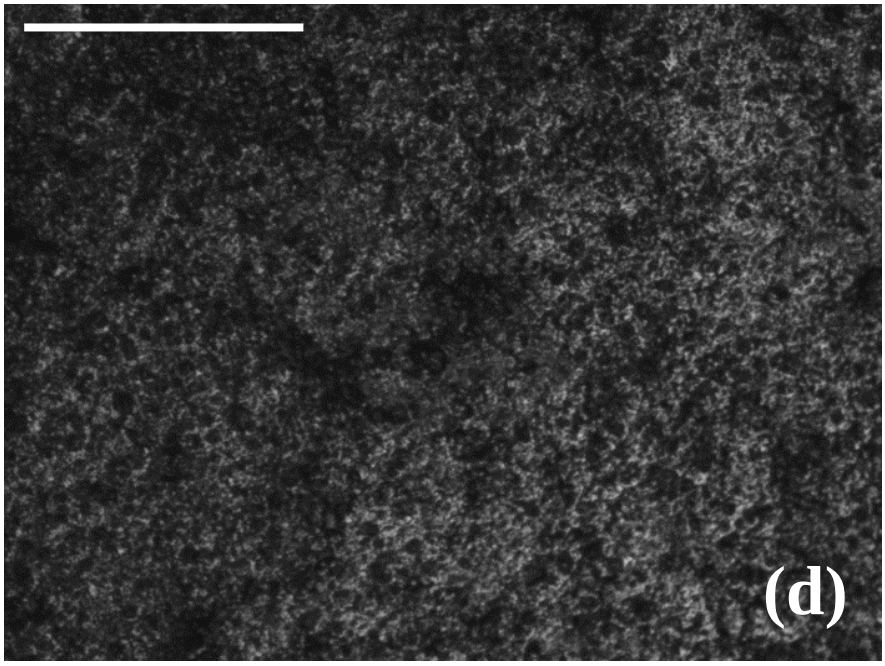
(d)

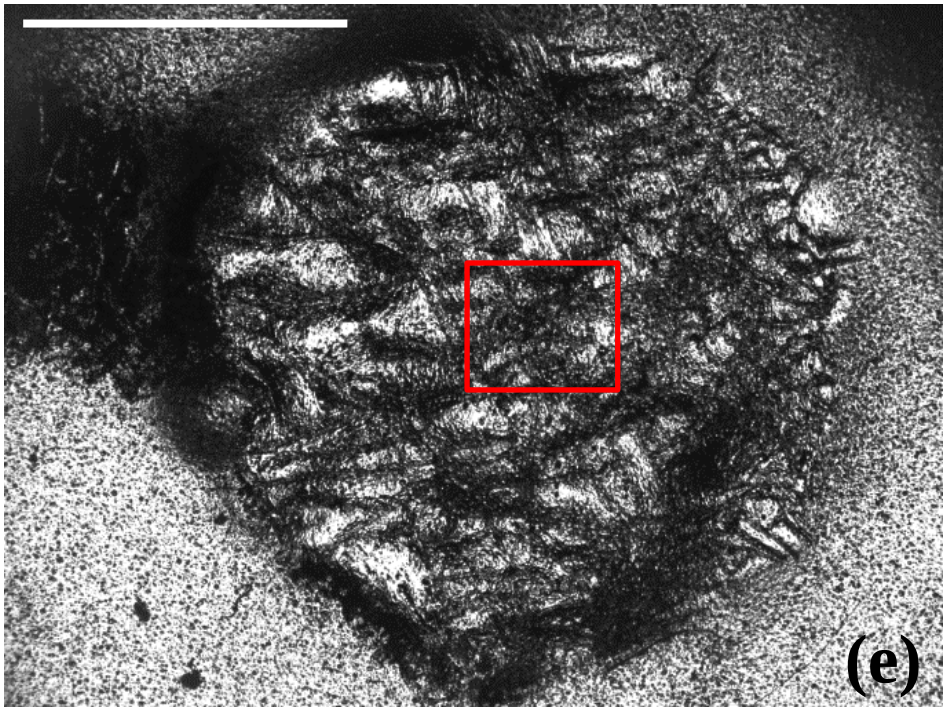
(e)

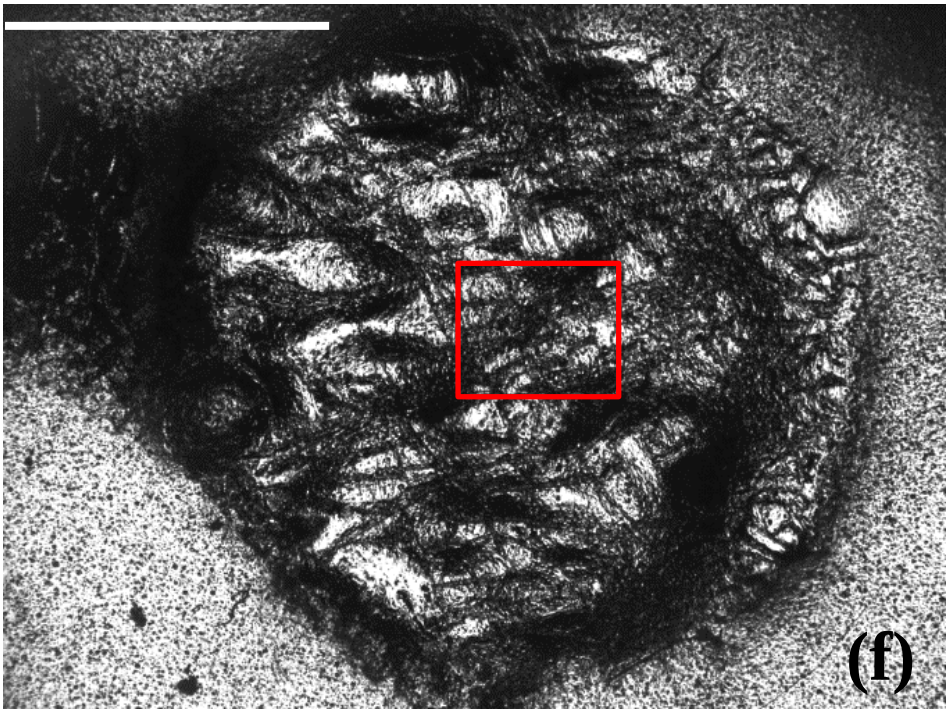
(f)

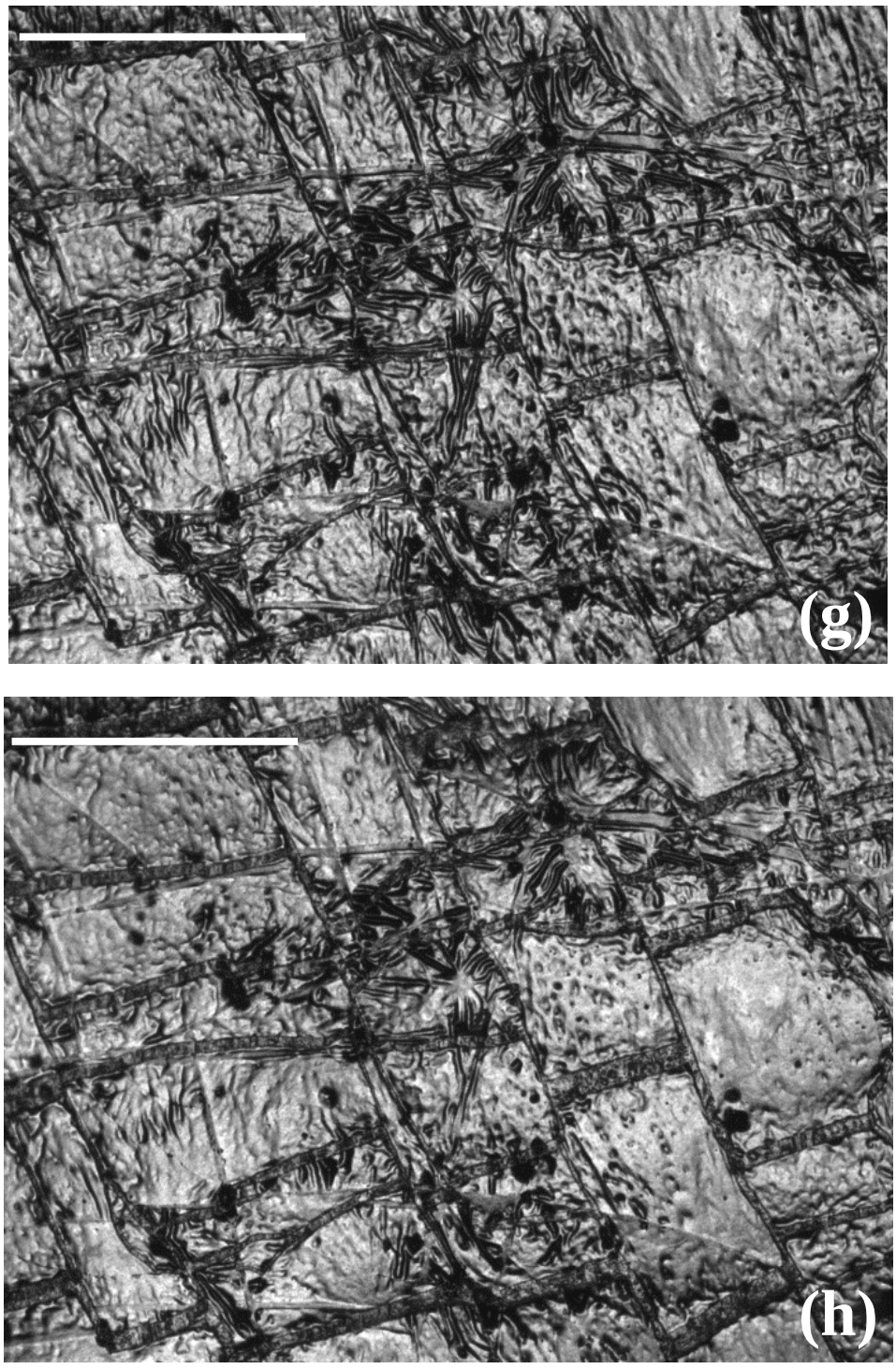

Fig. 3. 16. Optical microscope images of compliant electrodes (a) before and (b) after the application of 33.4 V/μm with scale bars 1.5 mm, and (c) before and (d) after the application of 33.4 V/μm with scale bars 300 μm, and compliant electrodes with thin alloy coating (e) before and (f) after the application of 33.4 V/μm with scale bars 1.5 mm, and (g) before and (h) after the application of 33.4 V/μm with scale bars 300 μm. Gaps shown in (e-h) have already been created before this testing.

It is concluded that Au-Pd thin coating layer could be beneficial to enhance the signal for measurement of surface displacement. However, measured displacement is highly discontinuous due to the poor adhesion of the Au-Pd layer and the electrodes. As a result, the obtained data can mislead the surface displacement measurement. Additionally, the elastic modulus difference could potentially cause the restriction of the DE deformation. The elastic modulus for Au-Pd alloy is in the range of GPa while that of elastomer is in the range of kPa. As a result, the deformation of the DEs or DE nanocomposite could be restricted.

3.3.9 Thickness Strain of DE Nanocomposites Filled with MWNTs

The thickness strain of nanocomposites is detected and the electromechanical response is compared with that of pristine DEs. It is demonstrated that the introduction of MWNTs enhances the electromechanical property of DEs. DE nanocomposites filled with MWNTs show higher thickness strain under any applied electric field as shown in Fig. 3.17. For example, at $30\,V/\mu m$, introduction of 0.75 wt. % MWNTs enhanced the electromechanical response of DE by 3 times, while 1.5 times for DE with 0.50 wt. % MWNTs. In addition, at magnitude of thickness strain 10 %, the required electric field is reduced for 30 % and 18 % for DE nanocomposites with 0.75 wt. % MWNTs and 0.50 wt. % MWNTs respectively.

As proposed by Pelrine [22], the thickness strain of HS III DEs are proportional to the square of applied electric fields. If we assume that the thickness strain of DE nanocomposites filled with 0.75 wt. % MWNTs also follow the Pelrine model, the required electric field reduction could be up to 57.7 % at fixed thickness strain 10 %. However, the measured electric field reduction is 30 % which is about the half of the calculated values. This shows that DE nanocomposites filled

with MWNTs follows a unique path deviated from Pelrine models, following the larger exponent of applied electric fields.

As will be discussed in the following chapters, at low concentration of MWNTs (up to 0.75 wt. %), the dielectric property of DE nanocomposites is much more sensitive to the introduction of MWNTs than mechanical property of the DE nanocomposites. As a result, higher dielectric constant attracts more charges on the electrodes resulting in larger stress while the mechanical property change MWNTs introduce is limited at low MWNT concentration. In addition, the coupling effect of electrical and mechanical properties might have been involved in the electromechanical response, resulting in the effective improvement of electromechanical response of DE nanocomposites filled with MWNTs.

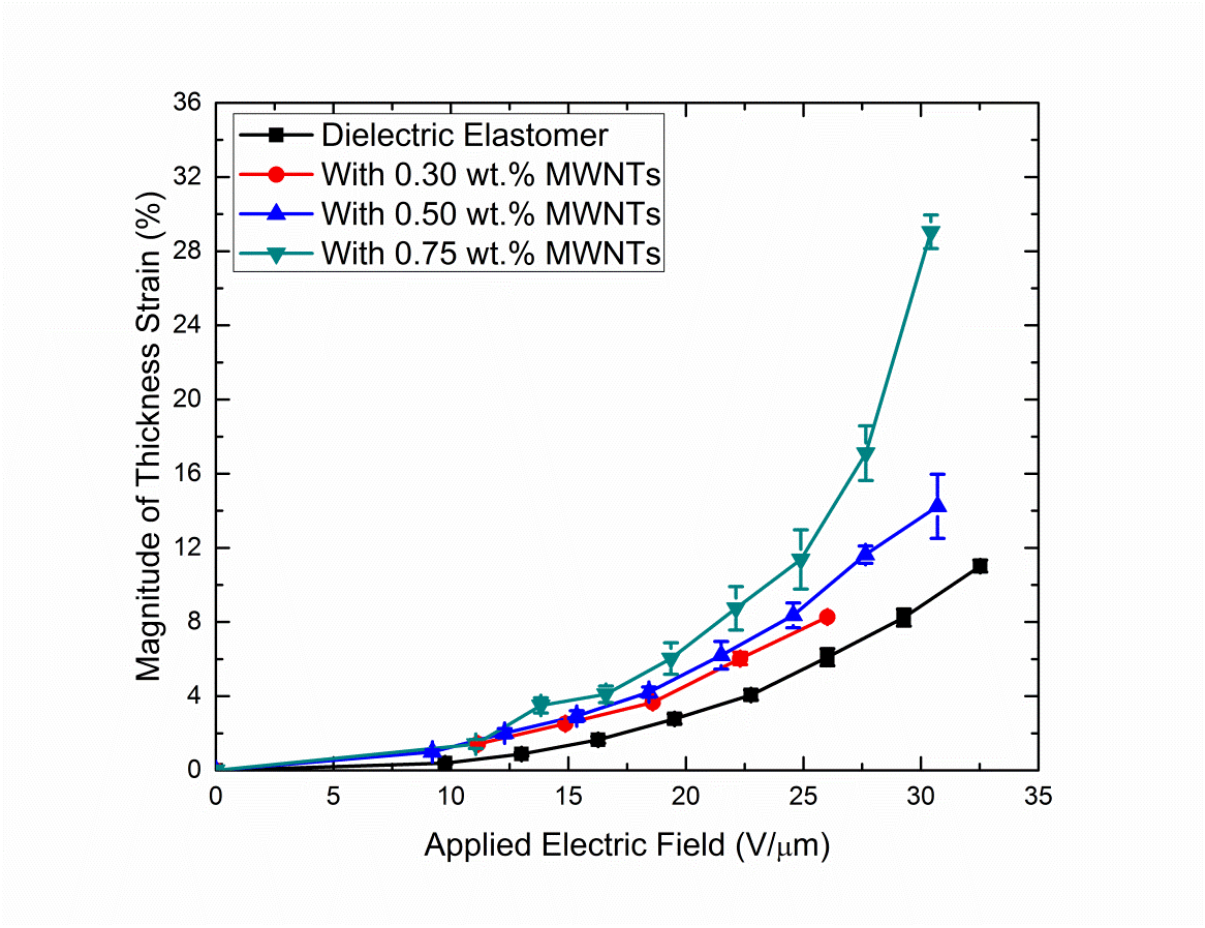

Fig. 3. 17. Measured thickness strain under applied electric fields of DEs and DE nanocomposites filled with MWNTs.

3.3.10 Percolation Threshold for DE Nanocomposites Filled with MWNTs

Percolation threshold is the point where the conductivity and dielectric properties of materials abruptly changes. Ideally, higher concentration of MWNTs can enable higher dielectric constant for DE nanocomposites. However, higher concentration of MWNTs can make the DE nanocomposites conductive, which leads to fail for DEs and DE nanocomposites. The electrical conduction is due to the formation of conduction paths formed by conductive fillers in the material, and at the same time, the percolation threshold is strongly related to the material processing.

Fig. 3.18 shows the moment of burning of a DE nanocomposite film with 0.75 wt. % MWNTs at $22.2\,\mathrm{V/\mu m}$. This shows that DE nanocomposites filled with 0.75 wt. % MWNTs is reaching or close to the percolation threshold point. As a result, the application of high electric field causes the electric conduction, leading to the heat generation and burning around the conduction paths. Thus, DE nanocomposites with more than 0.75 wt. % are not tested as they are likely to be more conductive.

The electrical conduction measurement of DE nanocomposites with CNTs and the associated results will be discussed in the next chapter.

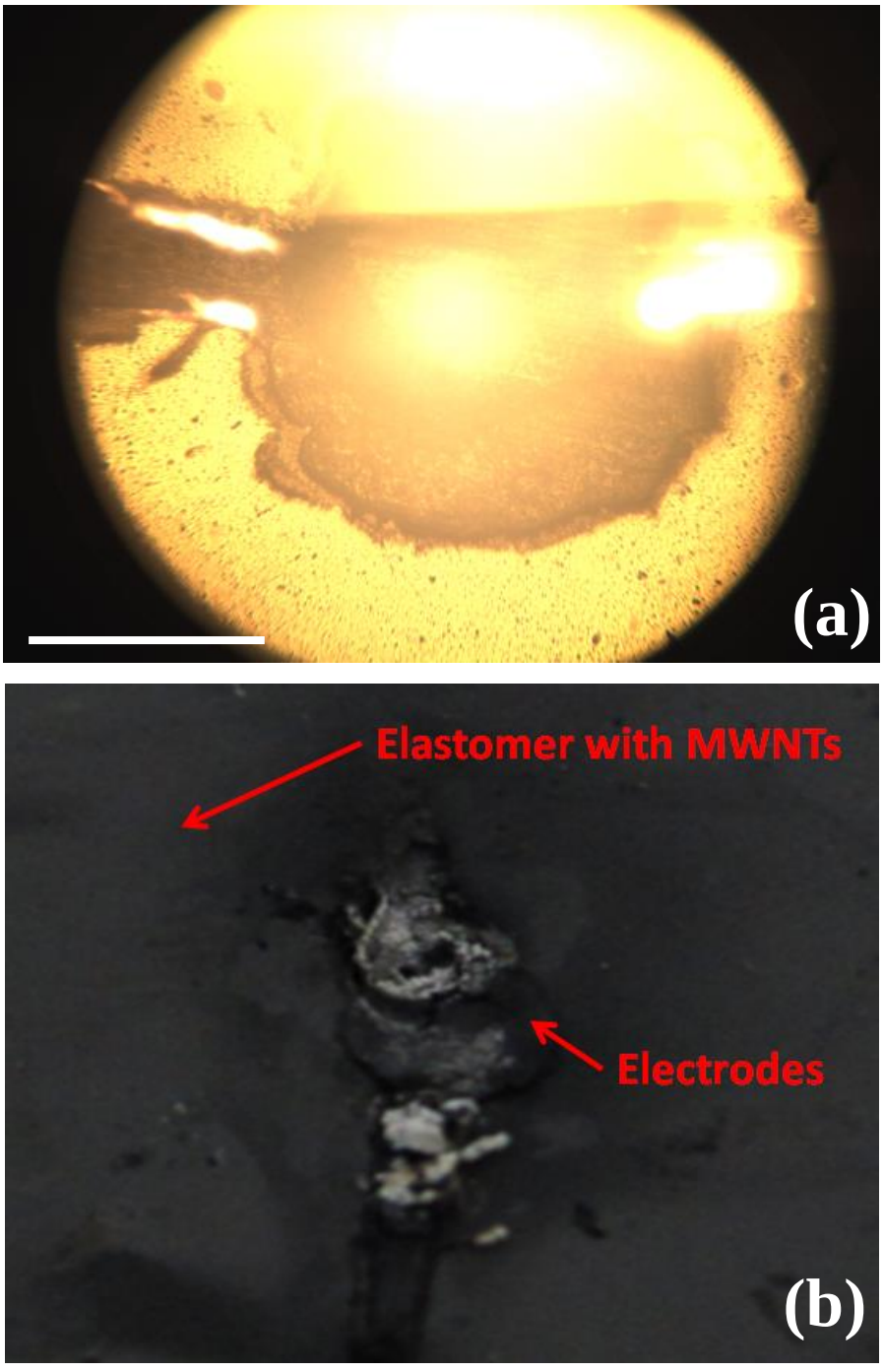

Fig. 3. 18. (a) The moment of burning and (b) after the burning of a DE nanocomposite film (158 μm) filled with 0.75 wt. % MWNTs as a result of electrical conduction when electric field is applied (22.1 V/μm). The scale bar in (a) is 1.5 cm.

3.3.11 Conductive Samples (SWNTs)

DE nanocomposites filled with SWNTs are also tested to investigate the electromechanical property. When voltage is applied to the nanocomposite films, the film becomes conductive in an equilibrium state shown in Fig. 3.19. From Fig. 3.19 and Ohm's Law, the resistance is calculated as $1.454 \cdot 10^5 \Omega$ which is close to the resistance value ($1.500 \cdot 10^5 \Omega$) of the resistor in the circuit. This indicates that the nanocomposite film ($137.1\,\mu m$) filled with 0.3 wt. % SWNTs becomes conductive under applied high voltage, and there is consistent current flowing in the circuit.

The displacement measurement is shown in Fig. 3.20. It can be clearly seen that the displacement from case 1 and 3 (same surface) are both deforming towards expanding direction while that from case 2 and 4 (same surface) are deforming towards the shrinking direction. Furthermore, the displacement magnitude of case 1 and 2, 3 and 4 are very similar, indicating that the displacement of the film might have been caused by the deflection of the film, not by the thickness strain of the DE nanocomposite film. Also, the measured thickness strain for the nanocomposite is much smaller than that of pure DEs shown in Fig. 3.20. The measured thickness strain is due to the local non-uniform deflection of the film or the roughness of the electrodes considering the thickness of the specimen is $137.1\,\mu m$.

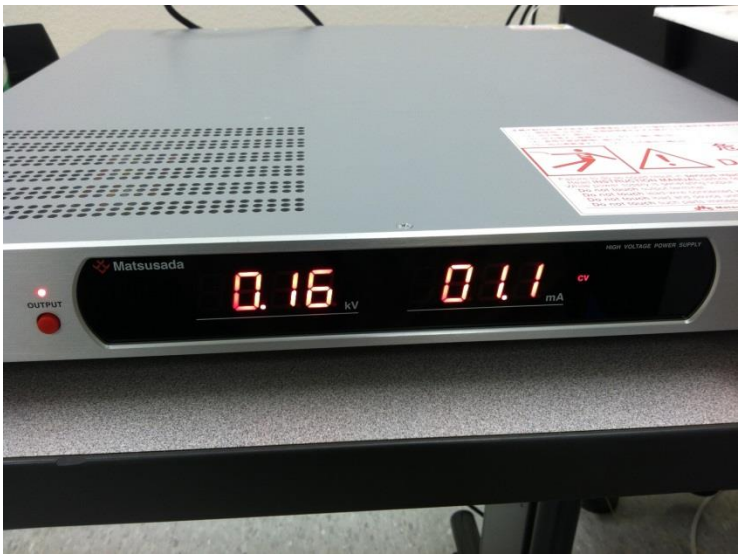

Fig. 3. 19. Power supplier (Matsusada AU-10P30-LC) used in the displacement measurement by laser Doppler vibrometer.

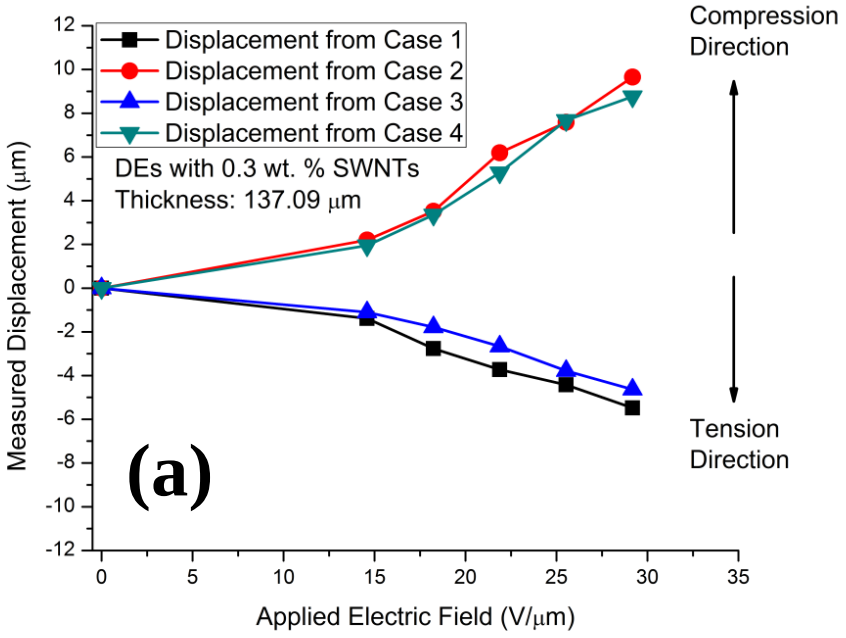

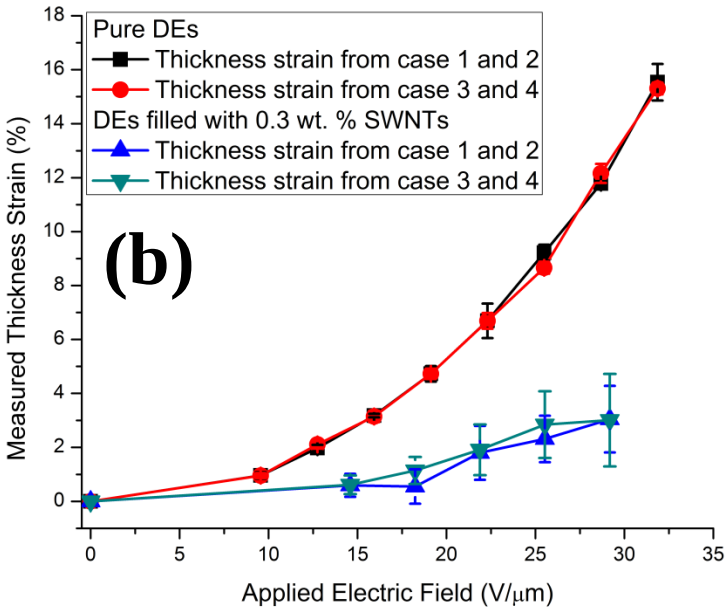

Fig. 3. 20. (a) Measured displacement and (b) measured thickness strain of DE nanocomposite filled with SWNTs.

The DEs filled with SWNTs show electrical conduction although DEs filled with MWNTs with same weight concentration does not. This is because a MWNT is made up of multilayers carbon sheets while a SWNT is made of a single layer. For instance, let's consider a MWNT with 10 layers for simplicity. Under a certain concentration, 10-layer MWNT can only have 100 carbon nanotubes while SWNTs can have 1000 single-layer carbon nanotubes assuming MWNTs and SWNTs have the same length. This results in higher probability for SWNTs to form conduction paths inside the nanocomposite. As a result, DEs filled with SWNTs tend to be more conductive than DEs filled with SWNTs.

For conductive DE nanocomposite with SWNTs, the small deformation is detected by vibrometer. However, the deformation is not caused by the electromechanical response of the nanocomposite as the DE nanocomposites filled with 0.3 wt. % SWNTs are electrically conductive.

3.4Conclusions

It is experimentally demonstrated that, with addition of MWNTs, the electromechanical response of DEs have been enhanced. Under the fixed applied electric field, such as $30\ V/\mu m$, the nanocomposites show about improvement by 3 times in the induced thickness strain. In addition, thickness strain is achieved even with less required electric field. This has verified effective improvement in the electromechanical properties of DE nanocomposites filled with MWNTs under the applied electric fields. The electromechanical response enhancement in vertical direction in Fig. 3.17 shows that the addition of MWNTs as filler is the potential solution to further enhance the energy harvesting applications. In addition, the reduction of required electric fields has shown an approach to the realization of applications which requires electrical to mechanical signal conversion such as actuators or artificial muscles.

Furthermore, Laser Doppler vibrometer is demonstrated to be a direct and effective approach to precisely capture the electromechanical properties of the dielectric elastomers and dielectric elastomer nanocomposites filled with MWNTs.

Chapter 4 Experimental Study of Dielectric and Mechanical Properties of Dielectric Elastomer Nanocomposites Filled with Carbon Nanotubes.

4.1 Introduction

In order to enhance the electromechanical response of polymer composite materials, introduction of ferroelectric materials such as $BaTiO_3$ nanoparticles [43-45], $PbTiO_3$ [47, 48] and CNTs [52] has been attempted as mentioned in the previous chapter. In this study, CNTs have been introduced to DE matrix to enhance the electromechanical response of DE nanocomposites. Thus, it is important to understand how the addition of CNTs to DEs changes the overall materials properties.

A various factors can affect the dielectric and mechanical properties of composite materials with high aspect ratio fillers: amount of fillers, filler shape, filler aspect ratio [121-123], filler dispersion, distance between each filler [124], waviness of the fillers [125], interaction between fillers and matrix, and orientation of the fillers. In addition, materials processing [98], CNT types [81] are also the dominating factors.

In this chapter, measurement of dielectric and mechanical properties of DE nanocomposites filled with randomly oriented CNTs is carried out. The dielectric and mechanical properties of DE nanocomposites are revealed.

4.2 Materials, Fabrication, Characterization and Dielectric Properties

Alumilite HS III RTV high strength mold-making silicone rubber is chosen as a dielectric elastomer material in this study. Two sets of 0.50 wt. % and 0.75 wt. % of MWNTs are added as fillers to dielectric elastomers. MWNTs are purchased from Cheap Tubes, Inc., having outer diameter 20-30 nm, inside diameter 5-10 nm, and 95 wt. % purity. The fabrication process is described in the previous chapter.

Spin coating technique is utilized to prepare DE nanocomposite films for electromechanical and dielectric property measurement. Both sides of the film specimens are coated with silver based electrodes with diameter 16.67 mm using Ted Pella, Inc. fast drying silver paint for capacitance measurement. This MIM (Metal-Insulator-Metal) is measured using HP 4280A 1MHz C Meter/C-V plotter at room temperature 24 ℃ shown in Fig. 4.1, and dielectric constant is further extracted from the measured capacitance. At least 10 measurements are carried out for each specimen.

For mechanical property analysis of DE nanocomposites filled with CNTs, the geometry of cylindrical specimens with 9.5 mm in diameter and 9.5 mm in height is prepared, following ASTM Standard D 5992-96 [126] on dynamic testing of vulcanized rubber and rubber-like materials using vibratory methods as shown in Fig. 4.2.

Fig. 4. 1. HP 4280A 1MHz C Meter / C-V plotter used for capacitance measurement.

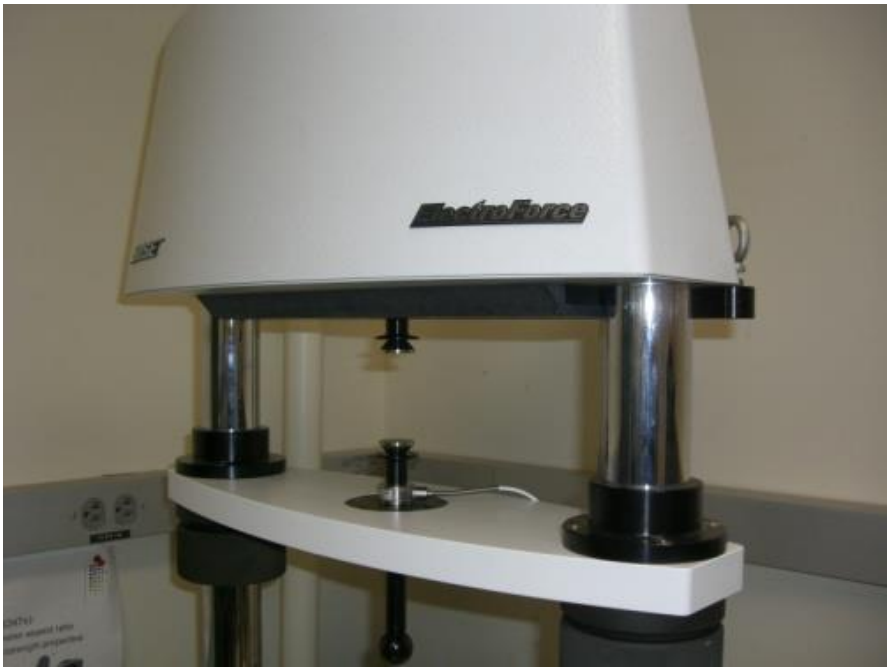

Fig. 4. 2. BOSE ElectroForce 3200 dynamic mechanical analysis (DMA) machine.

4.3 Results and Discussion

4.3.1 Dielectric Constant and Electrical Conductivity Measurement of DE Nanocomposites Filled with CNTs

Both sides of the film specimens are coated with silver based electrodes with diameter 16.67 mm using Ted Pella, Inc. fast drying silver paint for capacitance measurement as shown in Fig. 4.3.

Fig. 4.4 shows the extracted dielectric constant for DEs and DE nanocomposites as a function of weight fraction of MWNTs. DEs and DE nanocomposites with 0.3 wt. % MWNTs show similar dielectric constant while that of DEs with 0.5 or 0.75 wt. % MWNTs show the improvement by 28 % and 40 % respectively. This is due to the space-charge polarization by the conductive MWNTs associated with Maxwell-Wagner Effects [101, 127].

Fig. 4.5 shows the electrical conductivity of DEs and DE nanocomposites filled with MWNTs as a function of weight fraction of MWNTs. DEs and DE nanocomposites filled with MWNTs do not show the significant changes in the electrical conductivity. Although DEs filled with 0.75 wt. % MWNTs do not show significant change in terms of electrical conductivity compared to pure DEs without mechanical loading, conduction paths can be easily formed under compression as mentioned in the previous chapter and Fig. 3.18.

Furthermore, dielectric constant is measured for DEs with SWNTs. Fig. 4.6 shows the extracted dielectric constant of DEs and DE nanocomposites filled with CNTs. Even for the same concentration of CNTs, addition of SWNTs has significantly enhanced the dielectric constant of the nanocomposites. This is associated with the conductivity shown in Fig. 4.7. The significant

improvement in dielectric constant is enabled by the concentration of conducive fillers close to the electrical percolation threshold associated with a power law relationship mentioned in [49, 68, 128, 129]. Moreover, SWNTs have longer aspect ratio due to the smaller diameter (usually 1-2 nm) assuming SWNTs and MWNTs have their length in similar dimension. The number of SWNTs tend to be larger than that of MWNTs under the same weight fraction because MWNTs are consisted of multilayers while a single layer for SWNTs. Accordingly, it is easier for SWNTs to form electrical conduction paths. As a result, DEs with 0.3 wt. % in the previous chapter is not actuated by applied electric field due to the electrical conduction of the specimen.

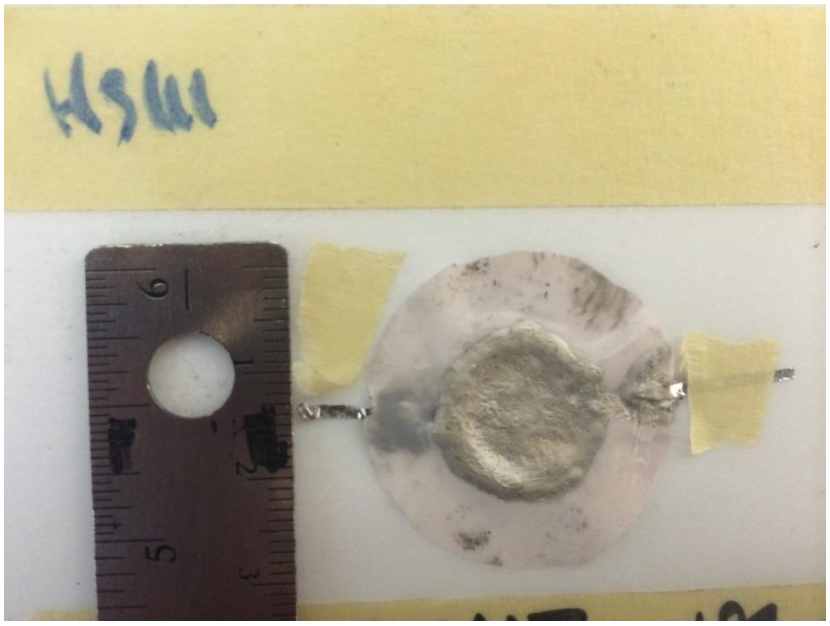

Fig. 4. 3. DE film specimen coated with diameter 16.67 mm using Ted Pella, Inc. fast drying silver paint.

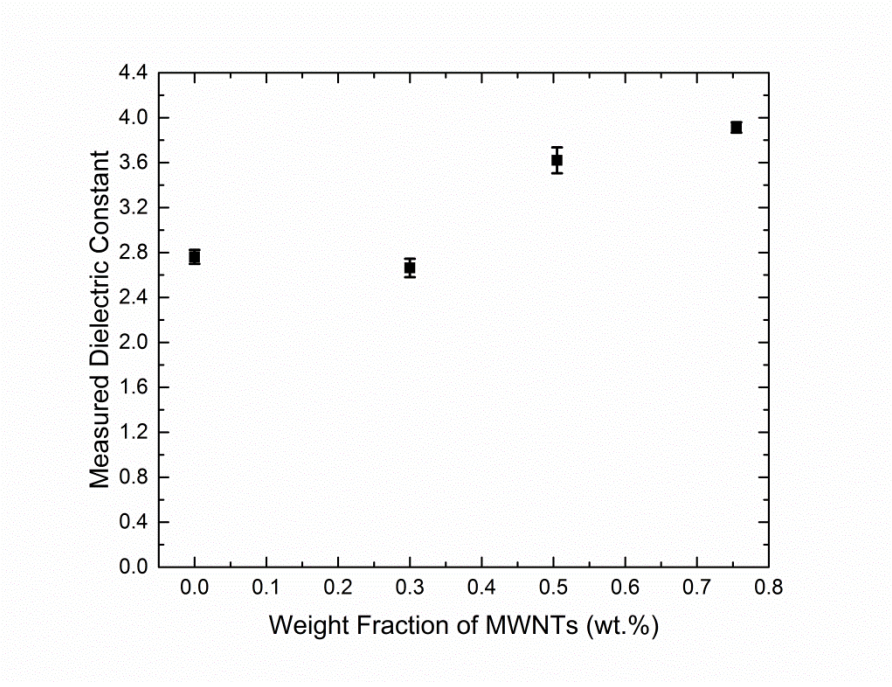

Fig. 4. 4. Extracted dielectric constant for DEs and DE nanocomposites with MWNTs.

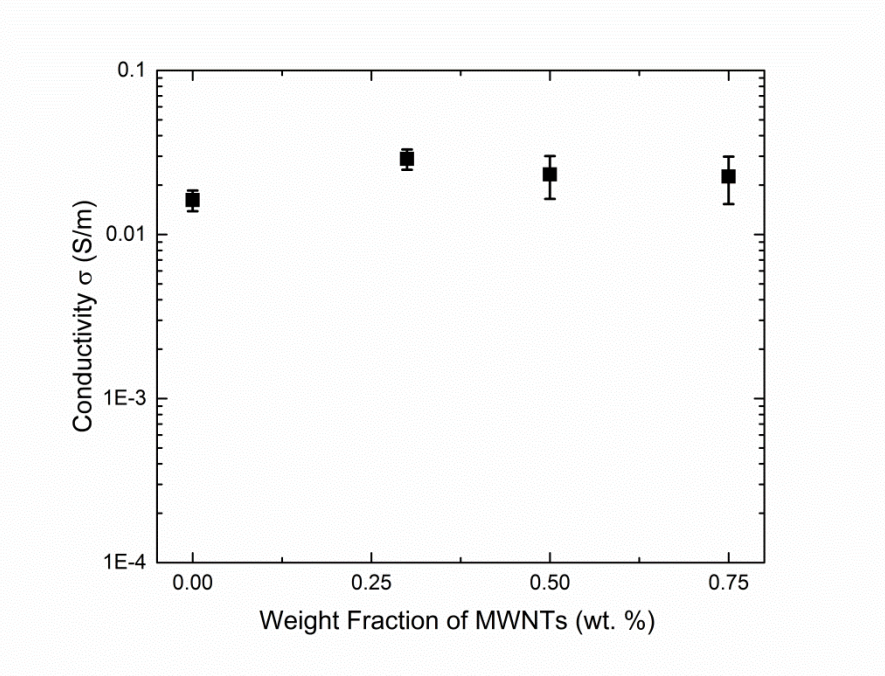

Fig. 4. 5. Measured conductivity of DEs and DE nanocomposites with MWNTs.

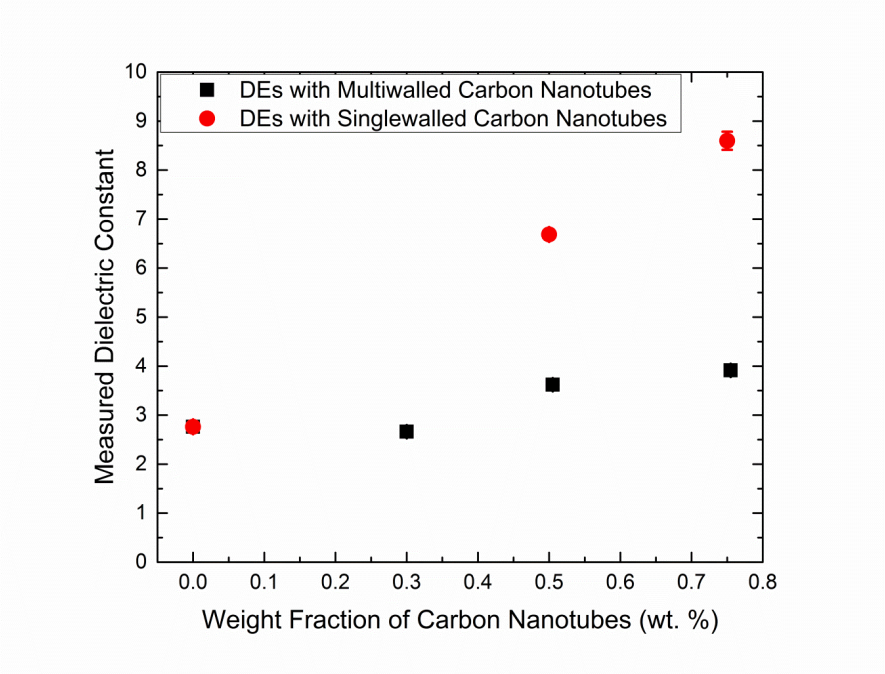

Fig. 4. 6. Extracted dielectric constant for DEs and DE nanocomposites with CNTs.

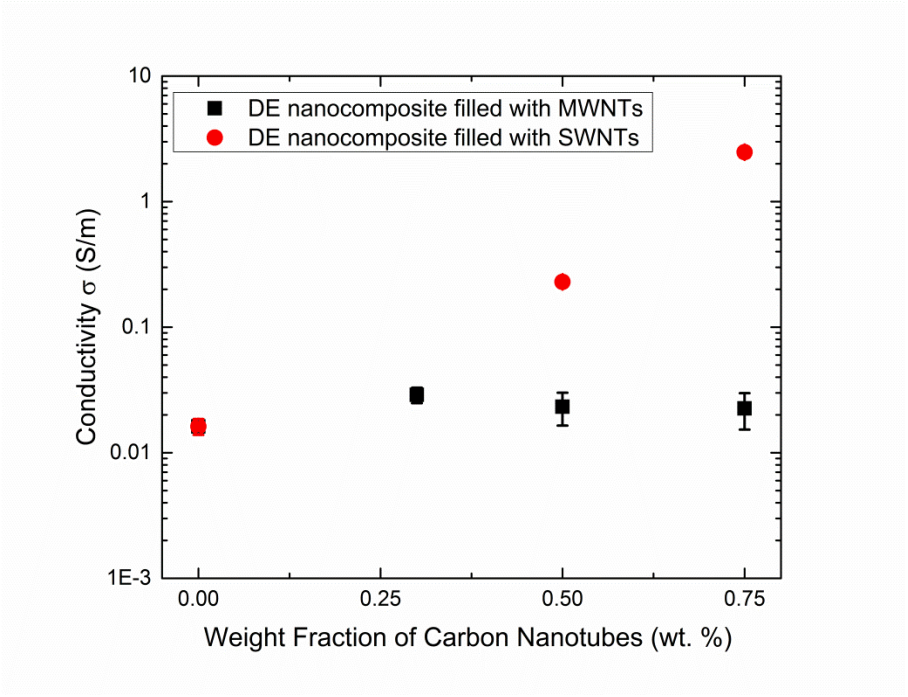

Fig. 4. 7. Measured conductivity of DEs and DE nanocomposites with MWNTs and SWNTs.

4.3.2 Static Mechanical Property of DE Nanocomposites Filled with MWNTs

Fig. 4.8 shows the measured displacement of DEs in static cases. Once the applied electric field is applied, the displacement reaches the equilibrium instantaneously, and stays in the equilibrium until the applied electric field is removed. As a result, it can be assumed that HS III DE can reach its relaxed state momentarily, under static compression loading. Thus, viscoelasticity is not considered in this section.

Fig. 4.9 shows the measured effective stress as a function of the stretch ratio in the loading direction. It is shown the effective stress due to the addition of MWNTs is increased by 10 % and 5.0 % for DEs with 0.75wt. % and 0.50 wt. % MWNTs respectively for wide range of stretch

ratio λ_3 in loading direction. This result is smaller than the enhancement of dielectric constant of DE nanocomposites reported in the previous section, which is 40 % and 28 % respectively. This shows that the dielectric properties of DE nanocomposites are more sensitive to the addition of MWNTs than mechanical properties under small concentration of MWNTs. This could be due to the bonding strength between the DE matrix and MWNTs which will be discussed in the next section. Due to the imperfect bonding between DE matrix and MWNTs, DE matrix and MWNTs slide from each other under compression loading, resulting in smaller reinforcement in the measured effective stress.

At larger concentration of MWNTs, dielectric constant cannot be defined due to the electrical conduction of DE nanocomposites although mechanical properties of DE nanocomposites are to be strengthened drastically due to the network formation of MWNTs [75, 98].

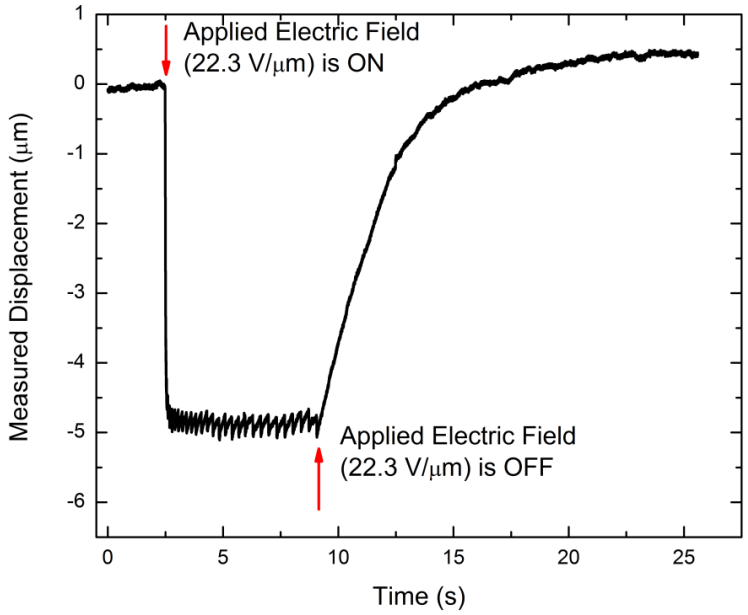

Fig. 4. 8. Measured displacement by laser Doppler vibrometer on applying and removing the electric field.

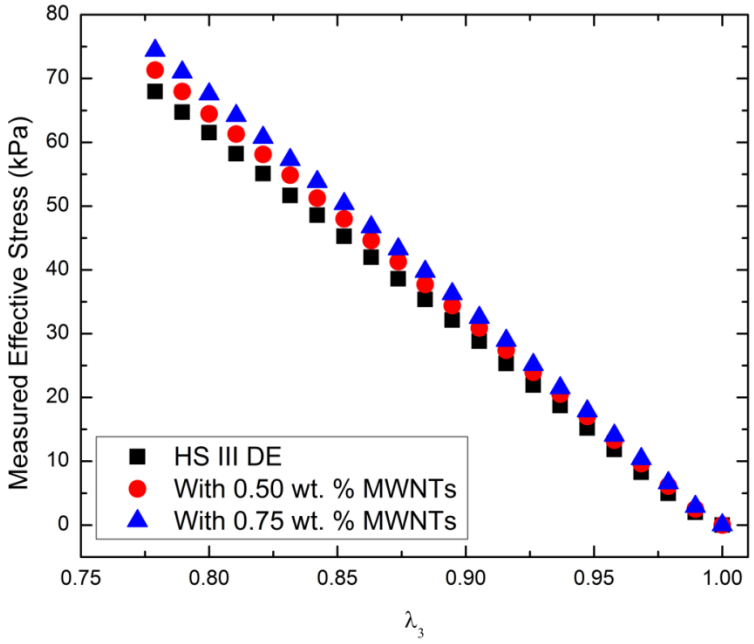

Fig. 4. 9. Measured static mechanical property of DEs and DE nanocomposites filled with MWNTs.

4.3.3 Amplitude and Frequency Dependence

The dependence of dynamic strain amplitude of dynamic mechanical properties is investigated and the results are shown in Fig. 4.10. The dynamic strain sweep is from 1.0 % up to 10.4 % at fixed pre-strain 10.0 % with frequency of 10 Hz.

At fixed frequency, although the gradual decrease of the storage moduli is observed for DEs and DE nanocomposites, the amplitude of the sinusoidal curve has very limited effect on the storage modulus of DEs and DE nanocomposites within the measured strain amplitude. This verifies that DEs and DE nanocomposites are still in elastic regions although thickness strain amplitude is

applied up to about 11 %. At fixed strain amplitudes in Fig. 4.10 (a) and (d), storage moduli show the increase with the increased concentration of MWNTs. This is due to the elastic moduli of MWNTs whose elastic moduli are in the range of GPa.

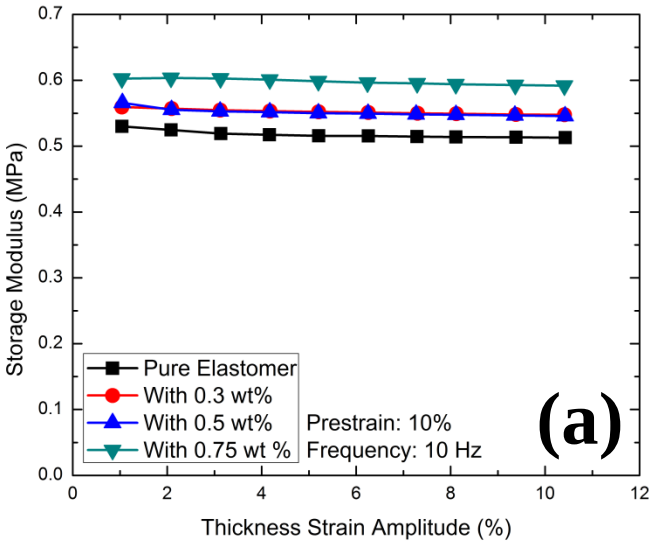

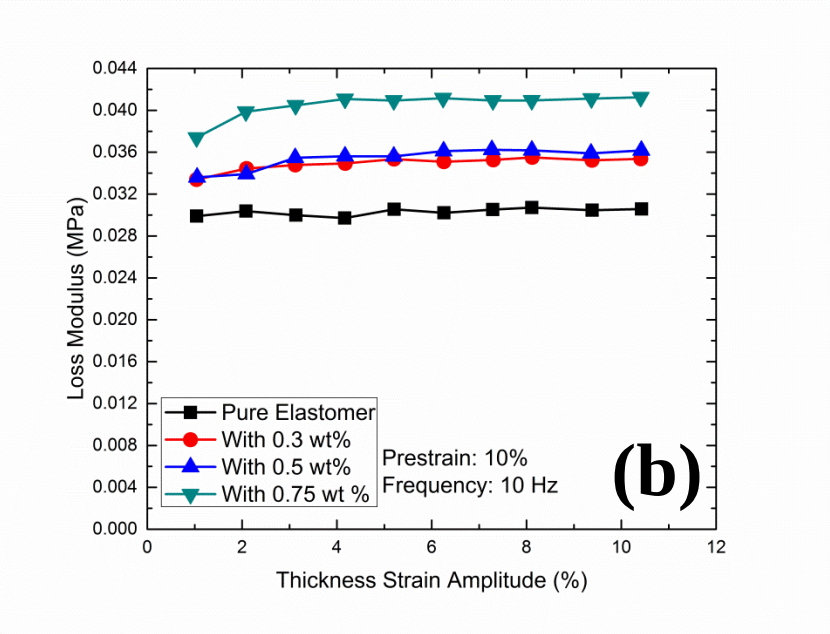
Loss Modulus (MPa)
0.044
0.040
0.036
0.032
0.028
0.024
0.020
0.016
0.012
0.008
0.004
0.000
0
2
4
6
8
10
12
Thickness Strain Amplitude (%)
Pure Elastomer
With 0.3 wt%
With 0.5 wt%
With 0.75 wt %
Prestrain: 10%
Frequency: 10 Hz
(b)

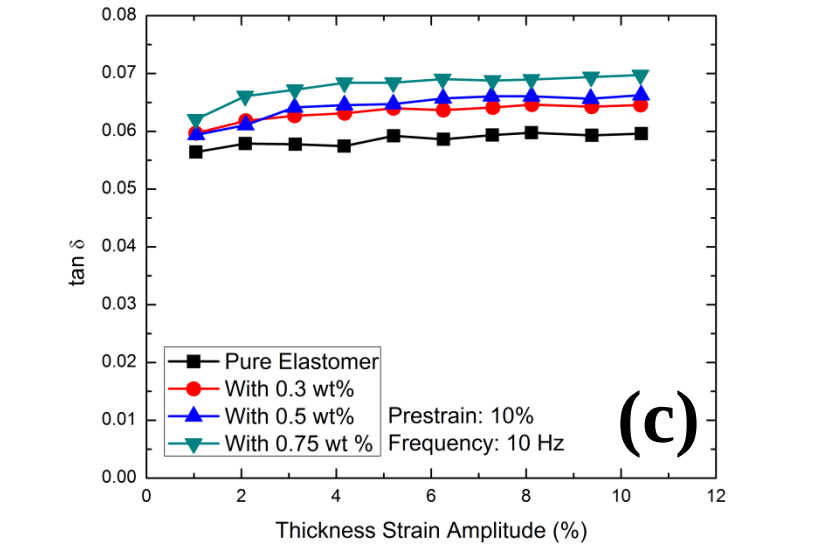
tan δ
0.08
0.07
0.06
0.05
0.04
0.03
0.02
0.01
0.00
0
2
4
6
8
10
12
Thickness Strain Amplitude (%)
Pure Elastomer
With 0.3 wt%
With 0.5 wt%
With 0.75 wt %
Prestrain: 10%
Frequency: 10 Hz
(c)

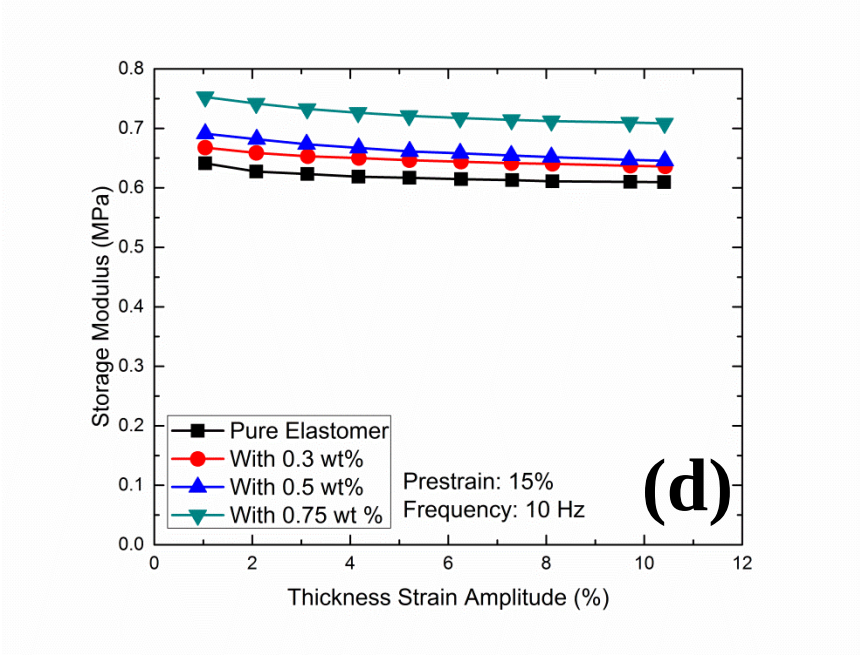
Storage Modulus (MPa)
Thickness Strain Amplitude (%)
Pure Elastomer
With 0.3 wt%
With 0.5 wt%
With 0.75 wt %
Prestrain: 15%
Frequency: 10 Hz
(d)

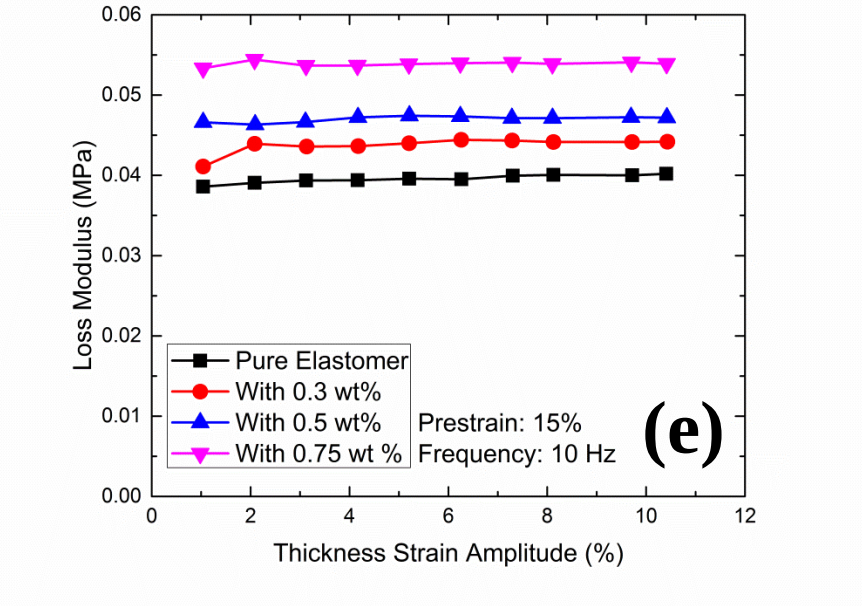
Loss Modulus (MPa)
Thickness Strain Amplitude (%)
Pure Elastomer
With 0.3 wt%
With 0.5 wt%
With 0.75 wt %
Prestrain: 15%
Frequency: 10 Hz
(e)

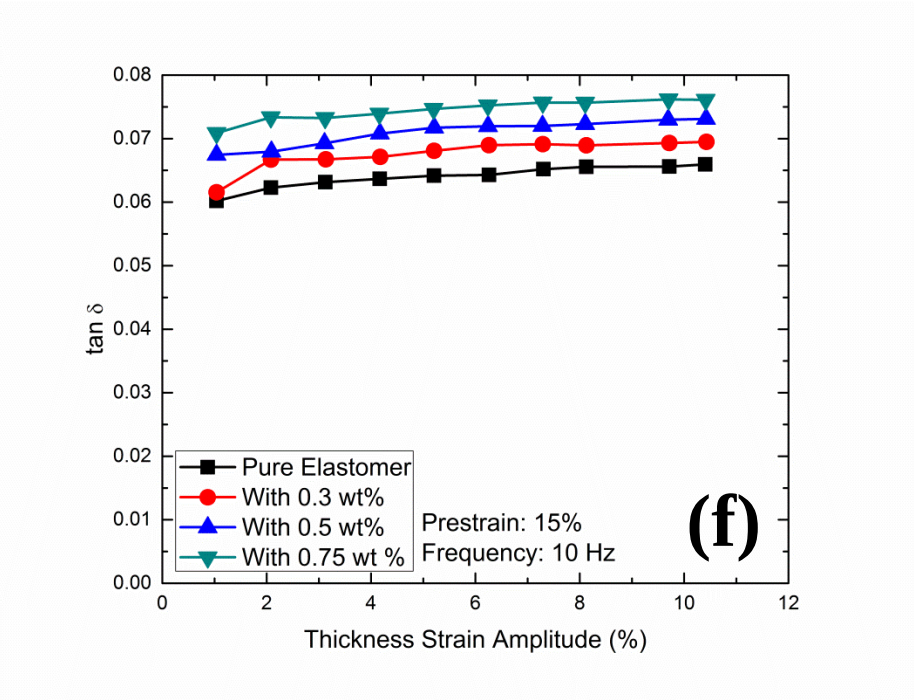

Fig. 4. 10. (a) Storage modulus, (b) loss modulus and (c) loss factor of DEs and DE nanocomposites filled with MWNTs with 10 % pre-strain at 10 Hz. (d) Storage modulus, (e) loss modulus and (f) loss factor of DEs and DE nanocomposites filled with MWNTs with 15 % pre-strain at 10 Hz.

The addition of MWNTs results in higher loss modulus and loss factor. Regardless of the pre-strain, the addition of 0.75 wt. % MWNTs increases loss factor by 15 %. This means that the interaction between DEs and MWNTs causes energy loss under cyclic loading although MWNTs are usually considered to be elastic materials [130]. As the amplitude increases, elastomers which have initially been bonded to the filler tend to be partially debonded from MWNTs, resulting in local sliding and friction at the interphase between the DE matrix and MWNTs. When the amplitude is larger than 5 %, the loss modulus and $\tan\delta$ reaches constant values for DE nanocomposites. This might indirectly show that the no more net partial debonding of DEs from MWNTs is progressing once the strain amplitude goes beyond 5 % at the fixed frequency.

Further changes of storage, loss moduli and loss factor depend on the frequency of applied cyclic loadings. Fig. 4.11 shows the storage and loss moduli and associated loss factor ($\tan\delta$) of DEs and DE nanocomposites with MWNTs as a function of frequency of the dynamic loading. Storage and loss moduli are found to increase with frequency, which reflects the linear viscoelastic nature of elastomer composites at small strains [131].

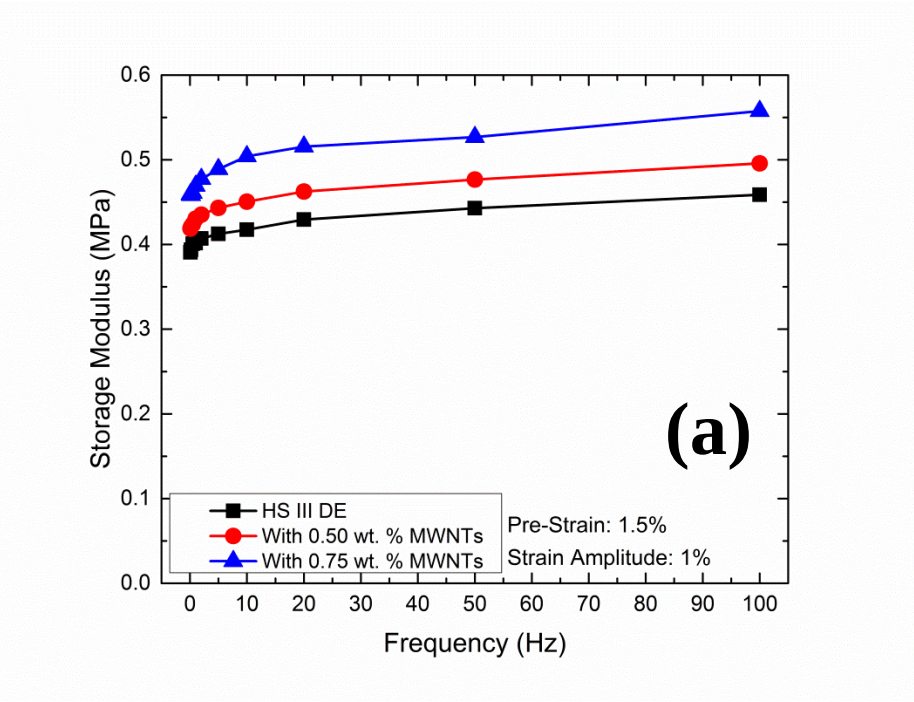

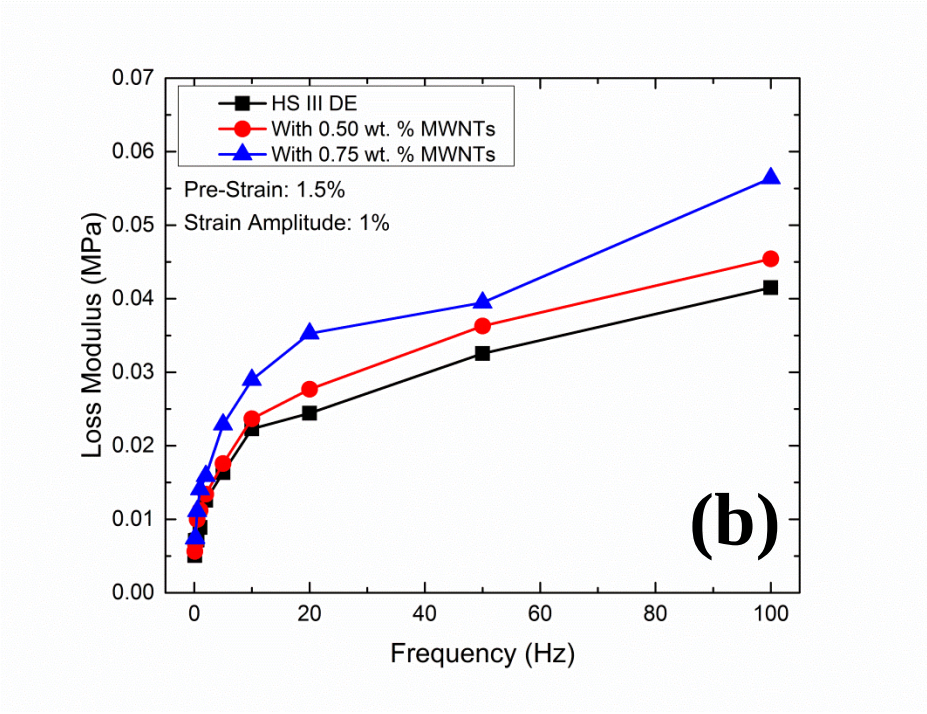

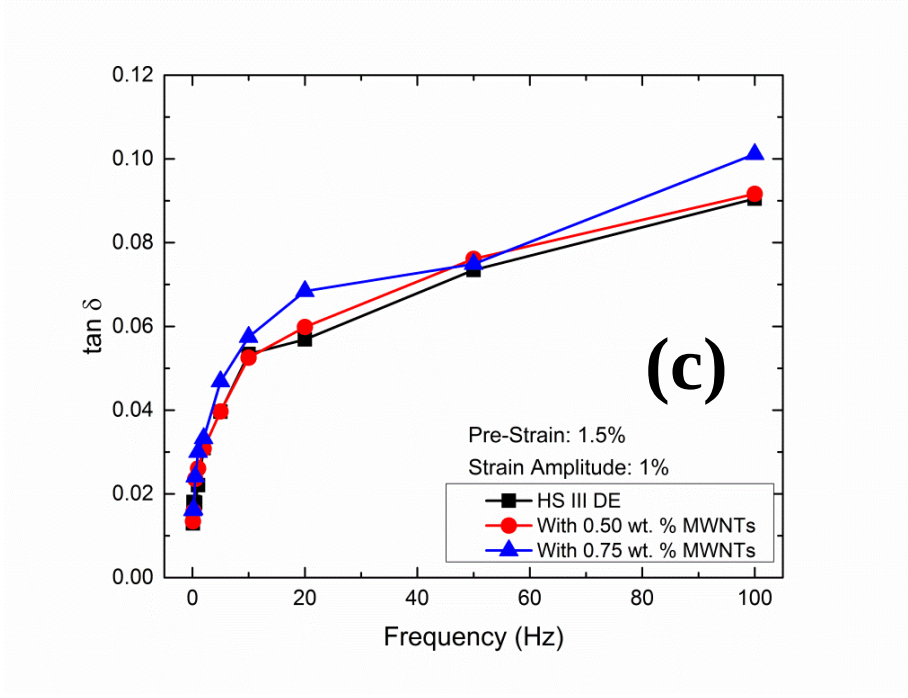

Fig. 4. 11. (a) Storage modulus, (b) loss modulus and (c) loss factor of DEs and DE nanocomposites filled with MWNTs under cyclic loading with varying frequency with pre-strain 1.5 %, strain amplitude 1 %.

4.4 Conclusions

This chapter investigates the dielectric and mechanical properties of DEs and DE nanocomposites. It is experimentally demonstrated that dielectric property of DEs is more sensitive to the addition of MWNTs than mechanical property of DEs at low MWNT concentration. This could explain the enhanced electromechanical response of DE nanocomposites. Enhanced dielectric properties enable more charges to accumulate on the electrodes, resulting in the larger stress between the electrodes. Meanwhile, less change in mechanical properties further improves the deformation enabled by the enhanced stress.

Dynamic mechanical analysis reveals that the interface between DE matrix and MWNTs is one of the primary factors deciding the mechanical properties of DE nanocomposites. This has posted the future work to analyze the interface effect by investigating the DE nanocomposites filled with pristine MWNTs or functionalized MWNTs as functionalized MWNTs enable stronger bonding between DE matrix and MWNTs and better dispersion [81, 83].

Chapter 5 Filler Orientation Effect on Relative Permittivity of Dielectric Elastomer Nanocomposites Filled with Carbon Nanotubes

5.1 Introduction

Electro active polymers (EAPs) have been attracting attention in the field of electro-mechanical actuation and sensing. Dielectric elastomers (DEs), an emerging area of EAPs, have been showing promising functionalities as energy harvesting materials [5, 6] as well as actuating materials for potential applications such as artificial muscles, capacitors, sensors, and even generators due to their high electromechanical efficiency, durability, stability, lightweight, low cost, and easy processing [1, 6, 9, 19, 22]. Despite the advantages of DEs, technical challenges must be resolved for wider applications. A high electric field of at least 10-30 $V/\mu m$ is required for the actuation of DEs, which limits the practical applications especially in biomedical fields [6, 11]. A common solution to the disadvantages of DEs is to enhance their relative permittivity by implementing ceramic powders with high dielectric constant such as TiO_2 particles [42], $BaTiO_3$ nanoparticles [43-45] and $PbTiO_3$ [47, 48] to generate high electromechanical responses with lower applied field level. However, high loading, up to 20-30 vol.% of these particles are required for meaningful increase, at which the ceramic powders filled composite materials could lose its flexibility, leading to limited improvement of the electromechanical response. Recently, carbon nanotubes have been reported to efficiently enhance the relative permittivity with a small loading fraction up to 2 wt. % due to its high aspect ratio and conductivity while avoiding the unwanted increase of the materials rigidity [49-52].

A various factors can affect the effective dielectric constant of composite materials with high aspect ratio fillers: amount of fillers, filler shape [132], filler aspect ratio, filler dispersion, distance between each filler [124], waviness of the fillers [125, 133], interaction between fillers and matrix [134], and orientation of the fillers. Different filler orientation may cause anisotropic dielectric constant. As a result, fillers parallel to the applied electric field can significantly enhance the effective dielectric constant, while the ones perpendicular to the applied electric field do not have primary impact on the effective dielectric constant. Many theories have been developed to predict the effective dielectric constant of composite materials such as Maxwell-Garnett (MG) rule of mixture [135, 136], and finite-element-based approaches [45, 137]. Some works have also focused on the filler orientation effects on both electrical and mechanical properties in extreme cases [132, 138-140]. The experimental efforts have been done on the alignment of MWNTs [139, 141], and characterization of the dielectric constant electromagnetic properties of aligned ceramic based nanowires [140] and polymer based composites with aligned MWNTs [138, 142-144]. However, detailed specific relationship between the filler orientation parameter and the associated effective dielectric constant value, especially for composite materials with fillers of high aspect ratio and rod-like shape, has not been revealed yet. Thus, it is demanded to investigate how the filler orientation can affect the overall materials properties while the filler orientation transits from one to another.

In this chapter, finite element analysis (FEA) is performed in three-dimensional (3D) unit cell models to investigate the filler orientation effect on the dielectric properties of dielectric elastomer nanocomposites with high aspect-ratio fillers. A statistical approach is employed to obtain a comprehensive understanding on how the mean angle of the MWNTs is associated with the theoretical effective angle when MWNTs are randomly dispersed in the dielectric elastomers.

Specifically, we fabricate, characterize and simulate the dielectric elastomer nanocomposites with randomly orientated MWNTs. Experimental results are compared with predictions given by FEA. We also show the approaches on how to reduce the model sizes to achieve less numerical efforts without sacrificing the accuracy of the results. Finally, the relationship between the mean filler angle and the corresponding effective dielectric constant is revealed.

5.2 Materials, Fabrication, and Characterization

Alumilite HS III RTV high strength mold-making silicone rubber is chosen as a dielectric elastomer material in this study. Under our materials processing method, dielectric elastomers with MWNT concentration above 0.75 wt. % are close to or reaching the electrical percolation threshold and showing electrical conductivity. Thus, two sets of 0.50 wt. % and 0.75 wt. % of MWNTs are added as fillers to dielectric elastomers to investigate the materials dielectricity. MWNTs are purchased from Cheap Tubes, Inc., having diameters of 20-30 nm with 95 wt. % purity.

The fabrication process are consisted of six steps: (1) grinding the pristine MWNT aggregates with a mortar and pestle, (2) stirring and dispersing MWNTs in acetone solution by ultrasonic processor (Sonics & Materials, Inc., VCX 130) for hours, (3) pouring the dielectric elastomer matrix into the solution followed by accelerated evaporation of acetone with a hot plate, (4) adding the curing agent followed by mixing, (5) vacuum degasing the mixture for minutes, and (6) spin coat the materials to obtain thin film specimens with controlled thickness. Grinding and solution mixing with ultra-sonication are utilized to break the Van der Waals forces between

MWNTs, and to improve MWNTs dispersion and also to minimize the formation of MWNT aggregates [79, 94, 95]. Vacuum degasing is utilized to eliminate air voids. The nanocomposite films are fabricated on silicon wafer substrates using Laurell spin coater, and the typical thickness is between 150 to 160 μm measured by Digital Instruments Dektek 3 surface profiler.

For the nanocomposite film with MWNTs of concentration 0.75 wt. %, a cross section of a fractured surface is imaged by using FEI Quanta 3D FEG scanning electron microscope (SEM) to examine the microstructures. MWNTs after ultra-sonication process mentioned above are observed by using FEI/Philips CM-20 transmission electron microscope (TEM) to obtain the typical filler aspect ratio. Both sides of the film specimens are coated with silver based electrodes with diameter 16.67 mm using Ted Pella, Inc. fast drying silver paint for capacitance measurement. This MIM (Metal-Insulator-Metal) is measured using HP 4280A 1MHz C Meter/C-V plotter at room temperature 24 ℃, and dielectric constant is further extracted from the measured capacitance. At least 10 measurements are carried out for each specimen.

5.3 Finite Element Methodology

5.4.2 Periodic Boundary Conditions and Materials Properties

Three-dimensional finite element analysis (FEA) is performed using commercially available FEA software, COMSOL Multiphysics (version 4.4). The geometry of the unit cell is set to be a half cubic due to the symmetry of the top half and bottom half. Using symmetries can reduce the model size from a cubic to a cuboid shown in Fig. 5.1.

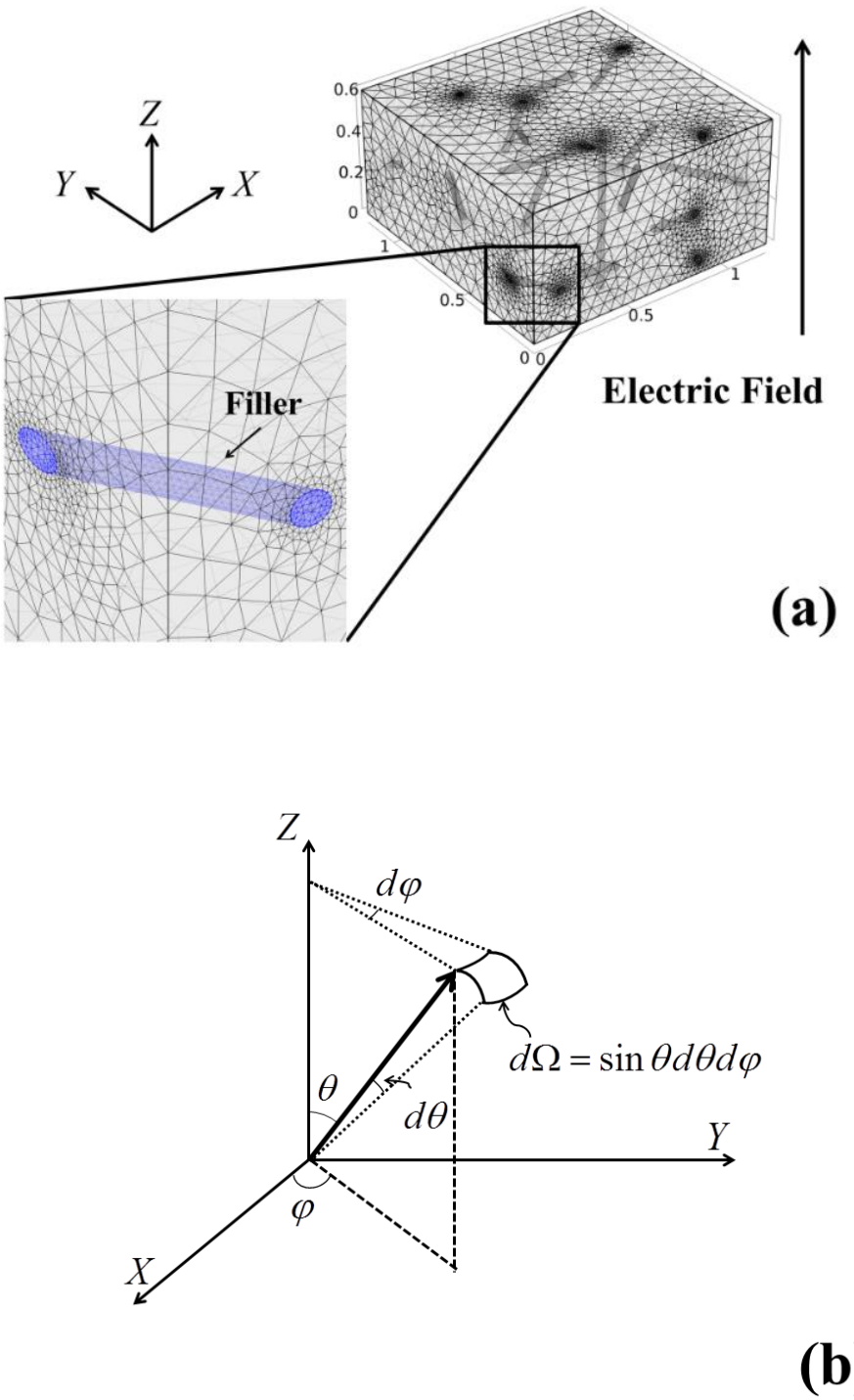

Fig. 5. 1. (a) The unit cell model used in FEA; (b) the coordinate system used to define the filler orientation.

A unit cell is a fundamental repeating block of the representative material microstructure, and therefore the continuity of the structures has to be satisfied. To assure the continuity of the electric field and the potential at the edges, periodic geometry and periodic boundary conditions are applied. For any points on the corresponding opposite boundaries, the potential is set to be identical. Fixed voltage values are applied on the Z plane shown in Fig. 5.1 (a). The effective dielectric constant is calculated over the entire domains using the following relation.

$$\langle D \rangle = \varepsilon_{eff} \langle E \rangle$$

where $\langle D \rangle$ is the volume average of electric displacements, and $\langle E \rangle$ is the volume average of electric fields in Z -direction.

The material properties used in this study are listed in Table. 5.1. Although MG rule of mixture predicts the increase of the effective dielectric constant with the dielectric constant of the fillers, it does not consider the effects of the high aspect ratio and its distribution, and the rod-like shape of MWNTs. For nanocomposites with fillers of high aspect ratio and rod-like shape, the effective dielectric constant of the nanocomposites is not sensitive to the dielectric constant of MWNTs when the contrast between the dielectric constant of MWNTs and that of dielectric elastomer is large enough [45]. For instance, when the filler dielectric constant varies from 5000 to 120000, the effective dielectric constant of the nanocomposites increases for 3.4 %, from 3.81 to 3.94, in a model with filler aspect ratio 20 and filler weight fraction of 0.75 %. For this reason, the dielectric constant of MWNTs is set to be 90000 experimentally obtained at 1Hz from Basu et al.[50, 145] even though the exact value for MWNTs used in this study is unknown.

Table. 5. 1. Material property input used in FEA.

Material	Dielectric constant	Diameter	Aspect ratio
MWNTs	90000 [50]	30 nm	20
Dielectric Elastomer	2.8	-	-

Ultra-sonication and grinding during the fabrication process introduce the breakage of MWNTs, resulting in the shortened aspect ratio [95-99]. It is reported that the aspect ratio strongly depends on the material processing, and 420, 80 and 8 are reported as MWNT average aspect ratio under different treatments even for the same MWNTs [98]. Ten MWNTs after ultra-sonication are examined in TEM, and the average diameter 30 nm with average length 600 nm is observed. Fig. 5.2 shows one of the fillers observed using TEM. Although the exact MWNT aspect ratio distribution in the nanocomposites is unknown, 20 is a reasonable value as reported in literature [98, 99]. In this study, MWNTs are represented by cylinders with diameter of 30 nm and aspect ratio of 20.

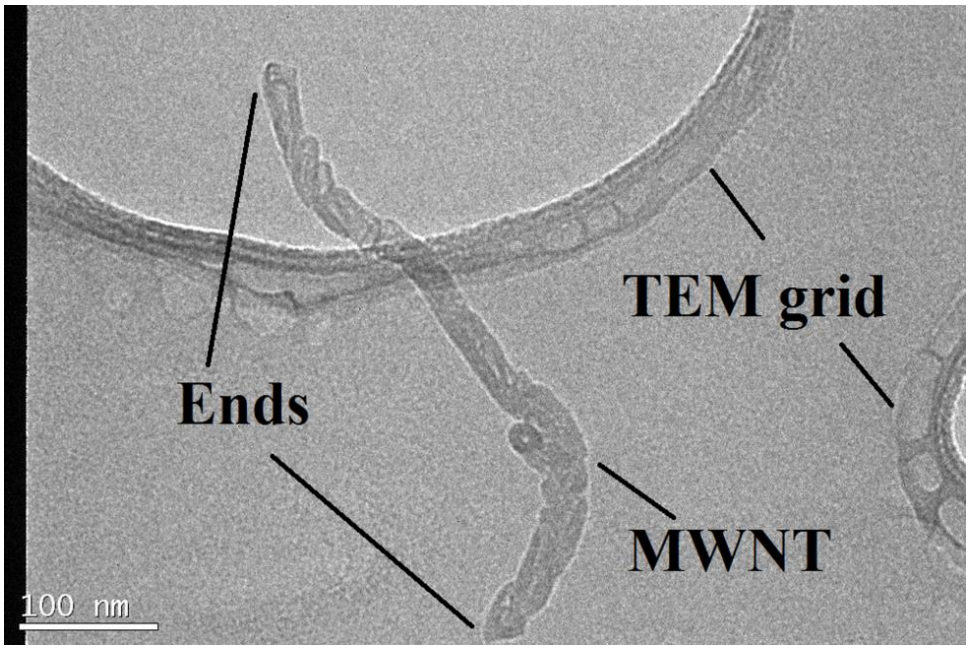

Fig. 5. 2. TEM image of a typical MWNT after ultra-sonication (before mixing with dielectric elastomer matrix).

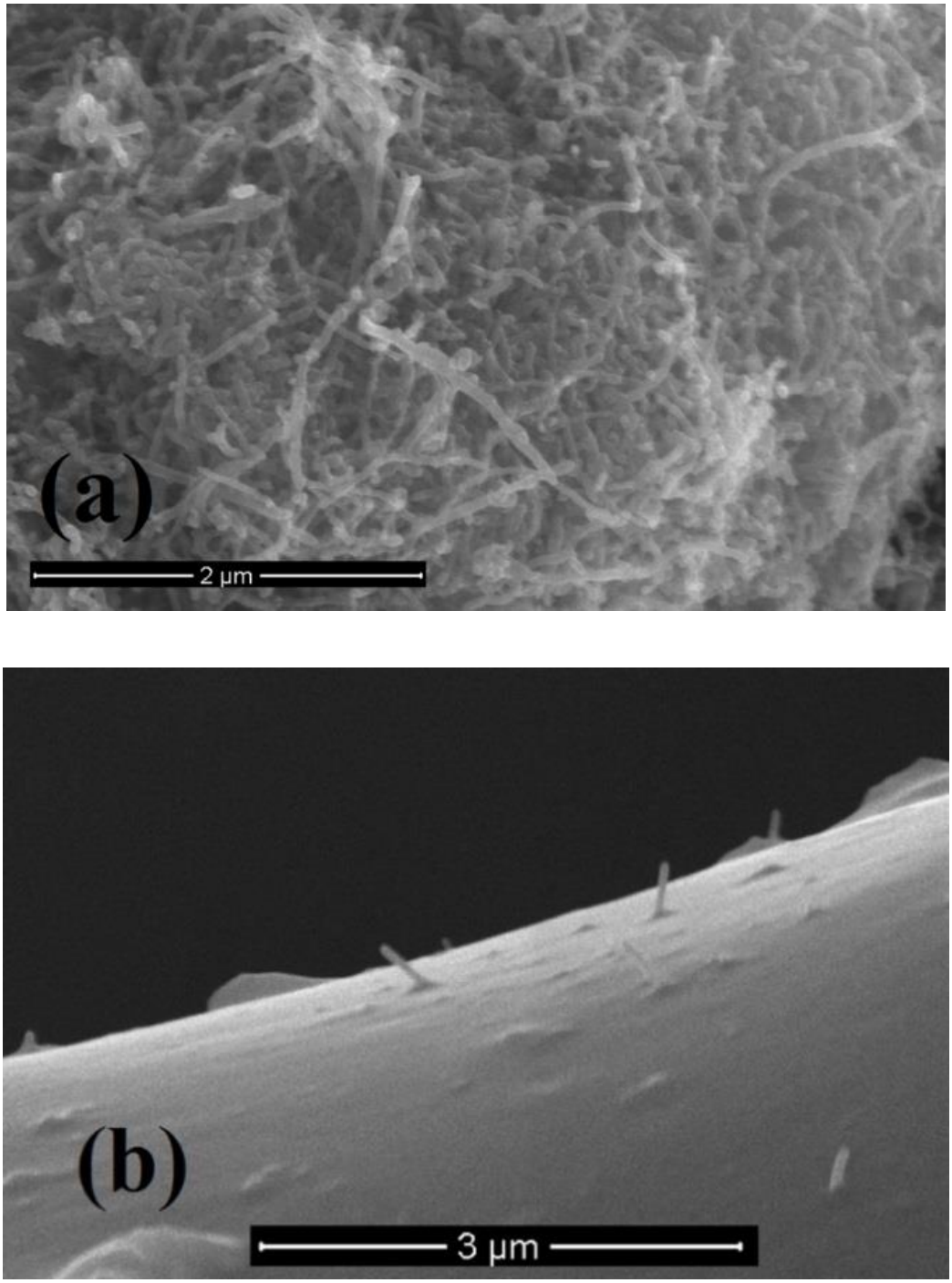

Fig. 5. 3. SEM images showing (a) pristine MWNTs before processing and (b) the randomly oriented MWNTs in a cross section.

Figure 5.3 (a) shows the pristine MWNTs before processing. After the fabrication process, a micrograph of a cross section of the nanocomposite with 0.75 wt. % MWNTs is taken as shown in Fig. 5.3 (b), and the microstructure of the nanocomposite is obtained. During the fabrication process of the dielectric elastomer nanocomposites, no electric field is introduced. Therefore, the orientation of the MWNTs inside the nanocomposite is considered to be pure random (mis-oriented).

5.4.3 Theoretical Effective Angle in a Random Orientation Model

To investigate the effective angle parameters in a random orientation model, cylinder-shaped fillers are generated with random angle θ and φ without overlapping each other as shown in Fig. 5.1 (b). To ensure the uniform distribution of the angle parameters, spherical uniform distribution is employed.

The angles θ and φ are defined as $0 \le \theta \le \pi$, $-\pi \le \varphi \le \pi$. Due to the spherical symmetry, the range can be reduced to $0 \le \theta \le \pi/2$, and $-\pi/2 \le \varphi \le \pi/2$. An area element Ω is defined as $d\Omega = \sin\theta d\theta d\varphi$ in a unit sphere shown in Fig. 5.1 (b). The probability that a point sits in an infinitesimal cone can be described as $P(\Omega)d\Omega$ with the normalization specified as $\int P(\Omega)d\Omega = 1$. Over a unit quarter sphere, $P(\Omega) = 1/\pi$. From $P(\Omega)d\Omega = P(\theta,\varphi)d\theta d\varphi$, $P(\theta,\varphi) = \sin\theta/\pi$ is obtained. Therefore, the effective angle $\langle\bar{\theta}\rangle$ of a model with randomly oriented fillers can be described as

$$\left\langle \bar{\theta} \right\rangle = \int_{-\pi/2}^{\pi/2} \int_{0}^{\pi/2} \theta P(\theta, \varphi) d\theta d\varphi = 1 \text{radian} = 57.3^{\circ}$$

5.4.4 Numerical Accuracy of the Models

Ten-node tetrahedral elements are used in the space domain for unit-cell FEA. Typical models of all cases are shown in Table. 5.2 along with the number of ten-node tetrahedral elements and the computed effective dielectric constant values. Although the number of elements, nodes and computed values are different from each model due to the difference in geometry, sufficiently refined meshes are applied to all the models to ensure calculations are sufficiently accurate. Table. 5.2 shows that the mesh refinement results in small changes. For models with 5 or 9 fillers, the difference of the values provided by "normal" mesh and "extra fine" mesh is less than 0.03 % as shown in Table. 5.2, demonstrating that the additional mesh refinements are not required for those models. By contrast, for models with 20 or 40 fillers, at least "finer" mesh is required due to the complexity of the geometry, resulting in much longer computing time. For models with 20 or 40 fillers, the difference of the mesh density caused less than 0.79 % difference in the calculated values. Therefore, it is judged that the "normal" mesh provides sufficiently accurate results for models with 5 or 9 fillers, while "finer" mesh for models with 20 or more fillers.

Table. 5. 2. Comparison of results by representative models for different finite element meshes for nanocomposites with 0.75 wt. % fillers.

Mesh description	Normal	Fine	Finer	Extra Fine
Number of tetrahedral elements	48896	145382	413702	915856
Dielectric constant (5 fillers)	3.640	3.640	3.639	3.639
Number of tetrahedral elements	69171	189507	704397	1462136
Dielectric constant (9 fillers)	4.007	4.007	4.003	4.002
Number of tetrahedral elements	-*	-*	1410948	3073279
Dielectric constant (20 fillers)	-	-	3.861	3.850
Number of tetrahedral elements	-*	-*	1903693	5978299
Dielectric constant (40-fillers)	-	-	3.569	3.597

*- indicates that the geometry cannot be meshed by the given mesh categories.

5.4Results and Discussion

5.4.1 Orientation Parameter θ and φ

The influence of the orientation parameters is systematically investigated. Ten models with randomly oriented five, nine, twenty, and forty fillers are examined. Fig. 5.4 (a)-(d) illustrate the

trend that the effective dielectric constant increases with the decrease of the mean orientation angle θ. The correlation coefficient is calculated to investigate the relationship between the effective dielectric constant and the orientation parameters shown in Table. 5.3. Further, $|R_\theta|$ and $|R_\varphi|$ represent the correlation coefficient between the effective dielectric constant and θ or φ. Regardless of the number of fillers in models, strong correlation is found from $|R_\theta|$. On the other hand, weak correlation is found from $|R_\varphi|$. This demonstrates that effective dielectric constant along Z direction is primarily controlled by the parameter θ which relates the deviation from Z direction. In addition, φ has little influence on the effective dielectric constant along the applied electric field direction. Thus, the rest of the results and discussion are based on the orientation parameter θ.

Table. 5. 3. Correlation coefficient between the effective dielectric constant of the nanocomposites and the filler orientation parameter θ or φ.

Number of fillers in models	$\|R_\theta\|$	$\|R_\varphi\|$
5	0.954	0.139
9	0.797	0.0706
20	0.587	0.301
40	0.872	0.125

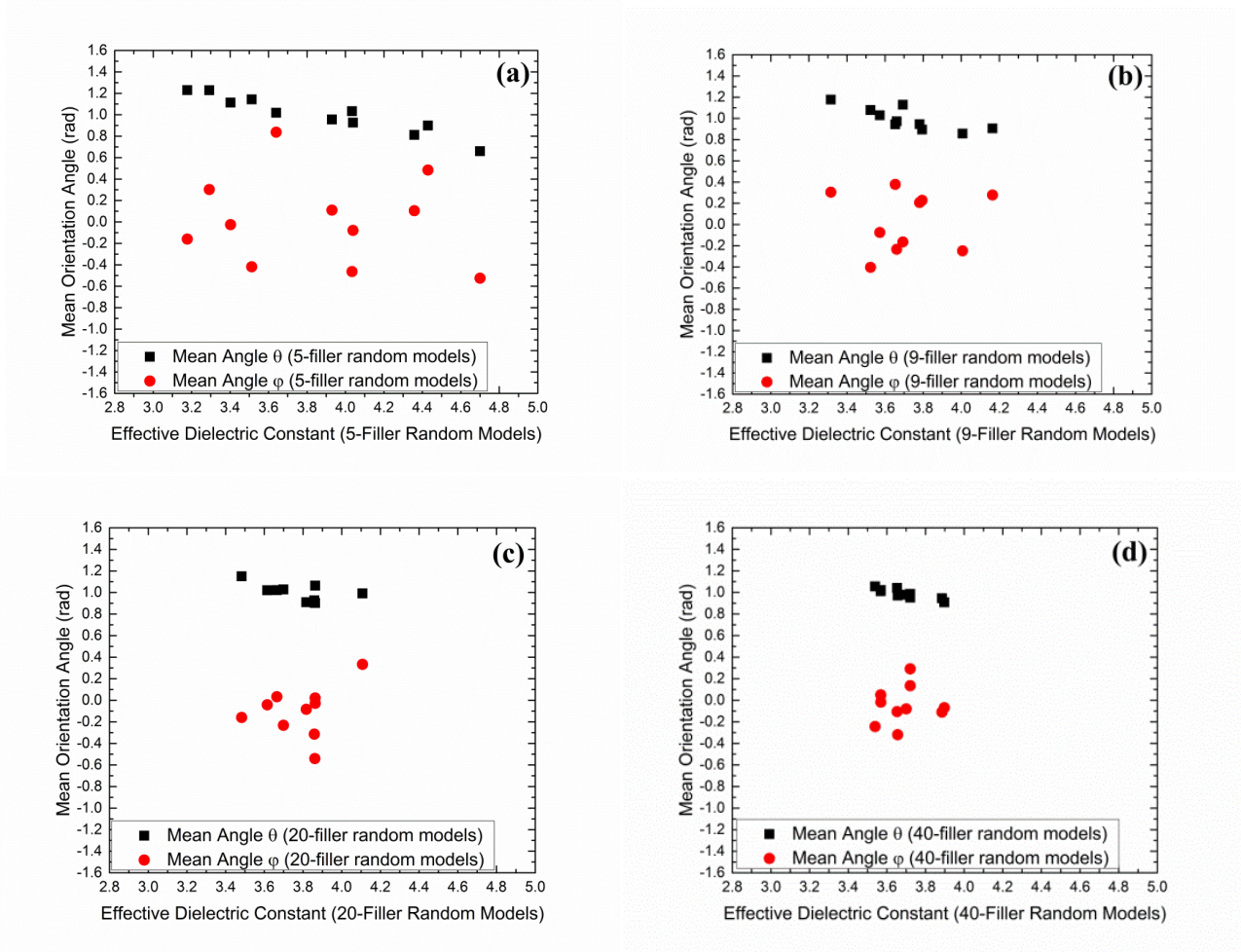

Fig. 5. 4. (a)-(d) Relationship between the orientation parameters and the effective dielectric constant of nanocomposites based on 10 random models with 5, 9, 20 or 40 fillers respectively.

5.4.2 Unit-Cell Model Size Effect

Various sizes of the 3D unit-cell models with randomly oriented fillers are studied for the comparison of unit-cell size effect and the numerical efforts. Models with 5, 9, 20 and 40 fillers shown in Fig. 5.5 are analyzed and compared. Ten models with randomly oriented fillers are created for each case. The results are shown in Fig. 5.6. The error bar is derived from one standard deviation based on ten models each. The calculated effective angle from Eq. (2), 1 radian (57.3°), has a good agreement with the mean angle of the random-orientation numerical models.

Five-filler models show the scattering of the effective dielectric constant varying from 3.36 to 4.36 while the models with nine or more fillers demonstrate the dispersion ranging from 3.46 to 3.97. The size of the error bar shrinks to 51% in size from five-filler models to nine-filler models, resulting in more consistent results. This is due to the larger number of orientation angles in a larger unit cell model with more fillers, resulting in more consistent dielectric constant values.

Table. 5. 4. Normalized minimum required computing time for models with 5, 9, 20 and 40 fillers.

Number of fillers in each model	5	9	20	40
Normalized minimum computing time	0.661	1.00	66.8	88.8

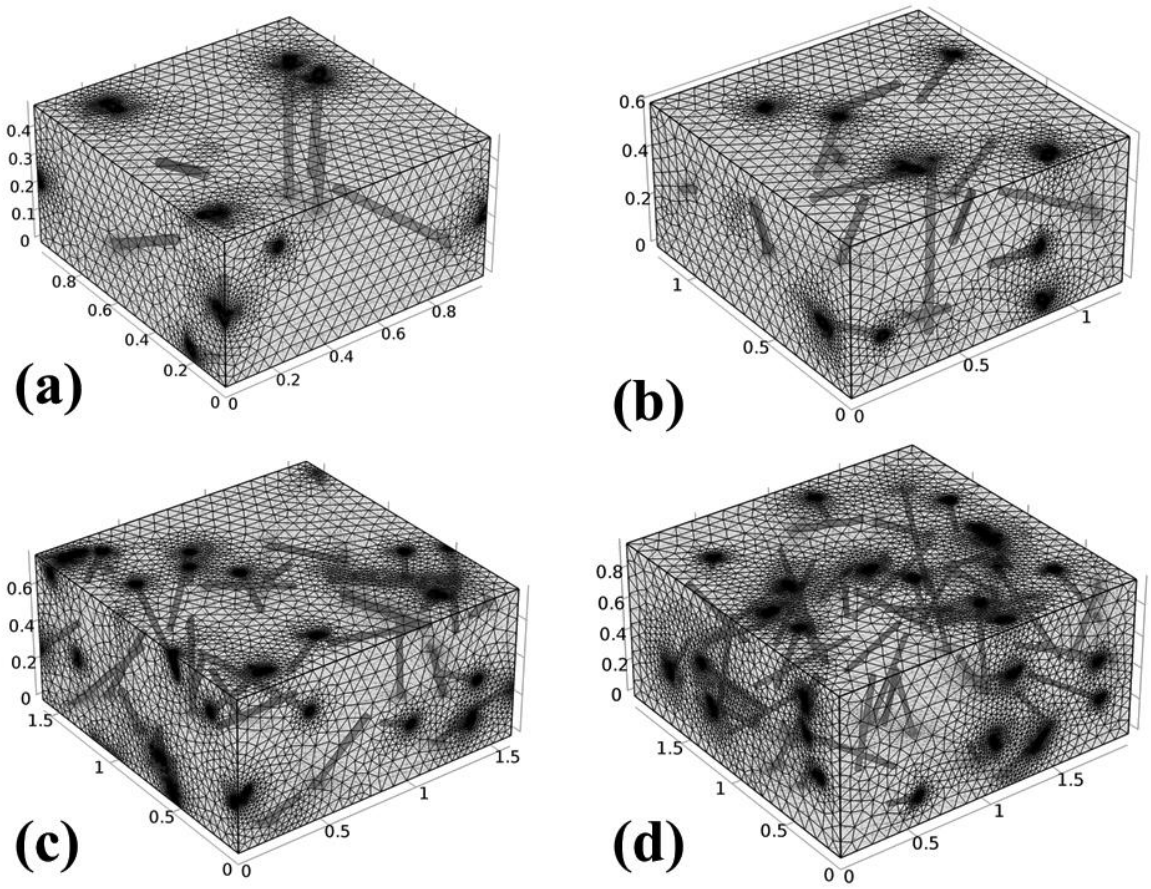

Fig. 5. 5. Examples of microstructures with "finer" mesh for 0.75 wt.% fillers: (a) 5-filler models, (b) 9-filler models, (c) 20-filler models, and (d) 40-filler models. Periodic geometry is defined at the boundaries for fillers. The unit in the axes is μm.

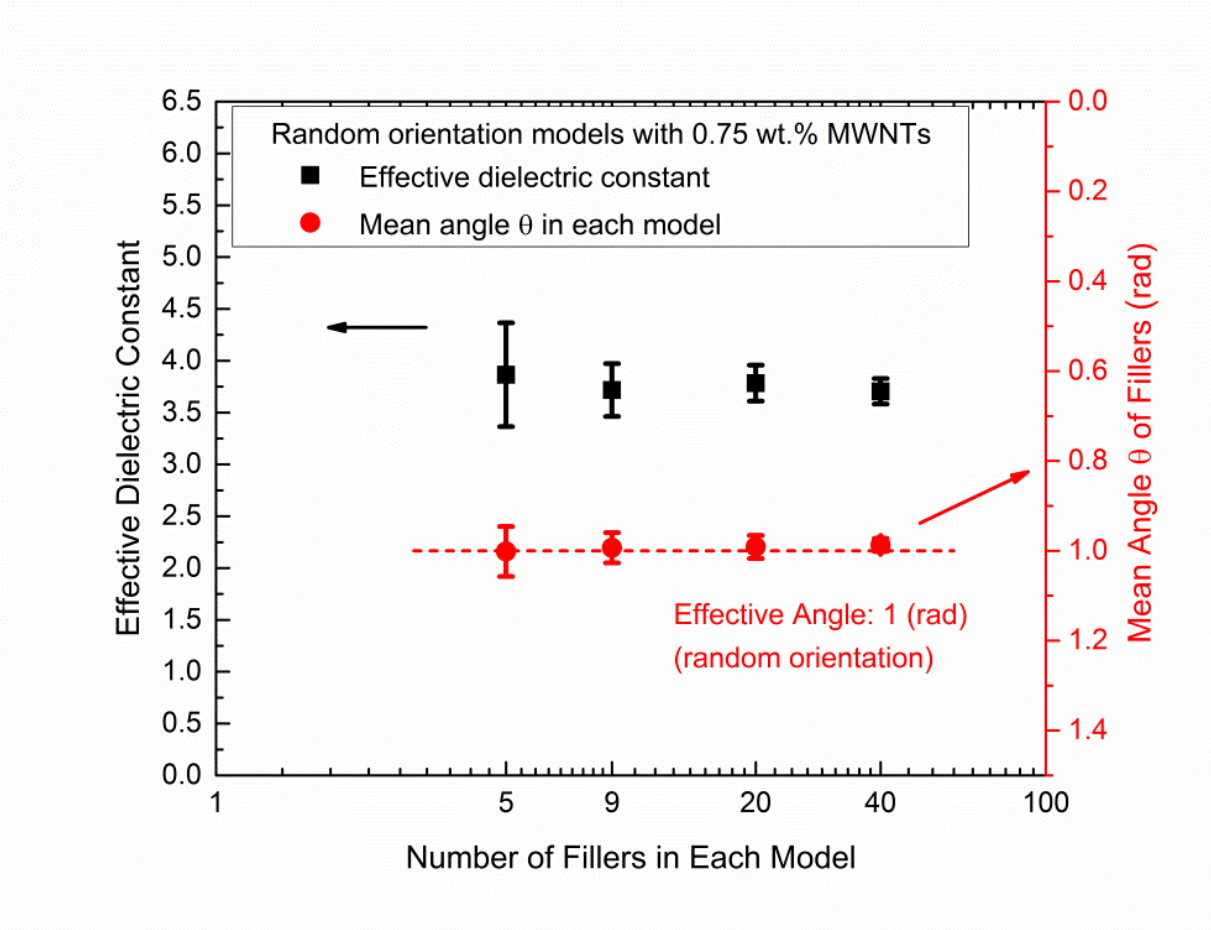

Fig. 5. 6. A comparison of (1) effective dielectric constant with respect to the unit cell size with the error bar derived from one standard deviation based on 10 models each; (2) a comparison of mean angle θ with respect to the unit cell size with the error bar derived from one standard deviation based on the mean values of 10 models each.

It is also illustrated in Fig. 5.6 that the deviation from the theoretical angle θ (1 radian) results in larger scattering of the effective dielectric constant, indicating that the dielectric property of the nanocomposites with randomly oriented fillers is significantly affected by the mean angle θ of the fillers in the microstructures. Furthermore, Table. 5.4 shows that a model with fillers greater than or equal to 20 requires much more numerical efforts compared to models with 9 fillers. This is due to the complicated geometry in models of 20 or more fillers which requires at least "finer" mesh, resulting in larger number of elements to solve as shown in Table. 5.3. As a result, the minimum required computing times was drastically increased for models with 20 or more fillers as shown in Table. 5.4. Although larger number of fillers could provide more consistent prediction, calculations are not affordable in most of the cases. Therefore, 9 fillers are determined to be sufficient to represent the microstructures of the nanocomposites with high aspect ratio fillers while keeping the numerical simplicity.

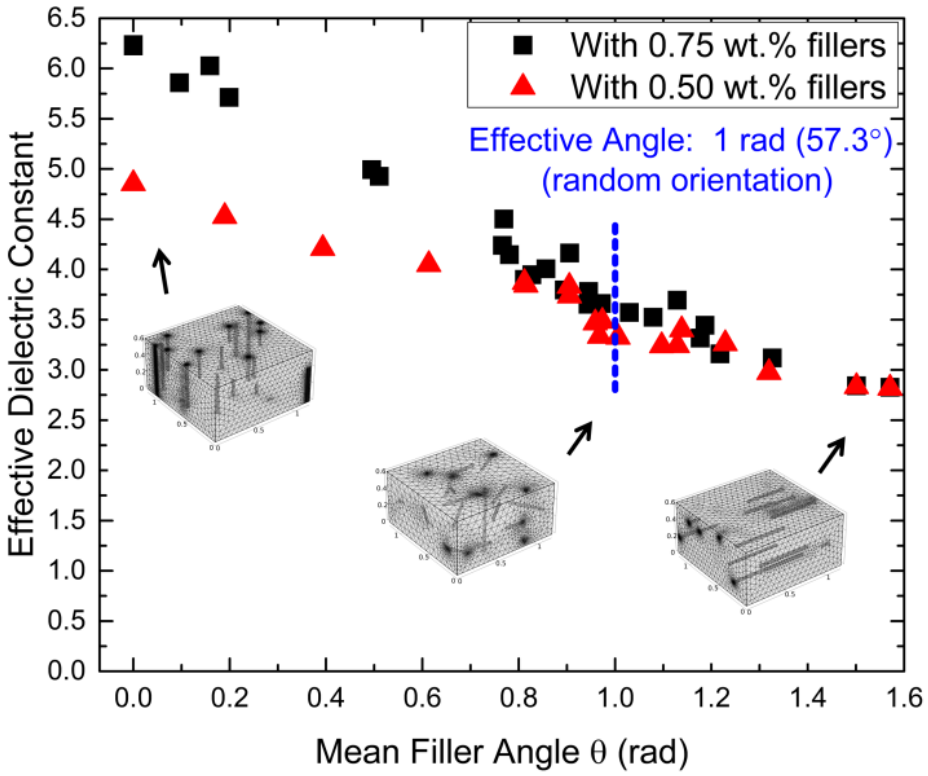

Fig. 5. 7. The relationship between the mean filler orientation parameter θ and the corresponding effective dielectric constant of the nanocomposites (9-filler models).

5.4.3 Filler Orientation Effect

Representative models with 9 fillers are utilized to investigate the filler orientation effect. The relationship between the effective dielectric constant and the mean filler angle θ is shown in Fig. 5.7. The FEA results show the effective dielectric constant variations as a function of mean filler angle θ. The FEA simulation demonstrates a trend of effective dielectric constant enhancement with the decrease of the mean filler angle θ of the microstructures. The effective dielectric constant ranges from 2.83 to 4.85 and from 2.83 to 6.23 for nanocomposites with 0.50 wt. % and 0.75 wt. % fillers respectively depending on the mean filler angle.

It is noted that the effective dielectric constant enhancement is not pronounced even with different MWNT concentrations when the mean filler angle θ is larger than 1 radian: effective dielectric constant ranges from 2.83 to 3.33 and from 2.83 to 3.73 for nanocomposites with 0.50 wt. % and 0.75 wt. % fillers respectively. By contrast, the amount of fillers significantly affects the effective dielectric constant, ranging from 3.33 to 4.85 and from 3.73 to 6.23 for nanocomposites with 0.50 wt. % and 0.75 wt. % fillers respectively, especially when the mean filler angle θ is below 1 radian. This is because as orientation angle θ of fillers decreases, fillers have longer paths in the direction along the applied electric field. As a result, under the fixed potential difference, larger electric displacement field can be induced, resulting in higher dielectric constant in the direction of the applied electric field.

Fig. 5.7 provides an estimate on how aligned the fillers need to be processed to get the desired dielectric constant enhancement. This implies that the microstructures of the nanocomposites can be predicted based on the effective dielectric constant. It is demonstrated that the most efficient enhancement of effective dielectric constant is to align the fillers along the applied electric field

while the least efficient approach is to align the fillers perpendicular to the applied electric field as reported in literature[146].

In addition, the relationship between the effective dielectric constant and the orientation angle parameter θ can provides the potential explanation on the reduction of the effective dielectric constant of MWNTs-filled nanocomposites reported in literature [147]. The stretch of the specimen introduces the compression along the applied electric field, resulting in the larger θ shown in Fig. 5.8. For simplicity, let's consider θ_i and θ_i' representing the orientation parameter of i^{th} filler projected on a plane parallel to the applied electric field before and after the stretch. $\theta_i' \geq \theta_i$ is valid for all the fillers due to the compression along the field. As a result, effective dielectric constant of the nanocomposites is lowered due to the larger orientation angle θ.

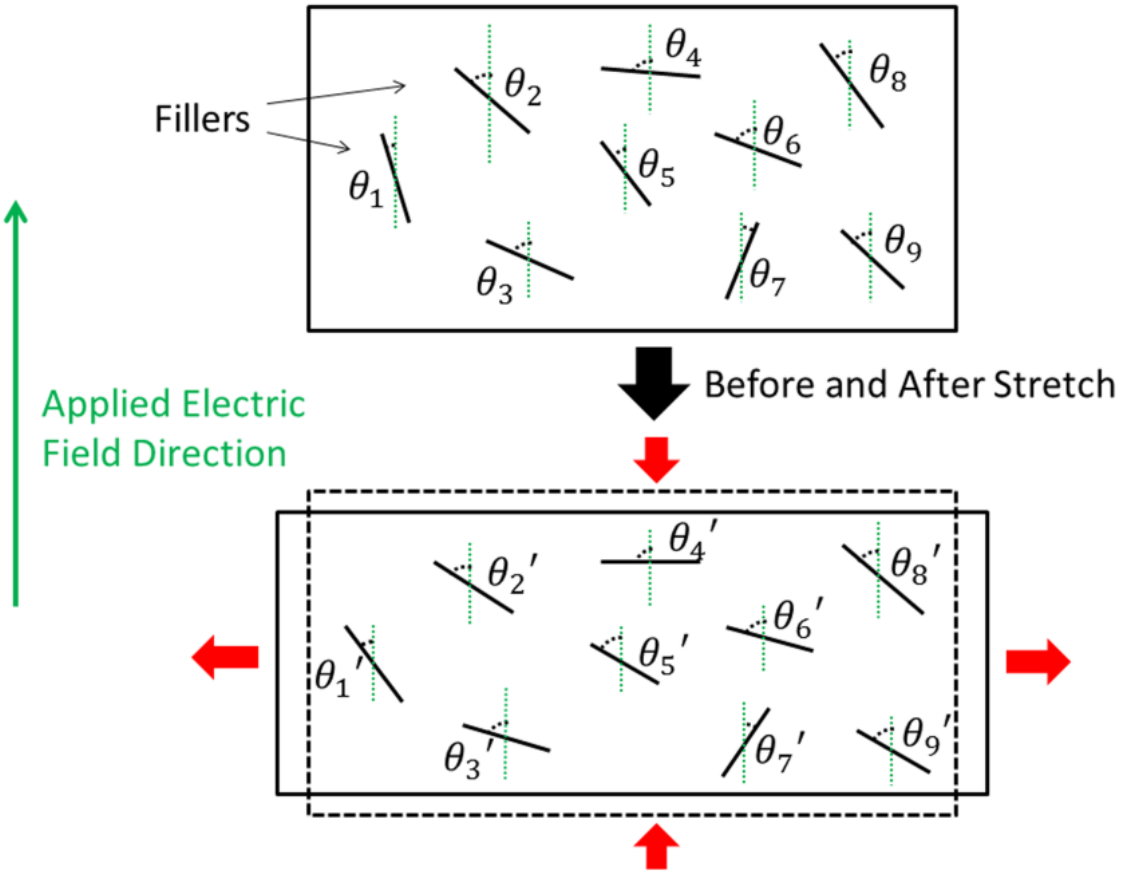

Fig. 5. 8. Schematic image of the filler orientation changes in 2-dimension simplified figure before and after stretching.

5.4.4 Acetone Effect

Although evaporation of acetone during the fabrication process is accelerated by a hot plate, there could be residue acetone left in the processed materials. A set of specimen of pure dielectric elastomer are prepared to investigate how the residue acetone could affect the effective dielectric constant of the materials as shown in Table. 5.5. The dielectric constant difference between the 2 specimens is 2.94 %. Both specimens show similar standard deviation from the measurements, 0.0650 (2.38 %) and 0.0794 (2.84 %) respectively for specimens without and with acetone. This demonstrates that residue acetone has little effects on the dielectric constant measurement although 2.94 % difference of the dielectric constant values could have derived from either measurement errors or residue acetone effect.

Table. 5. 5. Residue acetone effect on the measured dielectric constant based on 10 measurements for each specimen.

Material	Dielectric constant	Standard Deviation
Without Acetone	2.72	0.0650
With Acetone	2.80	0.0794

5.4.5 An Approach to Further Enhance the Dielectric Property of DE Nanocomposites.

Experimental results by the dielectric elastomer nanocomposites with several MWNTs concentrations are further compared with the proposed random-orientation models shown in Fig. 5.9. Models with fillers aligned parallel and perpendicular to the applied electric field are also plotted for comparison.

When it comes to nanocomposites with randomly oriented MWNTs, the measured effective dielectric constants have a good agreement with the prediction provided by FEA shown in Fig. 5.9. However, both the experiments and simulation imply that the effective dielectric constant enhancement is limited unless the nanocomposites are processed with filler alignment. It is also noted in Fig. 5.9 that the filler orientation is more influential than the amount of fillers to obtain the desired effective dielectric constant. For instance, to obtain effective dielectric constant 6.23, only 0.75 wt. % MWNTs are needed if they are all aligned parallel to the applied electric field. By contrast, twice or three times more MWNT concentration is required if the fillers are randomly oriented in the nanocomposites. However, higher loading of MWNTs may easily cause the loss of the insulation [49, 148] and to give rise to the aggregation of MWNTs, which destroys the electromechanical functions of dielectric elastomers.

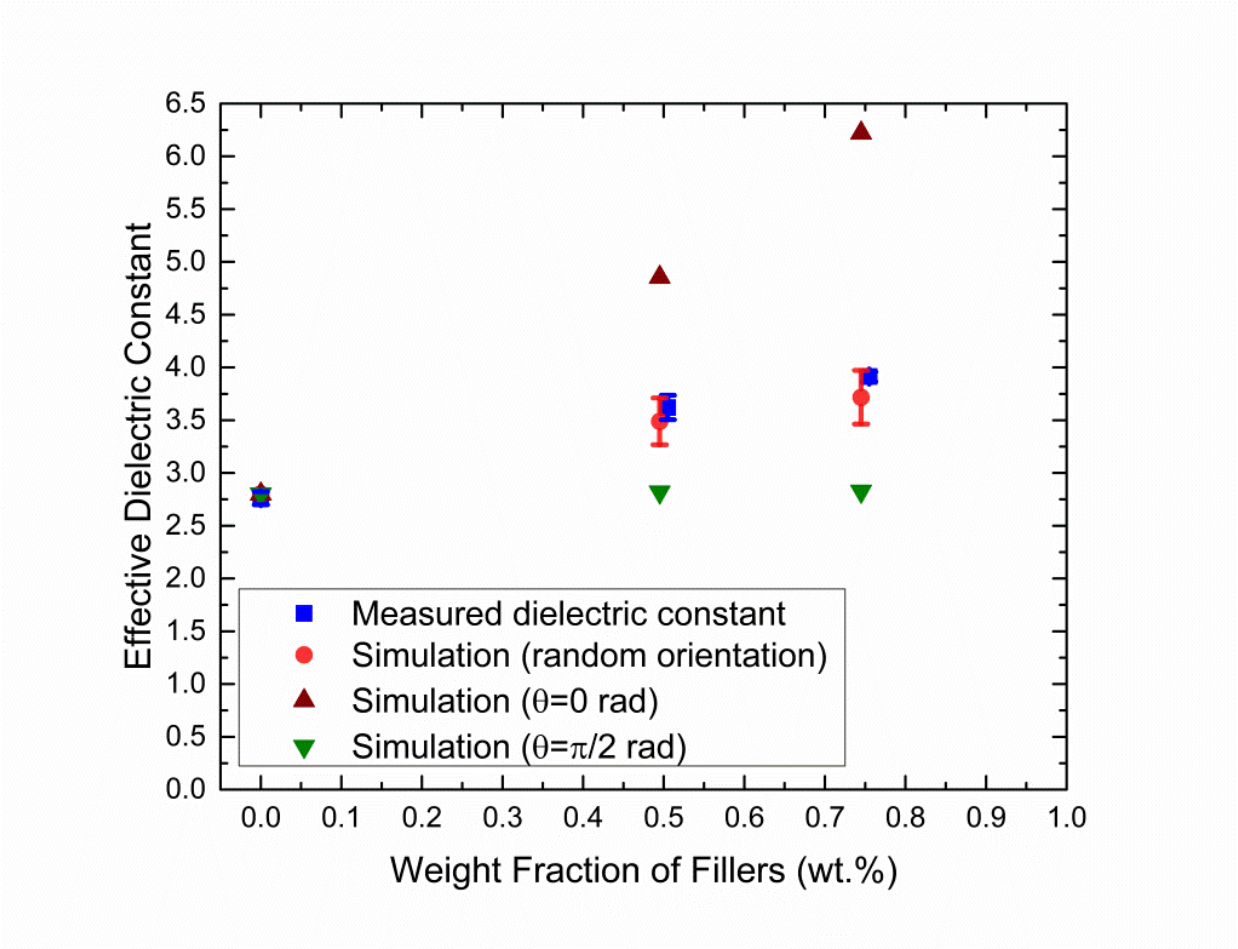

Fig. 5. 9. A comparison between the experimental data and FEA results. The error bar for random orientation models is derived from one standard deviation based on ten models.

5.4.6 Tortuosity Effect

Many research efforts have been made to investigate the waviness effect of high aspect ratio fillers inside the polymer matrix. Fisher, F. T., et al. utilized finite element analysis and micromechanics approach to investigate the waviness effect of CNTs on the mechanical properties of the Polymer/CNTs composites [125, 149, 150]. In their work, curved CNTs are described as cylinders with 2-dimensional sinusoidal curves. Much work has been dealing with filler waviness by introducing one cylinder with 2-dimensional sinusoidal or exponential curves [151, 152] in unit-cell representative models. Dendievel, R., et al. investigated the tortuosity effect of CNTs on the percolation threshold of polymer/CNTs composites [153]. In their work, it is summarized that the fiber tortuosity reduces the average aspect ratio, resulting in the increase of percolation threshold. A new approach to create the tortuosity is proposed by Herasati [154], and the tortuosity effects on mechanical properties are investigated for polymer/CNTs composites.

In this section, 3-dimensional fiber tortuosity is defined and finite element models are created using Digimat-FE [155]. Random orientation models with different fiber tortuosity are also proposed to investigate the filler tortuosity effects on the dielectric properties of dielectric elastomers filled with MWNTs.

11 control points are assigned to each filler, and there are 10 small segments for each filler. Each segment does not have to be the same in length. However, the tangents of any 2 segments at the control point they share need to be the same. The filler tortuosity is defined as the maximum acceptable change in orientation from one control point to the next [155]. In the fixed aspect ratio 20, the tortuosity 10 is not realistic. From the TEM image from Fig. 5.10, we assume the

typical tortuosity is 3 for filler with aspect ratio 20, and also investigation on the tortuosity of 1, 3 and 5 shown in Fig. 5.11 are conducted.

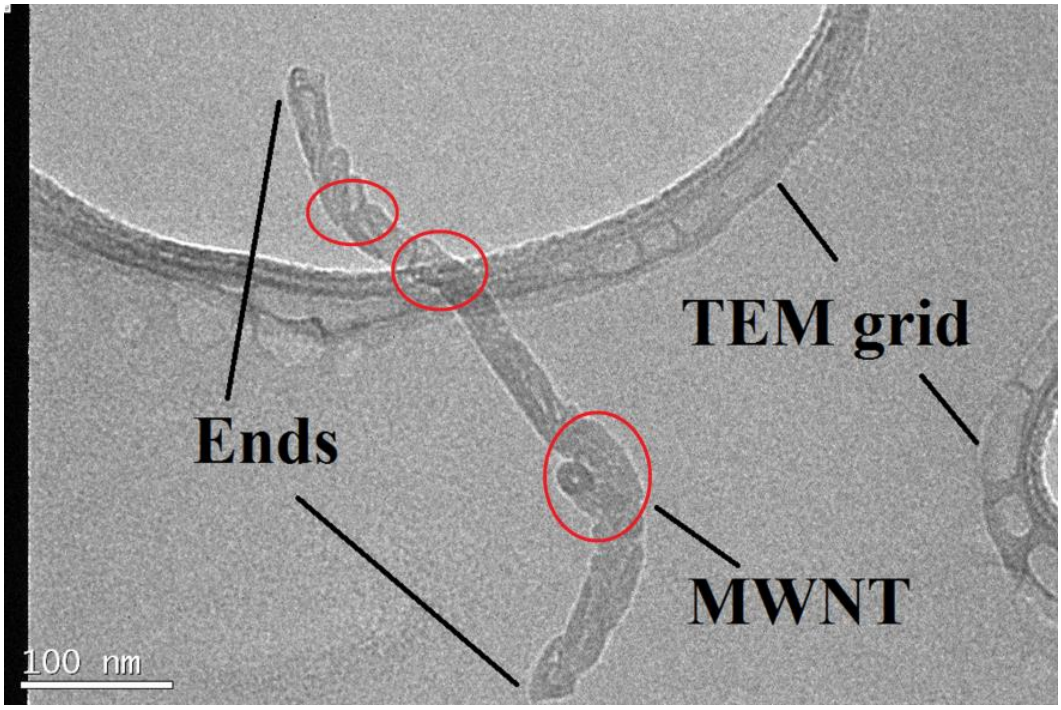

Fig. 5. 10. TEM image of a MWNT with tortuosity 3.

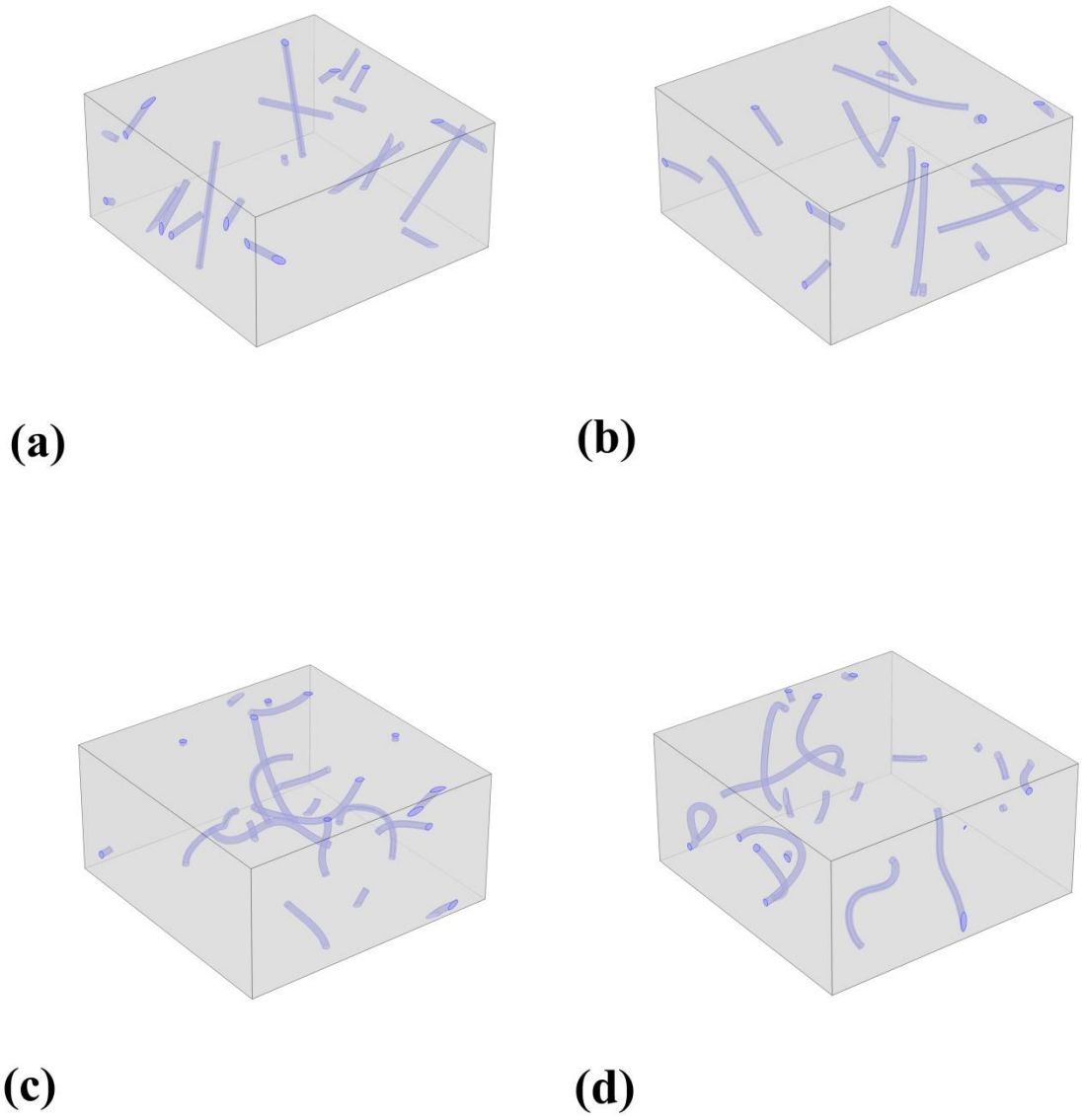

Fig. 5. 11. Examples of microstructures of nanocomposites with 0.75 wt.% fillers (9-filler models): One example of (a) waviness 0, (b) waviness 1, (c) waviness 3, and (d) waviness 5. Periodic geometry is defined at the boundaries for fillers.

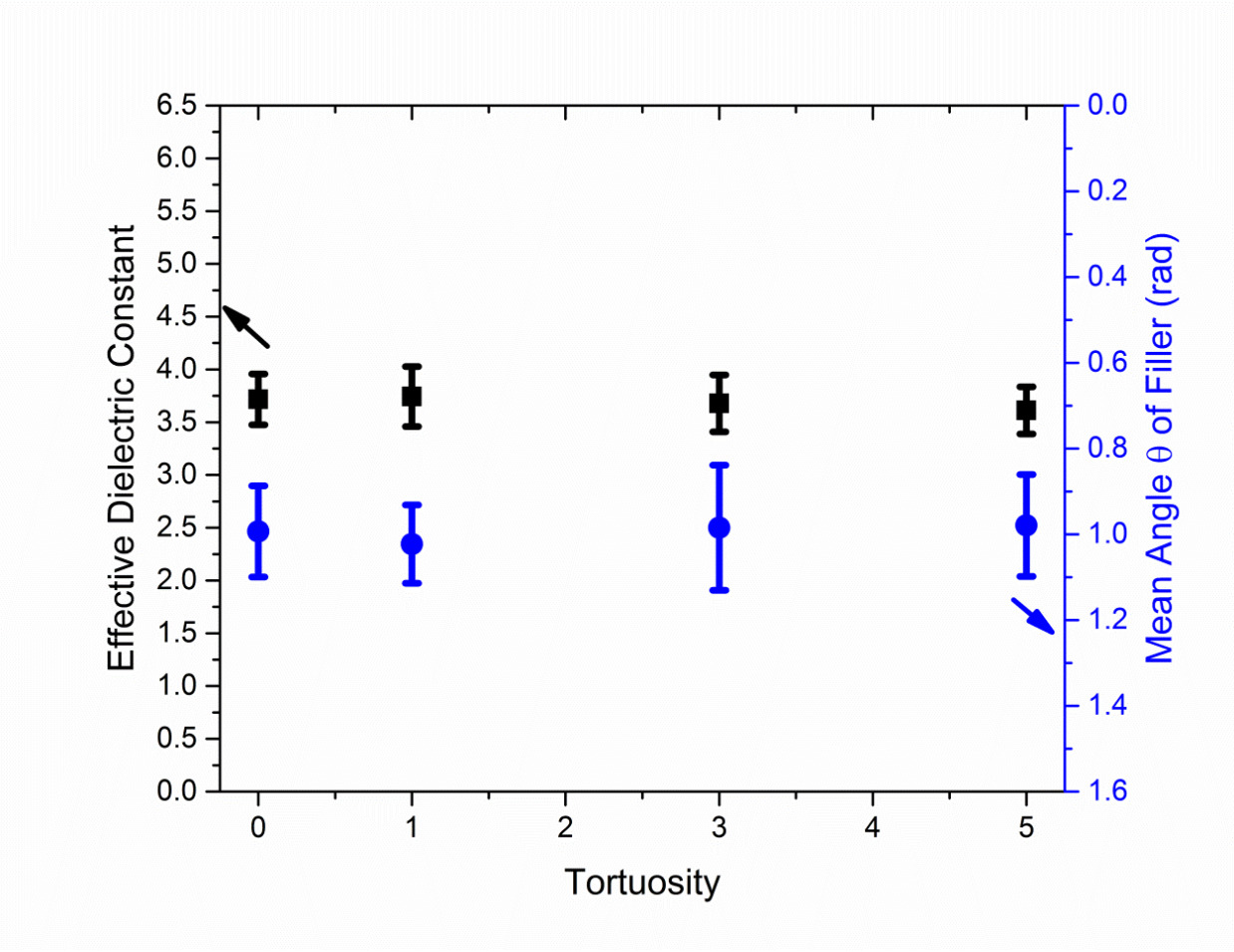

Fig. 5. 12. Effective dielectric constant calculated by FEA using 9-filler random orientation models with different tortuosity. The error bar is derived from one standard deviation based on ten models.

Fig. 5.12 shows the tortuosity effects on the DE nanocomposite dielectric constant. It can be observed that the dielectric constant of nanocomposites is not sensitive to the tortuosity when fillers are randomly oriented within the DE matrix.

One of the potential reasons is that the fillers are randomly oriented and placed within the models. Thus, the mean filler angle θ for each model with specific tortuosity is around 1 radian as shown in the Fig. 5.12. As mentioned earlier in this chapter, filler orientation plays an important role in determining the dielectric properties of nanocomposites. If fillers are aligned to certain degrees, such as 0 to 0.523 rad, then the tortuosity could become a significant factor.

The second potential reason is the fixed aspect ratio 20. The accurate aspect ratio of fillers in nanocomposites is unknown, and the aspect ratio distribution is also unknown as well. However, longer aspect ratio fillers, such as filler with aspect ratio 50 or 100, could have larger tortuosity factor due to its geometry [155]. More research will be done to reveal the aspect ratio effects coupled with tortuosity effects on the relative permittivity of DE nanocomposites.

5.5 Conclusions

This study systematically investigates the relationship between the filler orientation parameter and the effective dielectric constant of the nanocomposites. To ensure the simple and affordable FEA study, a unit cell model with nine fillers is determined to be sufficient to represent the microstructures of the nanocomposites. This provides a strategy allowing us to obtain the results with acceptable precision for a low computational cost.

It is shown that the orientation parameter φ perpendicular to the applied electric field has little effect on the effective dielectric constant along the electric field direction. The angle θ between fillers and axis parallel to the applied electric field serves a primary factor to control the dielectric property of the nanocomposites. It is demonstrated that the effective dielectric constant of the nanocomposite with high aspect ratio is strongly associated with the mean filler orientation in the microstructures. As a result, it is more efficient to control the microstructures in order to enhance the effective dielectric constant by aligning the fillers than simply increasing the filler concentrations which causes problems such as filler dispersion, stiffening of the materials and the reduction of the dielectric strength of the materials [43, 156]. This also addresses the possibility of controlling the effective dielectric constant by altering the orientation of the fillers either by processing [139] or external stimulus such as mechanical loading [157] while keeping the same amount of the fillers. In addition, the models can potentially explain the dielectric property change of the nanocomposites due to the filler orientation change under mechanical deformation.

Tortuosity effect on dielectric properties of DE nanocomposites is also investigated. It is demonstrated that tortuosity has little effect on the dielectric properties of DE nanocomposites filled with randomly oriented MWNTs. However, it has posted some possibilities that DE nanocomposites with longer aspect ratio fillers and/or with aligned fillers could be significantly affected by tortuosity in terms of dielectric property.

In summary, we have created representative models for nanocomposites with fillers. The proposed unit-cell models, controlled by filler orientation parameters, provide straightforward and successful predictions on the effective dielectric constant of the nanocomposites.

Chapter 6 Modeling of Mechanical Properties of Dielectric Elastomer Nanocomposites

6.1 Introduction

As described in the previous chapter, the basic ideas to improve dielectric elastomers are to: (1) achieve higher effective dielectric constant for larger energy storage and less required actuating voltage, and (2) keeping the material rigidity low while achieving (1) at the same time. A common improvement has been reported including implementing ceramic powders with high dielectric constant such as TiO_2 particles [42], $BaTiO_3$ nanoparticles [44, 45, 146] and $PbTiO_3$ [47]. However, high loading, up to 20-30 vol.% of these particles are required for meaningful increase, at which the ceramic powders filled composite materials could lose its flexibility, making the materials not suitable for the actual applications.

Recently, carbon nanotubes have been reported to efficiently enhance the relative permittivity with a small loading fraction up to 2 wt.% due to its high aspect ratio and conductivity while avoiding the unwanted increase of the materials rigidity [49-51].

A various factors can affect the mechanical properties of composite materials with high aspect ratio fillers: amount of fillers, filler shape, filler aspect ratio, filler dispersion, distance between each filler [124], waviness of the fillers [125], interaction between fillers and matrix, and orientation of the fillers. Different filler-orientation may cause anisotropic mechanical responses. Many works have been focusing on the mechanical properties of polymer based composite materials. Fisher et al. investigated the 2-dimensional waviness effects of CNTs on the mechanical properties of composite materials [125, 149]. Efforts have been taken to create the

unit-cell models with one filler to predict the mechanical properties of polymer composite materials [133, 134, 158-160]. Farsadi used FE method to investigate the effective response of embedded wavy inclusions of CNT within a matrix [161].

Furthermore, assigning the correct boundary conditions is essential to reasonable material property prediction provided by FEA. For unit-cell models, special boundary conditions need to be assigned due to the continuity of geometry and stress/strain field. Periodic boundary conditions have been proposed to satisfy both the geometry and fields for unit-cell models [162-168]. Application of periodic boundary conditions can guarantee the continuity of the displacement and the traction at the boundaries [162].

In this chapter, finite element analysis (FEA) is performed in three-dimensional (3D) unit cell models with nine high aspect ratio fillers are created to investigate the mechanical properties of DE nanocomposites. A statistical approach is employed to obtain an understanding on how the mean angle of the MWNTs is associated with the theoretical effective angle when MWNTs are randomly dispersed in DEs. Experimental results are also compared with predictions given by the FEA. Moreover, the 3-dimensional tortuosity effect by filler is investigated.

6.2 Finite Element Methodology

6.2.1 Displacement-Difference Periodic Boundary Conditions

Three-dimensional finite element analysis (FEA) is performed using commercially available FEA software, COMSOL Multiphysics (version 4.4). The geometry of the unit cell is set to be a half cubic due to the symmetry of the top half and bottom half. Using symmetries can reduce the

model size from a cubic to a cuboid shown the previous chapter. A unit cell is a fundamental repeating block of the representative material microstructure, and therefore the continuity of the structures has to be satisfied.

2 boundary conditions are compared: (1) Free Boundary Conditions (FBCs), and (2) Displacement-Difference Periodic Boundary Conditions (PBCs) [162, 169, 170]. FBCs only assign the displacement of the top plane and fix the displacement of the bottom plane, or called "plane-remains-plane" boundary conditions [164]. It was revealed that FBCs are over-constrained and violates the stress/strain periodicity conditions [164].

All the other 4 planes remain free to deform. As all the 4 side planes are free, the incompressible hyperelastic materials tend to inflate in *XY* direction in all the edges to conserve the volume, resulting in discontinuity of the geometry especially after the load is applied. Thus, deformed unit-cell model loses its periodicity as a repeating block.

To guarantee the continuity of the displacement and the traction at the boundaries, periodic boundary conditions are applied [162, 169, 170]. Displacement-difference periodic boundary condition (PBC) has been proven to guarantee the displacement and traction continuity, thus it is applied in the unit cell models in this study.

Consider a periodic unit cell structures. The geometry of the fillers is continuous at x^+ and x^- planes, y^+ and y^- planes, and z^+ and z^- planes, where "+" and "-" identify the pair of two opposite boundary surfaces in the unit cell models shown in Fig. 6.1.

The displacement field of the periodic boundary conditions can be described as

$$u_i = \bar{\varepsilon}_{ik} x_k + u_i^*$$

$$u_i^{j+} = \bar{\varepsilon}_{ik} x_k^{j+} + u_i^*$$

$$u_i^{j-} = \bar{\varepsilon}_{ik} x_k^{j-} + u_i^*$$

$$u_i^{j+} - u_i^{j-} = \bar{\varepsilon}_{ik} (x_k^{j+} - x_k^{j-}) = \bar{\varepsilon}_{ik} \Delta x_k^{j}$$

where $\bar{\varepsilon}_{ik}$ is the global average strain tensor of the periodic structures, u_i^* is the local fluctuation and the periodic part of the displacement components on the periodic boundary surfaces. "*j*+" and "*j*-" mean the directions along positive and negative X_j directions.

The difference of u_i^{j+} and u_i^{j-} is given as well. Since Δx_k^{j} are constants for each pair of the periodic boundary surfaces, $\bar{\varepsilon}_{ik} \Delta x_k^{j}$ is constant as long as the global strain is specified. It is note that $\bar{\varepsilon}_{ik} \Delta x_k^{j}$ does not contain the periodic term (u_i^*) any more, which makes it easier to apply the constraints in the finite element analysis using COMSOL Multiphysics.

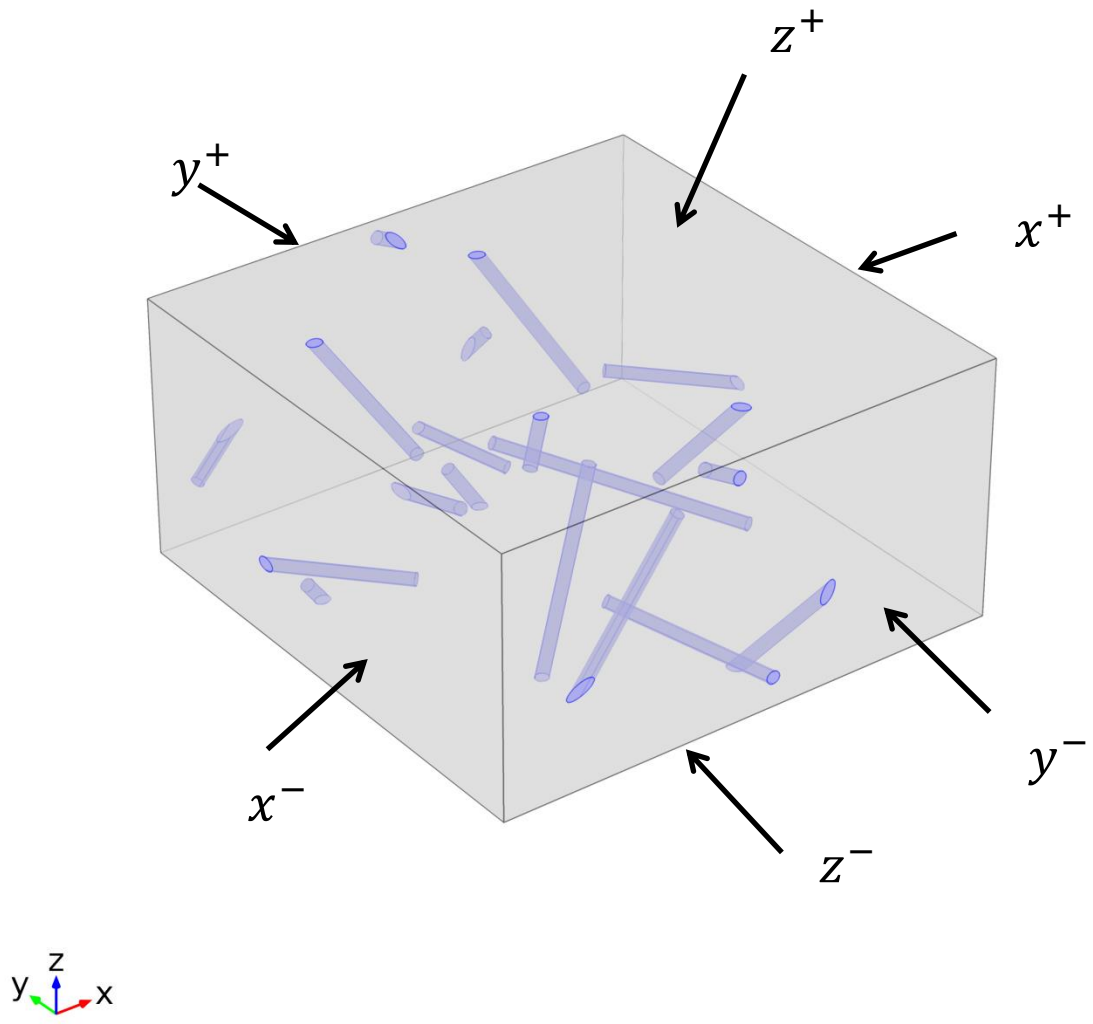

Fig. 6. 1. Assignment of the planes of unit-cell models to define boundary condition.

6.2.2 Hyperelastic Models and Materials Parameters

Rubbers and rubber-like materials usually exhibit extremely large strain, sometimes 10 times longer than its original length, and stress strain curve of those materials show non-linear behaviors [171]. As a result, those materials are usually modeled as incompressible hyperelastic materials.

Let's first consider the incompressible hyperelastic case. In nearly incompressible models, elastic strain energy density can be described as

$$W_s = W_{iso} + W_{vol}$$

where W_s is elastic strain energy density, W_{iso} the isochoric (also called volume-preserving) strain energy density, and W_{vol} volumetric (also called dilatational) strain energy density. The most commonly used form for volumetric strain energy density is:

$$W_{vol} = \frac{1}{2}\kappa(J_{el} - 1)^2$$

Neo-Hookean model is employed to calculate the material parameters used from experimental results. Neo- Hookean model [172] can be described as

$$W_s = W_{iso} + W_{vol} = \frac{1}{2}\mu(\overline{I}_1 - 3) + \frac{1}{2}\kappa(J_{el} - 1)^2$$

where μ Lamé coefficient, κ initial bulk modulus, and $\overline{I}_1$ the first invariant of the deviatoric part of the left Cauchy-Green deformation tensor and can be described as

$$\overline{I_1} = J_{el}^{-2/3}(\lambda_1^2 + \lambda_2^2 + \lambda_3^2), J_{el} = \lambda_1\lambda_2\lambda_3$$

For the simplest case, perfectly incompressible hyperelastic models are assumed. In perfectly incompressible model, $J_{el} = 1$. Thus, Neo-Hookean model can be simplified as

$$W_s = W_{iso} = \frac{1}{2}\mu(\overline{I_1} - 3)$$

$$\lambda_3 = \lambda, \lambda_1 = \lambda_2 = \frac{1}{\sqrt{\lambda}}$$

$$W_s = \frac{1}{2}\mu(\frac{2}{\lambda} + \lambda^2 - 3)$$

Cauchy stress is related to W_s under uniaxial compression by

$$\sigma_3 = \lambda_3 \frac{\partial W_s}{\partial \lambda_3} = \mu(\lambda^2 - \frac{1}{\lambda})$$

From the fitting shown in Fig. 6.2, Lamé coefficient μ is determined to be 98.4 kPa as shown in Table. 6.1. It needs to be noted here that static mechanical response is measured under fixed displacement as discussed in the previous chapter. Viscosity is not considered in this static case. Thus, Lamé coefficient μ discussed here is related to the relaxed elastic modulus.

Wide range of materials parameters are reported for carbon nanotubes [130, 134, 173, 174]. In this study, parameters from a literature [174] is used for FEA as shown in Table. 6.2. Also, MWNTs are to be assumed to be isotropic in all directions.

It is also noted that the perfect bonding between the DE matrix and carbon nanotubes is assumed. Although some research groups are introducing the concept of the interlayers between the matrix

and the fillers [134, 175], it is not realistic to experimentally investigate the interface between the matrix and the fillers, especially nano-fillers. Thus, in this section, interface concepts are not introduced. However, interlayers are a useful concept to understand the strength of bonding between the matrix and fillers [134].

Table. 6. 1. HS III dielectric elastomer materials parameters used in FEA.

Material	Lamé coefficient μ
Dielectric Elastomer	98.4 kPa

Table. 6. 2. MWNT materials parameters used in FEA [174].

Material	Young's Modulus	Poisson's Ratio
MWNTs	200 GPa	0.2

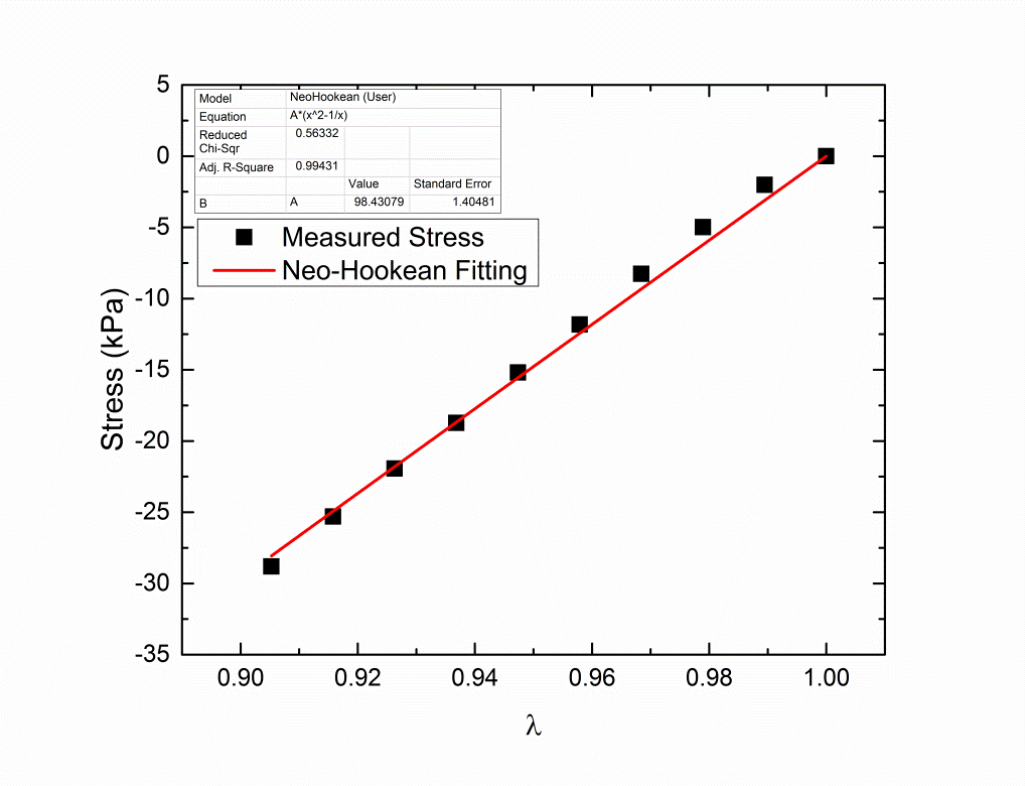

Fig. 6. 2. Fitting of compression testing results and Neo-Hookean models.

6.3 Results and Discussion

6.3.1 Periodic Boundary Conditions

To guarantee the continuity of the displacement and the traction at the boundaries, periodic boundary conditions are applied mentioned earlier.

Fig. 6.3 shows the static mechanical property of DE nanocomposites. It is experimentally shown that the introduction of 0.75 wt. % enhances the mechanical response of DE nanocomposites by 9 %. The numerical results by using either PBCs or FBCs are plotted as well. Fig. 6.3 shows the calculated result by FBCs is even lower than the mechanical response of the pristine DEs under

compression. This seems unreasonable as MWNTs have much higher elastic modulus, and contradictory to the experimental results at the same time.

On the other hand, the numerical results done by PBCs have shown the increase trend with the addition of 0.75 wt. % MWNTs to DEs by 20-25 %. Although the numerical results show higher enhancement of the mechanical property of DE nanocomposites than the experimental results, this reasoning can be associated with 2 factors which will be discussed later in this chapter.

In conclusion, PBCs have been proved to provide reasonable results coupled with FEA analysis although many earlier works have been based on FBCs.

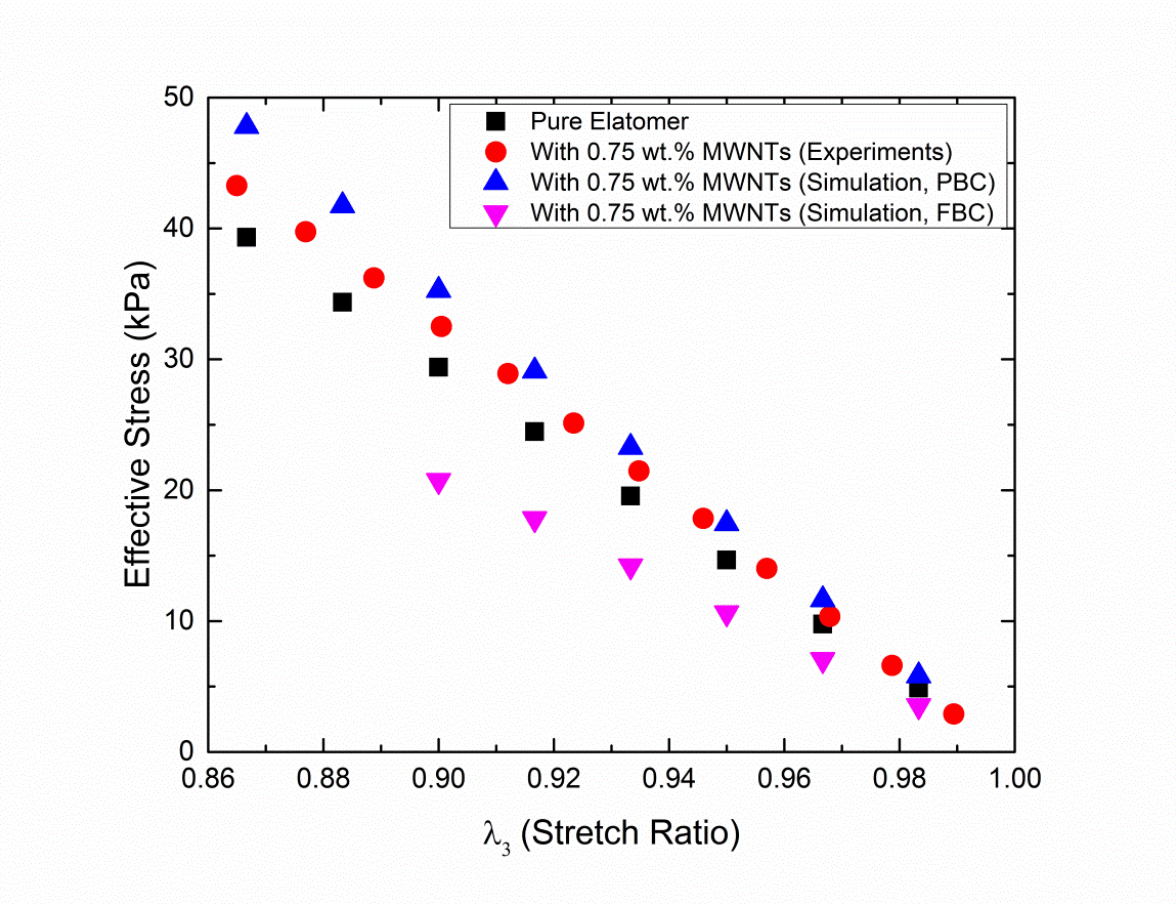

Fig. 6. 3. The relationship between the stretch ratio in thickness direction λ_3 and the effective strain measured or calculated.

6.3.2 Static Mechanical Response of DE nanocomposites

As we have seen, once the applied electric field is applied, the displacement reaches the equilibrium within a second, and stays in the equilibrium until the applied electric field is removed. As a result, it can be assumed that HS III DE can reach its relaxed state momentarily, under compression. Thus, viscoelasticity is not considered in this section.

Hyperelastic models are employed to investigate the relationship between the material stretch ratio and the relaxed stress state of DE nanocomposites.

Fig. 6.4 shows the static compression results. The increase of the measured effective stress of DE with 0.75 wt. % MWNTs is about 9 % even under large deformation at λ =0.78. This demonstrates that the mechanical property enhancement from the introduction of MWNTs is limited under static loading cases compared to the dielectric constant improvement, which is about 40 % enhancement with the introduction of 0.75 wt. % MWNTs.

Although the numerical results show higher enhancement of the mechanical property of DE nanocomposites than the experimental results, this reasoning can be associated with a few potential factors which will be discussed later in this chapter.

Based on the random orientation discussion mentioned in the previous chapter, MWNTs are assumed to be randomly distributed and oriented inside DE matrix. As discussed in the previous chapter, 9-filler models are utilized to investigate the mechanical properties of the DE nanocomposites filled with MWNTs.

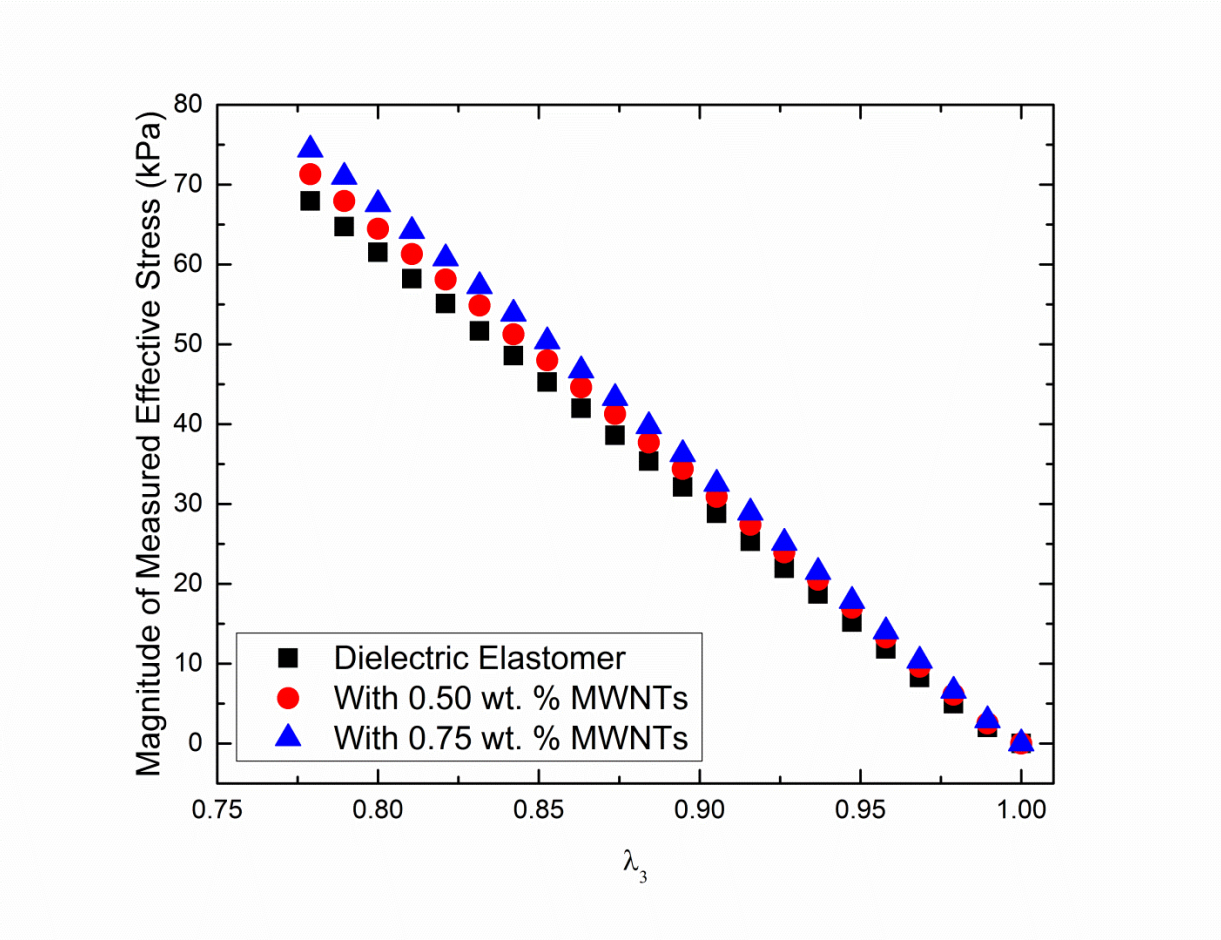

Fig. 6. 4. Measured static effective stress under compression testing of DEs and DE nanocomposites filled with MWNTs.

6.3.3 Filler Orientation Effects on Mechanical Response of DE nanocomposites

Filler orientation effects on mechanical properties of nanocomposites are investigated. 9-filler models are created as mentioned in the previous chapter. Fig. 6.5 shows the relationship between the calculated effective stress and the mean orientation angle θ of each model. The magnitude correlation coefficient is calculated to be 0.630, which shows medium correlation between the calculated effective stress by FEA and the mean orientation angle θ. However, the scattering of the data points can be observed from Fig. 6.5. The potential causes of the data scattering involve the number of fillers in the unit-cell models. Although 9 fillers are enough to investigate the orientation effects for dielectric properties, more fillers might be required for orientation effects for mechanical properties. In addition, bonding strength between DE matrix and MWNTs, and the dispersion of MWNTS as mentioned in chapter 2 and 4 are all affecting factors for mechanical analysis.

One potential reason to the gap shown in Fig. 6.3 between the calculation and experimental results could also be the orientation change due to the compression. Although, the filler orientation is random before the mechanical loadings, the mean orientation could change due to the compression as illustrated in Fig. 5.8 in the previous chapter. If this is the primary factor, the gap between the numerical and experimental results should be shrinking as the compression proceeds as the larger orientation angle θ results in smaller effective stress. However, this cannot be clearly validated from Fig. 6.5. As a result, it can be concluded that the filler orientation change due to the compression is not the primary cause of the gap mentioned above in the range currently tested in the compression test.

In summary, the orientation effect on mechanical properties has been carried out. Moderate correlation has been found between the effective stress and the mean filler orientation of unit cells. With the decrease of the mean filler orientation, the effective stress is reinforced. However, the orientation effect is not statistically meaningful yet, thus models with more fillers are to be test to validate the orientation effects on the mechanical properties of DEs and DE nanocomposites.

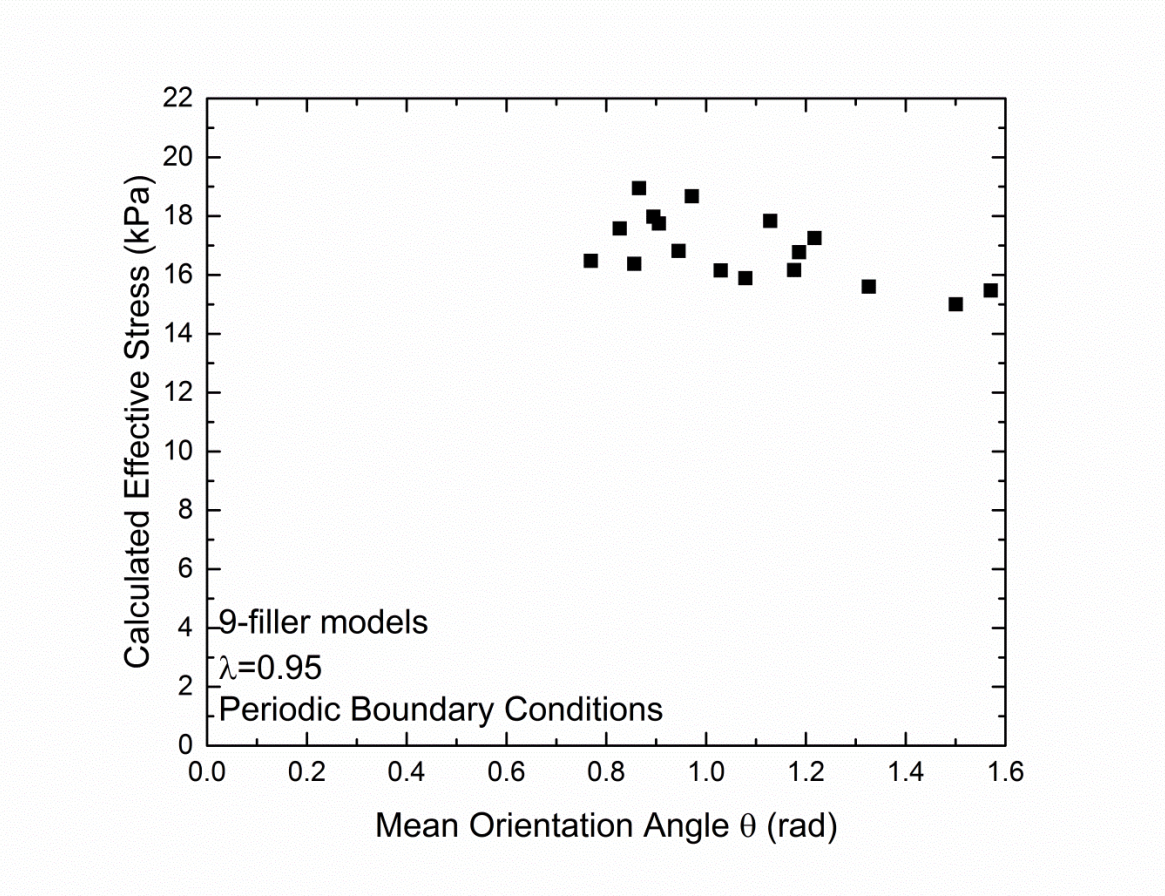

Fig. 6. 5. Filler orientation effects on static effective stress at stretch ratio in loading direction $\lambda = 0.95$. Calculated effective stress as a function of the mean orientation angle of the fillers in the unit-cell models.

6.3.4 Tortuosity effects and Aspect Ratio Effects on Mechanical Properties of DE Nanocomposites

Tortuosity has been defined in the previous chapter. The tortuosity effects on the mechanical properties of nanocomposites are to be discussed in this section. The periodic boundary conditions mentioned above are applied to the unit-cell models with 9 fillers. Tortuosity 1, 3 and 5 are investigated in this study. In the fixed aspect ratio 20, the tortuosity 10 is not realistic [155].

Fig. 6.6 and Table. 6.3 show the tortuosity effects on the effective stress of nanocomposites under $\lambda = 0.9$. Although the error bars are closely overlapping each other, the magnitude of the error bars is very closely related to the mean orientation deviation in the random orientation models. However, the mean effective stress shows slight decrease with tortuosity by 5-6%, showing the limited reduction of effective stress by tortuosity for fillers with aspect ratio 20. As a result, tortuosity cannot fully explain the gaps between the computed effective stress and the measured effective stress. Thus, this has posted the direction to further investigate another potential factor which is interface effects between the DE matrix and MWNTs.

Aspect ratio of MWNTs is also a deciding factor for mechanical properties of DE nanocomposites [121]. Although longer aspect ratio MWNTs tends to aggregate during the processing, it is reported that Young's modulus of the polymer composite filled with MWNTs is reinforced with the increase of MWNT aspect ratio [121]. However, tortuosity is more significant for higher aspect ratio MWNTs as tortuosity can easily shorten the effect aspect ratio of MWNTs.

More research is required to investigate the coupling effects of aspect ratio and tortuosity effects.

Table. 6. 3. The relationship between tortuosity, effective stress and mean angle θ.

Tortuosity	Effective Stress (kPa)	Error (One standard deviation, kPa)	Mean Angle θ (rad)	Error (One standard deviation, rad)
0	35.3	2.69	0.993	0.1064
1	33.2	1.91	1.023	0.0914
3	33.2	3.40	0.985	0.1459
5	33.4	3.27	0.979	0.1187

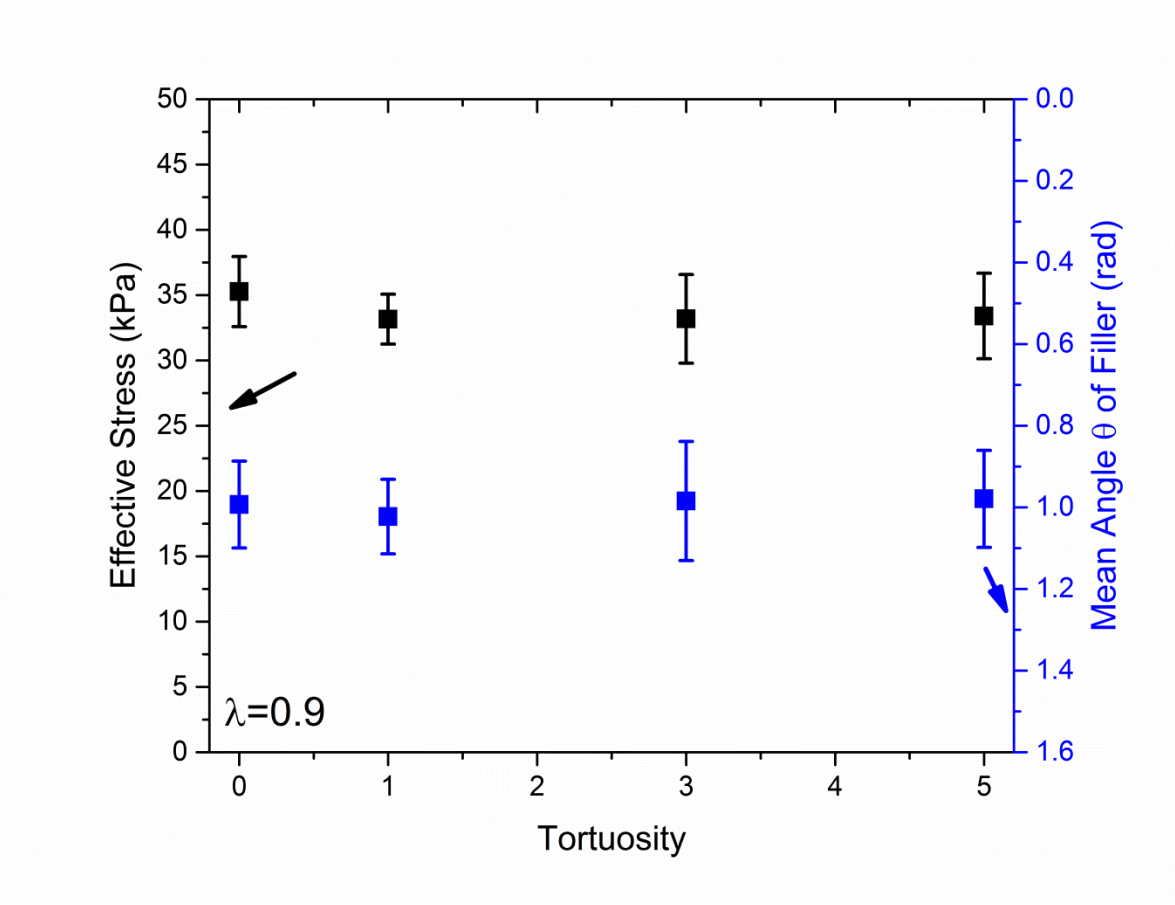

Fig. 6. 6. Effective stress calculated by FEA using 9-filler random orientation models with different tortuosity. The error bar is derived from one standard deviation based on ten models.

6.4 Conclusions

This chapter is focusing on the static mechanical properties of DE nanocomposites filled with MWNTs. The static mechanical property of DE nanocomposites filled with 0.5, 0.75 wt. % is experimentally investigated, and also numerically analyzed by FEA.

The results show the effective stress predicted by FEA is overestimated by 10-15 % compared to experimentally obtained stress. The potential causes to the gap between the experimental results and the computed results are the tortuosity of fillers, remaining aggregates of MWNTs [152] and the bonding between DE matrix and MWNTs.

Tortuosity effect study reveals that the reduction of effective stress of DE nanocomposites is limited under the assumption that aspect ratio of fillers is 20.

As mentioned in chapter 4, it is still likely that the aggregates of MWNTs are remaining in the DE nanocomposites, resulting in smaller effective stress. In addition, the results have posted the direction to further investigate the interface (bonding/debonding) effects between the DE matrix and MWNTs. In other word, mechanical properties of DE nanocomposite are processing dependent.

In conclusion, the mechanical property change due to the introduction of MWNTs is limited compared to the dielectric property change. As a result, the electromechanical response of DE nanocomposites filled with MWNTs is significantly enhanced due to the pronounced improvement in relative permittivity of DE nanocomposites filled with MWNTs, and limited mechanical change.

Chapter 7 Conclusions and Future Research

7.1.Conclusions

This dissertation is devoted to investigations of the development of DE nanocomposites as stretchable and flexible actuating materials. MWNTs are introduced to DE matrix to enhance the deforming properties. Both experimental and numerical works have been carried out to investigate the dielectric, mechanical and electromechanical properties of DE nanocomposites filled with MWNTs. As a final remark, the 2 major achievements in this dissertation are summarized below, followed by some suggestions on future work.

As the first major contribution, the novel smart DE nanocomposites filled with MWNTs have been developed, and their electromechanical properties are fully characterized via laser Doppler vibrometer. It is demonstrated that the addition of 0.75 wt. % MWNTs to DEs has enhanced the thickness strain by 3 times, and reduced the required electric field by 30 % to achieve the same amount of thickness strain compared to pristine DEs. This is due to the significant improvement of dielectric constant by the addition of MWNTs, and limited mechanical reinforcement at low MWNTs concentration. This opens up the option for DE nanocomposites as energy harvesting materials due to the enhanced thickness strain compared to conventional DEs.

The second major contribution includes the investigation of the filler orientation effects on relative permittivity of MWNTs in dielectric elastomer nanocomposites. To further improve the electromechanical properties at the fixed weight fraction of MWNTs, filler orientation turns out be a dominating factor. Unit-cell models are created to investigate the filler orientation effects on

the both dielectric and mechanical properties of dielectric elastomer nanocomposites. Nine fillers in the unit-cell models are found to be sufficient to represent the microstructures of dielectric elastomer nanocomposites while keeping the numerical simplicity. The proposed random orientation models show a good agreement with the experimental results of dielectric properties of DE nanocomposites. Furthermore, the proposed model is efficient in predicting the dielectric properties of DE nanocomposites with fillers of high aspect ratio while keeping the numerical simplicity. Lastly, the proposed model reveals the relationship between the microstructure of DE nanocomposites and the associated relative permittivity. The proposed model provides the prediction of the effective permittivity of dielectric elastomer nanocomposites as a function of the mean filler orientation of the microstructures. The results show the further improvement of relative permittivity of nanocomposites with the alignment of the fillers, leading to the further enhancement of electromechanical response of dielectric elastomer nanocomposites while keeping the MWNT concentration low.

7.2.Suggestions for Future Research

In the future research on the development of DE nanocomposites, in terms of experimental efforts, DE nanocomposites filled with SWNTs should be developed, while improving fabrication techniques is a continuing objective. In addition, to further investigate the interface effects between DE matrix and the MWNTs, functionalized MWNTs need to be introduced to the matrix and compared with the data obtained in this study.

As for the numerical modeling, tortuosity effects should be further investigated with varying aspect ratios. Interface models need to be developed to achieve better understanding on the mechanical properties of DE nanocomposites. Finally, electromechanical coupling models need to be developed to investigate the coupling effects of DE nanocomposites filled with MWNTs.

REFERENCE

[1] A. O'Halloran, F. O'Malley, and P. McHugh, "A review on dielectric elastomer actuators, technology, applications, and challenges," *Journal of Applied Physics,* vol. 104, p. 071101, Oct 1 2008.

[2] P. Chouinard and J. S. Plante, "Bistable Antagonistic Dielectric Elastomer Actuators for Binary Robotics and Mechatronics," *Ieee-Asme Transactions on Mechatronics,* vol. 17, pp. 857-865, Oct 2012.

[3] J. A. Rogers and Y. G. Huang, "A curvy, stretchy future for electronics," *Proceedings of the National Academy of Sciences of the United States of America,* vol. 106, pp. 10875-10876, Jul 7 2009.

[4] S. Wagner, S. P. Lacour, J. Jones, P.-h. I. Hsu, J. C. Sturm, T. Li, *et al.*, "Electronic skin: architecture and components," *Physica E: Low-dimensional Systems and Nanostructures,* vol. 25, pp. 326-334, 2004.

[5] S. J. A. Koh, X. Zhao, and Z. Suo, "Maximal energy that can be converted by a dielectric elastomer generator," *Applied Physics Letters,* vol. 94, p. 262902, 2009.

[6] P. Brochu and Q. Pei, "Advances in Dielectric Elastomers for Actuators and Artificial Muscles," *Macromolecular Rapid Communications,* vol. 31, pp. 10-36, 2010.

[7] X. Zhao and Z. Suo, "Electrostriction in elastic dielectrics undergoing large deformation," *Journal of Applied Physics,* vol. 104, p. 123530, 2008.

[8] Y. Liu, L. Liu, Z. Zhang, Y. Jiao, S. Sun, and J. Leng, "Analysis and manufacture of an energy harvester based on a Mooney-Rivlin–type dielectric elastomer," *EPL (Europhysics Letters),* vol. 90, p. 36004, 2010.

[9] I. A. Anderson, T. A. Gisby, T. G. McKay, B. M. O'Brien, and E. P. Calius, "Multi-functional dielectric elastomer artificial muscles for soft and smart machines," *Journal of Applied Physics,* vol. 112, p. 041101, 2012.

[10] Y. Bar-Cohen, S. Chiba, M. Waki, R. Kornbluh, and R. Pelrine, "Extending applications of dielectric elastomer artificial muscle," *Electroactive Polymer Actuators and Devices (EAPAD) 2007,* vol. 6524, pp. 652424-5, 2007.

[11] B. M. O'Brien, E. P. Calius, T. Inamura, S. Q. Xie, and I. A. Anderson, "Dielectric elastomer switches for smart artificial muscles," *Applied Physics A,* vol. 100, pp. 385-389, 2010.

[12] H. Stoyanov, M. Kollosche, S. Risse, D. N. McCarthy, and G. Kofod, "Elastic block copolymer nanocomposites with controlled interfacial interactions for artificial muscles with direct voltage control," *Soft Matter,* vol. 7, p. 194, 2011.

[13] M. Potz, M. Artusi, M. Soleimani, C. Menon, S. Cocuzza, and S. Debei, "Rolling dielectric elastomer actuator with bulged cylindrical shape," *Smart Materials and Structures,* vol. 19, p. 127001, 2010.

[14] Y. Bar-Cohen, R. Heydt, R. Kornbluh, J. Eckerle, and R. Pelrine, "Sound radiation properties of dielectric elastomer electroactive polymer loudspeakers," *Smart Structures and Materials 2006,* vol. 6168, pp. 61681M-8, 2006.

[15] K. Hochradel, S. J. Rupitsch, A. Sutor, R. Lerch, D. K. Vu, and P. Steinmann, "Dynamic performance of dielectric elastomers utilized as acoustic actuators," *Applied Physics A,* vol. 107, pp. 531-538, 2012.

[16] M. Aschwanden and A. Stemmer, "Polymeric, electrically tunable diffraction grating based on artificial muscles," *Optics Letters,* vol. 31, pp. 2610-2612, Sep 2006.

[17] E. Biddiss and T. Chau, "Dielectric elastomers as actuators for upper limb prosthetics: Challenges and opportunities," *Medical Engineering & Physics,* vol. 30, pp. 403-418, 2008.

[18] S. Son and N. C. Goulbourne, "Dynamic response of tubular dielectric elastomer transducers," *International Journal of Solids and Structures,* vol. 47, pp. 2672-2679, 2010.

[19] G. Kang, K.-S. Kim, and S. Kim, "Note: Analysis of the efficiency of a dielectric elastomer generator for energy harvesting," *Review of Scientific Instruments,* vol. 82, p. 046101, 2011.

[20] T. McKay, B. O'Brien, E. Calius, and I. Anderson, "An integrated, self-priming dielectric elastomer generator," *Applied Physics Letters,* vol. 97, p. 062911, 2010.

[21] T. G. McKay, B. M. O'Brien, E. P. Calius, and I. A. Anderson, "Soft generators using dielectric elastomers," *Applied Physics Letters,* vol. 98, p. 142903, 2011.

[22] R. Pelrine, R. Kornbluh, J. Joseph, R. Heydt, Q. B. Pei, and S. Chiba, "High-field deformation of elastomeric dielectrics for actuators," *Materials Science & Engineering C-Biomimetic and Supramolecular Systems,* vol. 11, pp. 89-100, Nov 2000.

[23] R. Pelrine, "High-Speed Electrically Actuated Elastomers with Strain Greater Than 100%," *Science,* vol. 287, pp. 836-839, 2000.

[24] T. Vu-Cong, C. Jean-Mistral, and A. Sylvestre, "Impact of the nature of the compliant electrodes on the dielectric constant of acrylic and silicone electroactive polymers," *Smart Materials and Structures,* vol. 21, p. 105036, Oct 2012.

[25] R. Pelrine, P. Sommer-Larsen, R. Kornbluh, R. Heydt, G. Kofod, Q. B. Pei, *et al.*, "Applications of dielectric elastomer actuators," *Smart Structures and Materials 2001: Electroactive Polymer Actuators and Devices,* vol. 4329, pp. 335-349, 2001.

[26] R. Shankar, T. K. Ghosh, and R. J. Spontak, "Dielectric elastomers as next-generation polymeric actuators," *Soft Matter,* vol. 3, p. 1116, 2007.

[27] X. Q. Zhang, C. Lowe, M. Wissler, B. Jahne, and G. Kovacs, "Dielectric elastomers in actuator technology," *Advanced Engineering Materials,* vol. 7, pp. 361-367, May 2005.

[28] G. Kofod, "Dielectric elastomer actuators," Ph.D., Department of Chemistry, The Technical University of Denmark, Denmark, 2001.

[29] Z. Suo, "Theory of dielectric elastomers," *Acta Mechanica Solida Sinica,* vol. 23, pp. 549-578, 2010.

[30] R. D. K. Ronald E. Pelrine, Jose P. Joseph, "Analysis of the electrostriction of polymer dielectrics with compliant electrodes as a means of actuation," *Sensors and Actuators A: Physical,* vol. 64, pp. 77-85, 1998.

[31] N. C. Goulbourne, "A constitutive model of polyacrylate interpenetrating polymer networks for dielectric elastomers," *International Journal of Solids and Structures,* vol. 48, pp. 1085-1091, 2011.

[32] G. Kofod, P. Sommer-Larsen, R. Kornbluh, and R. Pelrine, "Actuation Response of Polyacrylate Dielectric Elastomers," *Journal of Intelligent Materials Systems and Structures,* vol. 14, pp. 787-793, 2003.

[33] M. Pharr, J.-Y. Sun, and Z. Suo, "Rupture of a highly stretchable acrylic dielectric elastomer," *Journal of Applied Physics,* vol. 111, p. 104114, 2012.

[34] J. Qiang, H. Chen, and B. Li, "Experimental study on the dielectric properties of polyacrylate dielectric elastomer," *Smart Materials and Structures,* vol. 21, p. 025006, 2012.

[35] Z. Zhen, L. Liwu, D. Gang, S. Shouhua, L. Yanju, and L. Jinsong, "Silicone dielectric elastomers filled with carbon nanotubes and actuator," *Proceedings of the SPIE - The International Society for Optical Engineering,* vol. 7287, p. 72871, 2009 2009.

[36] D. M. Opris, M. Molberg, C. Walder, Y. S. Ko, B. Fischer, and F. A. Nüesch, "New Silicone Composites for Dielectric Elastomer Actuator Applications In Competition with Acrylic Foil," *Advanced Functional Materials,* vol. 21, pp. 3531-3539, 2011.

[37] S. Michel, X. Q. Q. Zhang, M. Wissler, C. Lowe, and G. Kovacs, "A comparison between silicone and acrylic elastomers as dielectric materials in electroactive polymer actuators," *Polymer International,* vol. 59, pp. 391-399, Mar 2010.

[38] Y. Bar-Cohen, H. R. Choi, K. Jung, N. H. Chuc, M. Jung, I. Koo, *et al.,* "Effects of prestrain on behavior of dielectric elastomer actuator," vol. 5759, pp. 283-291, 2005.

[39] G. Kofod, "The static actuation of dielectric elastomer actuators: how does pre-stretch improve actuation?," *Journal of Physics D-Applied Physics,* vol. 41, p. 11, Nov 2008.

[40] B. Li, H. L. Chen, J. H. Qiang, S. L. Hu, Z. C. Zhu, and Y. Q. Wang, "Effect of mechanical pre-stretch on the stabilization of dielectric elastomer actuation," *Journal of Physics D-Applied Physics,* vol. 44, p. 155301, Apr 2011.

[41] M. Wissler and E. Mazza, "Modeling of a pre-strained circular actuator made of dielectric elastomers," *Sensors and Actuators A: Physical,* vol. 120, pp. 184-192, 2005.

[42] G. Ouyang, K. Wang, and X. Y. Chen, "TiO2nanoparticles modified polydimethylsiloxane with fast response time and increased dielectric constant," *Journal of Micromechanics and Microengineering*, vol. 22, p. 074002, 2012.

[43] D. Yang, M. Tian, Y. Dong, H. Kang, D. Gong, and L. Zhang, "A high-performance dielectric elastomer consisting of bio-based polyester elastomer and titanium dioxide powder," *Journal of Applied Physics*, vol. 114, p. 154104, 2013.

[44] X. Huang, L. Xie, Z. Hu, and P. Jiang, "Influence of BaTiO3 Nanoparticles on Dielectric, Thermophysical and Mechanical Properties of Ethylene-Vinyl Acetate Elastomer/BaTiO3 Microcomposites," *Ieee Transactions on Dielectrics and Electrical Insulation*, vol. 18, pp. 375-383, Apr 2011.

[45] Z. P. Wang, J. K. Nelson, H. Hillborg, S. Zhao, and L. S. Schadler, "Dielectric constant and breakdown strength of polymer composites with high aspect ratio fillers studied by finite element models," *Composites Science and Technology*, vol. 76, pp. 29-36, Mar 4 2013.

[46] S. Javadi and M. Razzaghi-Kashani, "Dielectric elastomer actuators of silicone rubber-titanium dioxide composites obtained by dielectrophoretic assembly of filler particles," in *Electroactive Polymer Actuators and Devices*. vol. 7642, Y. BarCohen, Ed., ed Bellingham: Spie-Int Soc Optical Engineering, 2010.

[47] G. Gallone, F. Carpi, D. De Rossi, G. Levita, and A. Marchetti, "Dielectric constant enhancement in a silicone elastomer filled with lead magnesium niobate–lead titanate," *Materials Science and Engineering: C*, vol. 27, pp. 110-116, 2007.

[48] Y. Bai, Z. Y. Cheng, V. Bharti, H. S. Xu, and Q. M. Zhang, "High-dielectric-constant ceramic-powder polymer composites," *Applied Physics Letters,* vol. 76, pp. 3804-3806, Jun 2000.

[49] L. Wang and Z. M. Dang, "Carbon nanotube composites with high dielectric constant at low percolation threshold," *Applied Physics Letters,* vol. 87, p. 042903, Jul 2005.

[50] R. Basu and G. S. Iannacchione, "Dielectric response of multiwalled carbon nanotubes as a function of applied ac-electric fields," *Journal of Applied Physics,* vol. 104, p. 114107, Dec 2008.

[51] Z. M. Dang, L. Wang, Y. Yin, Q. Zhang, and Q. Q. Lei, "Giant dielectric permittivities in functionalized carbon-nanotube/electroactive-polymer nanocomposites," *Advanced Materials,* vol. 19, pp. 852-857, Mar 2007.

[52] F. Galantini, S. Bianchi, V. Castelvetro, and G. Gallone, "Functionalized carbon nanotubes as a filler for dielectric elastomer composites with improved actuation performance," *Smart Materials and Structures,* vol. 22, p. 055025, May 2013.

[53] S. L. Shi and J. Liang, "Effect of multiwall carbon nanotubes on electrical and dielectric properties of yttria-stabilized zirconia ceramic," *Journal of the American Ceramic Society*, vol. 89, pp. 3533-3535, Nov 2006.

[54] I. A. Anderson, T. Hale, T. Gisby, T. Inamura, T. McKay, B. O'Brien, *et al.*, "A thin membrane artificial muscle rotary motor," *Applied Physics A,* vol. 98, pp. 75-83, 2009.

[55] H. R. Choi, K. Jung, N. H. Chuc, M. Jung, I. Koo, J. Koo, *et al.*, "Effects of prestrain on behavior of dielectric elastomer actuator," in *Smart Structures and Materials 2005: Electroactive Polymer Actuators and Devices(EAPAD)*. vol. 5759, Y. B. Cohen, Ed., ed Bellingham: Spie-Int Soc Optical Engineering, 2005, pp. 283-291.

[56] C. Chiang Foo, S. Cai, S. Jin Adrian Koh, S. Bauer, and Z. Suo, "Model of dissipative dielectric elastomers," *Journal of Applied Physics,* vol. 111, p. 034102, 2012.

[57] T. He, L. Cui, C. Chen, and Z. Suo, "Nonlinear deformation analysis of a dielectric elastomer membrane–spring system," *Smart Materials and Structures,* vol. 19, p. 085017, 2010.

[58] T. He, X. Zhao, and Z. Suo, "Dielectric elastomer membranes undergoing inhomogeneous deformation," *Journal of Applied Physics,* vol. 106, p. 083522, 2009.

[59] J. Huang, T. Li, C. Chiang Foo, J. Zhu, D. R. Clarke, and Z. Suo, "Giant, voltage-actuated deformation of a dielectric elastomer under dead load," *Applied Physics Letters,* vol. 100, p. 041911, 2012.

[60] S. J. A. Koh, T. Li, J. Zhou, X. Zhao, W. Hong, J. Zhu, *et al.*, "Mechanisms of large actuation strain in dielectric elastomers," *Journal of Polymer Science Part B: Polymer Physics,* vol. 49, pp. 504-515, 2011.

[61] X. Zhao and Z. Suo, "Method to analyze electromechanical stability of dielectric elastomers," *Applied Physics Letters,* vol. 91, p. 061921, 2007.

[62] X. Zhao and Z. Suo, "Theory of Dielectric Elastomers Capable of Giant Deformation of Actuation," *Physical Review Letters,* vol. 104, p. 178302, 2010.

[63] J. Zhu, H. Stoyanov, G. Kofod, and Z. Suo, "Large deformation and electromechanical instability of a dielectric elastomer tube actuator," *Journal of Applied Physics,* vol. 108, p. 074113, 2010.

[64] W. Yuan, L. B. Hu, Z. B. Yu, T. Lam, J. Biggs, S. M. Ha, *et al.*, "Fault-Tolerant Dielectric Elastomer Actuators using Single-Walled Carbon Nanotube Electrodes," *Advanced Materials,* vol. 20, pp. 621-625, 2008.

[65] I. S. Park, K. J. Kim, J. D. Nam, J. Lee, and W. Yim, "Mechanical, dielectric, and magnetic properties of the silicone elastomer with multi-walled carbon a nanotubes as a nanofiller," *Polymer Engineering and Science,* vol. 47, pp. 1396-1405, Sep 2007.

[66] P. Pötschke, S. M. Dudkin, and I. Alig, "Dielectric spectroscopy on melt processed polycarbonate—multiwalled carbon nanotube composites," *Polymer,* vol. 44, pp. 5023-5030, 2003.

[67] Z. M. Dang, L. Wang, Y. Yin, Q. Zhang, and Q. Q. Lei, "Giant Dielectric Permittivities in Functionalized Carbon-Nanotube/ Electroactive-Polymer Nanocomposites," *Advanced Materials,* vol. 19, pp. 852-857, 2007.

[68] R. S. Underhill and B. W. Michalchuk, *Carbon nanotube-elastomer composites for use in dielectric polymer actuators*. Los Alamitos: Ieee Computer Soc, 2005.

[69] S. Iijima, "Helical Microtubules of Graphitic Carbon," *Nature,* vol. 354, pp. 56-58, Nov 1991.

[70] J. Song, C. M. Thurber, S. Kobayashi, A. M. Baker, C. W. Macosko, and H. C. Silvis, "Blends of polyolefin/PMMA for improved scratch resistance, adhesion and compatibility," *Polymer,* vol. 53, pp. 3636-3641, Jul 2012.

[71] T. Sekitani, Y. Noguchi, K. Hata, T. Fukushima, T. Aida, and T. Someya, "A rubberlike stretchable active matrix using elastic conductors," *Science,* vol. 321, pp. 1468-72, Sep 12 2008.

[72] B. Ashrafi, P. Hubert, and S. Vengallatore, "Carbon nanotube-reinforced composites as structural materials for microactuators in microelectromechanical systems," *Nanotechnology,* vol. 17, pp. 4895-4903, Oct 2006.

[73] P. Soonjae, L. Jae-Ik, K. Min-Ook, C. Taeyoung, O. Yongkeun, L. Soo-Chul, *et al.*, "Development of a flexible three-axis tactile sensor based on screen-printed carbon nanotube-polymer composite," *Journal of Micromechanics and Microengineering*, vol. 24, pp. 075012 (9 pp.)-075012 (9 pp.), July 2014.

[74] L. Bokobza, "Multiwall carbon nanotube elastomeric composites: A review," *Polymer*, vol. 48, pp. 4907-4920, Aug 2007.

[75] L. Ci, J. Suhr, V. Pushparaj, X. Zhang, and P. M. Ajayan, "Continuous carbon nanotube reinforced composites," *Nano Letters*, vol. 8, pp. 2762-2766, Sep 2008.

[76] Z. M. Liu and B. X. Han, "Synthesis of Carbon-Nanotube Composites Using Supercritical Fluids and Their Potential Applications," *Advanced Materials*, vol. 21, pp. 825-829, Feb 2009.

[77] A. Bachtold, P. Hadley, T. Nakanishi, and C. Dekker, "Logic circuits with carbon nanotube transistors," *Science*, vol. 294, pp. 1317-1320, Nov 2001.

[78] O. Breuer and U. Sundararaj, "Big returns from small fibers: A review of polymer/carbon nanotube composites," *Polymer Composites*, vol. 25, pp. 630-645, Dec 2004.

[79] L. Sun, G. L. Warren, J. Y. O'Reilly, W. N. Everett, S. M. Lee, D. Davis, *et al.*, "Mechanical properties of surface-functionalized SWCNT/epoxy composites," *Carbon*, vol. 46, pp. 320-328, Feb 2008.

[80] J. E. Riggs, Z. X. Guo, D. L. Carroll, and Y. P. Sun, "Strong luminescence of solubilized carbon nanotubes," *Journal of the American Chemical Society*, vol. 122, pp. 5879-5880, Jun 2000.

[81] M. C. Paiva, B. Zhou, K. A. S. Fernando, Y. Lin, J. M. Kennedy, and Y. P. Sun, "Mechanical and morphological characterization of polymer-carbon nanocomposites from functionalized carbon nanotubes," *Carbon,* vol. 42, pp. 2849-2854, 2004.

[82] L. W. Qu, Y. Lin, D. E. Hill, B. Zhou, W. Wang, X. F. Sun, *et al.*, "Polyimide-functionalized carbon nanotubes: Synthesis and dispersion in nanocomposite films," *Macromolecules,* vol. 37, pp. 6055-6060, Aug 2004.

[83] C. A. Mitchell, J. L. Bahr, S. Arepalli, J. M. Tour, and R. Krishnamoorti, "Dispersion of functionalized carbon nanotubes in polystyrene," *Macromolecules,* vol. 35, pp. 8825-8830, Nov 2002.

[84] H. L. Zeng, C. Gao, and D. Y. Yan, "Poly(epsilon-caprolactone)-functionalized carbon nanotubes and their biodegradation properties," *Advanced Functional Materials,* vol. 16, pp. 812-818, Apr 2006.

[85] L. Zhang, Q. Q. Ni, T. Natsuki, and Y. Q. Fu, "Carbon nanotubes/magnetite hybrids prepared by a facile synthesis process and their magnetic properties," *Applied Surface Science,* vol. 255, pp. 8676-8681, Jul 2009.

[86] Y.-h. Shih and M.-S. Li, "Adsorption of selected volatile organic vapors on multiwall carbon nanotubes," *Journal of Hazardous Materials,* vol. 154, pp. 21-28, Jun 15 2008.

[87] X. L. Xie, Y. W. Mai, and X. P. Zhou, "Dispersion and alignment of carbon nanotubes in polymer matrix: A review," *Materials Science & Engineering R-Reports,* vol. 49, pp. 89-112, May 2005.

[88] J. Ryszkowska, M. Jurczyk-Kowalska, T. Szymborski, and K. J. Kurzydlowski, "Dispersion of carbon nanotubes in polyurethane matrix," *Physica E-Low-Dimensional Systems & Nanostructures,* vol. 39, pp. 124-127, Jul 2007.

[89] H. Varela-Rizo, I. Rodriguez-Pastor, and I. Martin-Gullon, "Effect of solvent nature in casting-based carbon nanofiber/poly(methyl-methacrylate) nanocomposites," *Journal of Applied Polymer Science,* vol. 125, pp. 3228-3238, Aug 2012.

[90] D. Kazachkin, Y. Nishimura, S. Irle, K. Morokuma, R. D. Vidic, and E. Borguet, "Interaction of acetone with single wall carbon nanotubes at cryogenic temperatures: A combined temperature programmed desorption and theoretical study," *Langmuir,* vol. 24, pp. 7848-7856, Aug 5 2008.

[91] C. U. Lee and M. D. Dadmun, "Improving the dispersion and interfaces in polymer-carbon nanotube nanocomposites by sample preparation choice," *Journal of Polymer Science Part B-Polymer Physics,* vol. 46, pp. 1747-1759, Aug 2008.

[92] Y. H. Liao, O. Marietta-Tondin, Z. Y. Liang, C. Zhang, and B. Wang, "Investigation of the dispersion process of SWNTs/SC-15 epoxy resin nanocomposites," *Materials Science and Engineering a-Structural Materials Properties Microstructure and Processing,* vol. 385, pp. 175-181, Nov 15 2004.

[93] K. T. Lau, M. Lu, C. K. Lam, H. Y. Cheung, F. L. Sheng, and H. L. Li, "Thermal and mechanical properties of single-walled carbon nanotube bundle-reinforced epoxy nanocomposites: the role of solvent for nanotube dispersion," *Composites Science and Technology,* vol. 65, pp. 719-725, Apr 2005.

[94] R. Li and L. Z. Sun, "Dynamic mechanical behavior of magnetorheological nanocomposites filled with carbon nanotubes," *Applied Physics Letters,* vol. 99, p. 131912, Sep 2011.

[95] A. Montazeri and M. Chitsazzadeh, "Effect of sonication parameters on the mechanical properties of multi-walled carbon nanotube/epoxy composites," *Materials & Design,* vol. 56, pp. 500-508, Apr 2014.

[96] B. Fiedler, F. H. Gojny, M. H. G. Wichmann, M. C. M. Nolte, and K. Schulte, "Fundamental aspects of nano-reinforced composites," *Composites Science and Technology,* vol. 66, pp. 3115-3125, Dec 2006.

[97] K. L. Lu, R. M. Lago, Y. K. Chen, M. L. H. Green, P. J. F. Harris, and S. C. Tsang, "Mechanical damage of carbon nanotubes by ultrasound," *Carbon,* vol. 34, pp. 814-816, 1996.

[98] J. B. Bai and A. Allaoui, "Effect of the length and the aggregate size of MWNTs on the improvement efficiency of the mechanical and electrical properties of nanocomposites - experimental investigation," *Composites Part a-Applied Science and Manufacturing,* vol. 34, pp. 689-694, 2003.

[99] D. Qian, E. C. Dickey, R. Andrews, and T. Rantell, "Load transfer and deformation mechanisms in carbon nanotube-polystyrene composites," *Applied Physics Letters,* vol. 76, pp. 2868-2870, May 2000.

[100] M. Wissler and E. Mazza, "Electromechanical coupling in dielectric elastomer actuators," *Sensors and Actuators a-Physical,* vol. 138, pp. 384-393, Aug 2007.

[101] M. Iwamoto, *Maxwell–Wagner Effect*: Springer Netherlands, 2012.

[102] I. A. Tchmutin, A. T. Ponomarenko, V. G. Shevchenko, N. G. Ryvkina, C. Klason, and D. H. McQueen, "Electrical transport in 0-3 epoxy resin barium titanate carbon black polymer composites," *Journal of Polymer Science Part B-Polymer Physics,* vol. 36, pp. 1847-1856, Aug 1998.

[103] X. H. Zhang, G. Z. Liang, J. F. Chang, A. J. Gu, L. Yuan, and W. Zhang, "The origin of the electric and dielectric behavior of expanded graphite-carbon nanotube/cyanate ester composites with very high dielectric constant and low dielectric loss," *Carbon,* vol. 50, pp. 4995-5007, Nov 2012.

[104] S. L. Shi, L. Z. Zhang, and J. S. Li, "Electrical and dielectric properties of multiwall carbon nanotube/polyaniline composites," *Journal of Polymer Research,* vol. 16, pp. 395-399, Jul 2009.

[105] L. Flandin, T. Prasse, R. Schueler, K. Schulte, W. Bauhofer, and J. Y. Cavaille, "Anomalous percolation transition in carbon-black-epoxy composite materials," *Physical Review B,* vol. 59, pp. 14349-14355, Jun 1999.

[106] N. Yoshikawa, K. Kawahira, Y. Saito, H. Todoroki, and S. Taniguchi, "Estimation of microwave penetration distance and complex permittivity of graphite by measurement of permittivity and direct current conductivity of graphite powder mixtures," *Journal of Applied Physics,* vol. 117, p. 084105, 2015.

[107] J. Macutkevic, I. Kranauskaite, J. Banys, S. Moseenkov, V. Kuznetsov, and O. Shenderova, "Metal-insulator transition and size dependent electrical percolation in onion-like carbon/polydimethylsiloxane composites," *Journal of Applied Physics,* vol. 115, p. 213702, 2014.

[108] A. L. Efros and B. I. Shklovskii, "Critical Behaviour of Conductivity and Dielectric Constant near the Metal-Non-Metal Transition Threshold," *Physica Status Solidi B-Basic Research,* vol. 76, pp. 475-485, 1976.

[109] Z. Zhang, L. W. Liu, J. M. Fan, K. Yu, Y. J. Liu, L. Shi, *et al.*, "New silicone dielectric elastomers with a high dielectric constant - art. no. 692610," in *Modeling, Signal*

Processing, and Control for Smart Structures 2008. vol. 6926, D. K. Lindner, Ed., ed Bellingham: Spie-Int Soc Optical Engineering, 2008, p. 692610.

[110] J. Rossiter, B. Yap, and A. Conn, "Biomimetic chromatophores for camouflage and soft active surfaces," *Bioinspiration & Biomimetics,* vol. 7, p. 036009, 2012.

[111] Y. Jhong, D. Mikolas, T. Yeh, W. Fang, D. Shaw, J. Chen, *et al.*, "Characterization of nonlinear effects in a two-dimensional dielectric elastomer actuator," *Smart Materials and Structures,* vol. 19, p. 105027, 2010.

[112] Y. Liu, L. Liu, Z. Zhang, and J. Leng, "Dielectric elastomer film actuators: characterization, experiment and analysis," *Smart Materials and Structures,* vol. 18, p. 095024, 2009.

[113] D. Yang, M. Tian, Y. Dong, H. Liu, Y. Yu, and L. Zhang, "Disclosed dielectric and electromechanical properties of hydrogenated nitrile–butadiene dielectric elastomer," *Smart Materials and Structures,* vol. 21, p. 035017, 2012.

[114] P. Khodaparast, S. R. Ghaffarian, and M. R. Khosroshahi, "Effect of Different Electrode Materials on the Performance of Smart Composite Actuators Based on Dielectric Elastomers," *Key Engineering Materials,* vol. 334-335, pp. 985-988, 2007.

[115] M. Molberg, D. Crespy, P. Rupper, F. Nüesch, J.-A. E. Månson, C. Löwe, *et al.*, "High Breakdown Field Dielectric Elastomer Actuators Using Encapsulated Polyaniline as High Dielectric Constant Filler," *Advanced Functional Materials,* vol. 20, pp. 3280-3291, 2010.

[116] S. Hsien Low, L. Lynn Shiau, and G.-K. Lau, "Large actuation and high dielectric strength in metallized dielectric elastomer actuators," *Applied Physics Letters,* vol. 100, p. 182901, 2012.

[117] D. Yang, L. Zhang, H. Liu, Y. Dong, Y. Yu, and M. Tian, "Lead magnesium niobate-filled silicone dielectric elastomer with large actuated strain," *Journal of Applied Polymer Science,* vol. 125, pp. 2196-2201, 2012.

[118] F. M. Guillot, J. Jarzynski, and E. Balizer, "Electromechanical response of polymer films by laser Doppler vibrometry," *Journal of the Acoustical Society of America,* vol. 103, pp. 1421-1427, Mar 1998.

[119] Mitutoyo. Microscope Units and Objectives [Online].

[120] Y. Wei, P. Brochu, H. Soon Mok, and P. Qibing, "Dielectric oil coated single-walled carbon nanotube electrodes for stable, large-strain actuation with dielectric elastomers," *Sensors and Actuators: A Physical,* vol. 155, pp. 278-284, Oct. 2009.

[121] M. R. Ayatollahi, S. Shadlou, M. M. Shokrieh, and M. Chitsazzadeh, "Effect of multi-walled carbon nanotube aspect ratio on mechanical and electrical properties of epoxy-based nanocomposites," *Polymer Testing,* vol. 30, pp. 548-556, Aug 2011.

[122] N. T. Dintcheva, R. Arrigo, G. Nasillo, E. Caponetti, and F. P. La Mantia, "Effect of the nanotube aspect ratio and surface functionalization on the morphology and properties of multiwalled carbon nanotube polyamide-based fibers," *Journal of Applied Polymer Science,* vol. 129, pp. 2479-2489, Sep 2013.

[123] K. Shehzad, Z. M. Dang, M. N. Ahmad, R. U. R. Sagar, S. Butt, M. U. Farooq, *et al.*, "Effects of carbon nanotubes aspect ratio on the qualitative and quantitative aspects of frequency response of electrical conductivity and dielectric permittivity in the carbon nanotube/polymer composites," *Carbon,* vol. 54, pp. 105-112, Apr 2013.

[124] R. Simoes, J. Silva, R. Vaia, V. Sencadas, P. Costa, J. Gomes, *et al.*, "Low percolation transitions in carbon nanotube networks dispersed in a polymer matrix: dielectric properties, simulations and experiments," *Nanotechnology,* vol. 20, p. 035703, Jan 2009.

[125] F. T. Fisher, R. D. Bradshaw, and L. C. Brinson, "Fiber waviness in nanotube-reinforced polymer composites-1: Modulus predictions using effective nanotube properties," *Composites Science and Technology,* vol. 63, pp. 1689-1703, Aug 2003.

[126] "Standard Guide for Dynamic Testing of Vulcanized Rubber and Rubber-Like Materials Using Vibratory Methods," in *D 5992 – 96*, ed: ASTM.

[127] R. Tamura, E. Lim, T. Manaka, and M. Iwamoto, "Analysis of pentacene field effect transistor as a Maxwell-Wagner effect element," *Journal of Applied Physics,* vol. 100, p. 114515, Dec 2006.

[128] Z. M. Dang, C. W. Nan, D. Xie, Y. H. Zhang, and S. C. Tjong, "Dielectric behavior and dependence of percolation threshold on the conductivity of fillers in polymer-semiconductor composites," *Applied Physics Letters,* vol. 85, pp. 97-99, Jul 2004.

[129] C. W. Nan, "Physics of inhomogeneous inorganic materials," *Progress in Materials Science,* vol. 37, pp. 1-116, 1993.

[130] M. A. Bhuiyan, R. V. Pucha, J. Worthy, M. Karevan, and K. Kalaitzidou, "Defining the lower and upper limit of the effective modulus of CNT/polypropylene composites through integration of modeling and experiments," *Composite Structures,* vol. 95, pp. 80-87, Jan 2013.

[131] R. Li, "Dynamic Mechanical Behavior of Magnetorheological Nanocomposites," Ph.D., University of California, Irvine, 2011.

[132] C. Brosseau, A. Beroual, and A. Boudida, "How do shape anisotropy and spatial orientation of the constituents affect the permittivity of dielectric heterostructures?," *Journal of Applied Physics,* vol. 88, pp. 7278-7288, Dec 2000.

[133] A. Y. Matveeva, S. V. Pyrlin, M. M. D. Ramos, H. J. Bohm, and F. W. J. van Hattum, "Influence of waviness and curliness of fibres on mechanical properties of composites," *Computational Materials Science,* vol. 87, pp. 1-11, May 2014.

[134] M. A. Bhuiyan, R. V. Pucha, M. Karevan, and K. Kalaitzidou, "Tensile modulus of carbon nanotube/polypropylene composites - A computational study based on experimental characterization," *Computational Materials Science,* vol. 50, pp. 2347-2353, Jun 2011.

[135] A. Sihvola, "Mixing Rules with Complex Dielectric Coefficients," *Subsurface Sensing Technologies and Applications*, vol. 1, pp. 393-415, 2000.

[136] Z. M. Dang, J. K. Yuan, J. W. Zha, T. Zhou, S. T. Li, and G. H. Hu, "Fundamentals, processes and applications of high-permittivity polymer matrix composites," *Progress in Materials Science,* vol. 57, pp. 660-723, May 2012.

[137] V. Myroshnychenko and C. Brosseau, "Finite-element method for calculation of the effective permittivity of random inhomogeneous media," *Physical Review E,* vol. 71, p. 016701, Jan 2005.

[138] M. Felisberto, A. Arias-Duran, J. A. Ramos, I. Mondragon, R. Candal, S. Goyanes, *et al.*, "Influence of filler alignment in the mechanical and electrical properties of carbon nanotubes/epoxy nanocomposites," *Physica B-Condensed Matter,* vol. 407, pp. 3181-3183, Aug 2012.

[139] Y. F. Zhu, C. Ma, W. Zhang, R. P. Zhang, N. Koratkar, and J. Liang, "Alignment of multiwalled carbon nanotubes in bulk epoxy composites via electric field," *Journal of Applied Physics,* vol. 105, p. 054319, Mar 2009.

[140] H. X. Tang, M. H. Malakooti, and H. A. Sodano, "Relationship between orientation factor of lead zirconate titanate nanowires and dielectric permittivity of nanocomposites," *Applied Physics Letters,* vol. 103, p. 222901, Nov 2013.

[141] H. Garmestani, M. S. Al-Haik, K. Dahmen, R. Tannenbaum, D. S. Li, S. S. Sablin, *et al.*, "Polymer-mediated alignment of carbon nanotubes under high magnetic fields," *Advanced Materials,* vol. 15, p. 1918, Nov 2003.

[142] D. S. Bychanok, M. A. Kanygin, A. V. Okotrub, M. V. Shuba, A. G. Paddubskaya, A. O. Pliushch, *et al.*, "Anisotropy of the electromagnetic properties of polymer composites based on multiwall carbon nanotubes in the gigahertz frequency range," *Jetp Letters,* vol. 93, pp. 607-611, Jul 2011.

[143] P. Kuzhir, A. Paddubskaya, D. Bychanok, A. Nemilentsau, M. Shuba, A. Plusch, *et al.*, "Microwave probing of nanocarbon based epoxy resin composite films: Toward electromagnetic shielding," *Thin Solid Films,* vol. 519, pp. 4114-4118, Apr 2011.

[144] M. Urvakis, A. Kupreviciute, J. Banys, J. Macutkevic, B. Mayoral, and T. McNally, "Effect of annealing and biaxial deformation on the dielectric properties of composites of multiwall carbon nanotubes and poly(ethylene terephthalate)," *Journal of Nanophotonics,* vol. 6, p. 061708, Oct 2012.

[145] R. Basu and G. S. Iannacchione, "High-resolution dielectric spectroscopy and electric-field dependence of carbon allotropes including multiwall and single-wall nanotubes," *Applied Physics Letters,* vol. 92, p. 052906, Feb 2008.

[146] V. Tomer, C. A. Randall, G. Polizos, J. Kostelnick, and E. Manias, "High- and low-field dielectric characteristics of dielectrophoretically aligned ceramic/polymer nanocomposites," *Journal of Applied Physics,* vol. 103, p. 034115, Feb 2008.

[147] Z. M. Dang, S. H. Yao, and H. P. Xu, "Effect of tensile strain on morphology and dielectric property in nanotube/polymer nanocomposites," *Applied Physics Letters,* vol. 90, p. 012907, Jan 2007.

[148] X. M. Zeng, X. F. Xu, P. M. Shenai, E. Kovalev, C. Baudot, N. Mathews, *et al.*, "Characteristics of the Electrical Percolation in Carbon Nanotubes/Polymer Nanocomposites," *Journal of Physical Chemistry C,* vol. 115, pp. 21685-21690, Nov 2011.

[149] R. D. Bradshaw, F. T. Fisher, and L. C. Brinson, "Fiber waviness in nanotube-reinforced polymer composites-II: modeling via numerical approximation of the dilute strain concentration tensor," *Composites Science and Technology,* vol. 63, pp. 1705-1722, Aug 2003.

[150] F. T. Fisher, R. D. Bradshaw, and L. C. Brinson, "Effects of nanotube waviness on the modulus of nanotube-reinforced polymers," *Applied Physics Letters,* vol. 80, pp. 4647-4649, Jun 2002.

[151] C. H. Tsai, C. Zhang, D. A. Jack, R. C. Liang, and B. Wang, "The effect of inclusion waviness and waviness distribution on elastic properties of fiber-reinforced composites," *Composites Part B-Engineering,* vol. 42, pp. 62-70, Jan 2011.

[152] J. Nafar Dastgerdi, G. Marquis, and M. Salimi, "The effect of nanotubes waviness on mechanical properties of CNT/SMP composites," *Composites Science and Technology,* vol. 86, pp. 164-169, 24 2013.

[153] R. Dendievel, F. Dalmas, L. Chazeau, J. Y. Cavaille, and C. Gauthier, "Carbon nanotube-filled polymer composites. Numerical simulation of electrical conductivity in three-dimensional entangled fibrous networks," *Acta Materialia*, vol. 54, pp. 2923-2931, June 2006.

[154] S. Herasati and L. Zhang, "A new method for characterizing and modeling the waviness and alignment of carbon nanotubes in composites," *Composites Science and Technology*, vol. 100, pp. 136-142, 2014.

[155] e-Xstream, "Digimat 5.0.1 Manual," ed, 2013.

[156] Z. P. Wang, J. K. Nelson, J. J. Miao, R. J. Linhardt, L. S. Schadler, H. Hillborg, *et al.*, "Effect of High Aspect Ratio Filler on Dielectric Properties of Polymer Composites: A Study on Barium Titanate Fibers and Graphene Platelets," *Ieee Transactions on Dielectrics and Electrical Insulation*, vol. 19, pp. 960-967, Jun 2012.

[157] H. X. Tang, Y. R. Lin, and H. A. Sodano, "Enhanced Energy Storage in Nanocomposite Capacitors through Aligned PZT Nanowires by Uniaxial Strain Assembly," *Advanced Energy Materials*, vol. 2, pp. 469-476, Apr 2012.

[158] U. A. Joshi, S. C. Sharma, and S. P. Harsha, "Effect of carbon nanotube orientation on the mechanical properties of nanocomposites," *Composites Part B-Engineering*, vol. 43, pp. 2063-2071, Jun 2012.

[159] Y. F. Zhang, Z. H. Xia, and F. Ellyin, "Nonlinear viscoelastic micromechanical analysis of fibre-reinforced polymer laminates with damage evolution," *International Journal of Solids and Structures*, vol. 42, pp. 591-604, Jan 2005.

[160] N. Montinaro and A. Pantano, "Parameters influencing the stiffness of composites reinforced by carbon nanotubes - A numerical-analytical approach," *Composite Structures,* vol. 109, pp. 246-252, Mar 2014.

[161] M. Farsadi, A. Ochsner, and M. Rahmandoust, "Numerical investigation of composite materials reinforced with waved carbon nanotubes," *Journal of Composite Materials,* vol. 47, pp. 1425-1434, May 2013.

[162] Z. Xia, C. Zhou, Q. Yong, and X. Wang, "On selection of repeated unit cell model and application of unified periodic boundary conditions in micro-mechanical analysis of composites," *International Journal of Solids and Structures,* vol. 43, pp. 266-278, 2006.

[163] L. Shuguang, "On the nature of periodic traction boundary conditions in micromechanical FE analyses of unit cells," *IMA Journal of Applied Mathematics,* vol. 77, pp. 441-450, Aug. 2012.

[164] Z. H. Xia, Y. F. Zhang, and F. Ellyin, "A unified periodical boundary conditions for representative volume elements of composites and applications," *International Journal of Solids and Structures,* vol. 40, pp. 1907-1921, Apr 2003.

[165] X. F. Wang, X. W. Wang, G. M. Zhou, and C. W. Zhou, "Multi-scale analyses of 3D woven composite based on periodicity boundary conditions," *Journal of Composite Materials,* vol. 41, pp. 1773-1788, Jul 2007.

[166] I. Bardi, J. Tharp, and R. Petersson, "Homogenization of Periodic Structures Using the FEM," *Ieee Transactions on Magnetics,* vol. 50, p. 4, Feb 2014.

[167] S. Jacques, I. De Baere, and W. Van Paepegem, "Application of periodic boundary conditions on multiple part finite element meshes for the meso-scale homogenization of

textile fabric composites," *Composites Science and Technology*, vol. 92, pp. 41-54, Feb 2014.

[168] J. Aboudi and M. Ryvkin, "The analysis of localized effects in composites with periodic microstructure," *Philosophical Transactions of the Royal Society a-Mathematical Physical and Engineering Sciences,* vol. 371, p. 12, Jun 2013.

[169] K. Xu and X. W. Xu, "Finite element analysis of mechanical properties of 3D five-directional braided composites," *Materials Science and Engineering a-Structural Materials Properties Microstructure and Processing,* vol. 487, pp. 499-509, Jul 2008.

[170] H. W. Zhang, J. K. Wu, J. Lu, and Z. D. Fu, "Extended multiscale finite element method for mechanical analysis of heterogeneous materials," *Acta Mechanica Sinica,* vol. 26, pp. 899-920, Dec 2010.

[171] L. Lampani and P. Gaudenzi, "3D Finite Element Analyses of Multilayer Dielectric Elastomer Actuators with Metallic Compliant Electrodes for Space Applications," *Journal of Intelligent Material Systems and Structures,* vol. 21, pp. 621-632, Apr 2010.

[172] COMSOL, "Nonlinear Structural Materials Module User's Guide," 4.3 ed, 2012.

[173] M. F. Yu, O. Lourie, M. J. Dyer, K. Moloni, T. F. Kelly, and R. S. Ruoff, "Strength and breaking mechanism of multiwalled carbon nanotubes under tensile load," *Science,* vol. 287, pp. 637-640, Jan 2000.

[174] R. Li and L. Z. Sun, "A micromechanics-based viscoelastic model for nanocomposites with imperfect interface," *International Journal of Damage Mechanics,* vol. 22, pp. 967-981, Sep 2013.

[175] M. G. Todd and F. G. Shi, "Characterizing the interphase dielectric constant of polymer composite materials: Effect of chemical coupling agents," *Journal of Applied Physics*, vol. 94, pp. 4551-4557, Oct 2003.

Appendix: Commands to Run COMSOL Multiphysics in a Batch Mode on High Performance Computing Facilities Available at University of California, Irvine.

“qsub.sh”

```
#!/bin/bash

# DO NOT SET THE -cwd flag for a /scratch job


#$ -cwd

#$ -q cee

#$ -pe openmp 32


# specify the genuine bash interpreter

#$ -S /bin/bash


# specify the name of the job displayed in 'qstat' output

#$ -N comsol
```

```
# email me when things happen

#$ -notify



# at this address

#$ -M yuw2@uci.edu



# these are the things I want to be notified about

# b=begin; e=end; a=abort; s=suspend

#$ -m beas



# set the output file name

#$ -e comsol.err



# set the error file name

#$ -o comsol.out



# make sure you have a clean module env
```

```
module purge


# this job requires comsol

module load comsol


# finally execute the application with the output tagged with the ${hn} suffix

#comsol batch -inputfile YOURINPUT -outputfile YOUROUTPUT


echo "Here's the module environment:"

module list


echo ${HOSTNAME}


date
```

“submit.sh”

```
#! /bin/bash

date >> history

echo $* >> history

file=tmp.sge

cat /share/pub/yuw2/comsol/qsub.sh > $file

echo $* >> $file

qsub $file

rm -f $file
```